DETECTING CROPPING ACTIVITIES USING LANDSAT AND SPOT-6 IMAGERY IN KERINCI SEBLAT NATIONAL PARK, INDONESIA

ELVIA WIRYADI

COLLEGE OF SCIENCE AND ENGINEERING
FLINDERS UNIVERSITY
SOUTH AUSTRALIA

A Research project submitted as part of the requirement for admission to the degree of

MASTER OF GEOSPATIAL INFORMATION SCIENCE

JUNE 2019

TABLE OF CONTENTS

DECLARATION

I, **Elvia Wiryadi,** certify that this thesis does not incorporate without acknowledgment any material previously submitted for a degree or diploma in any university and, to the best of my knowledge and belief, does not contain any material previously published or written by another person except where due reference is made in the text.

Signature   Date: June 2019

Elvia Wiryadi

ABSTRACT

In Indonesia, the expansion of agriculture has become one of the drivers of deforestation, particularly with regard to farmland adjacent. Conservation areas such as national parks, nature reserve, and wildlife reserves are examples of forested areas that are most vulnerable to the threat of deforestation. Data on change in land use and in particular the existence of cropping within the protected forest areas is required as the initial attempt in understanding and preventing deforestation, followed by further actions such as law enforcement and collaboration with various organizations.

By adopting a remotely sensed approach using satellite images, this research aims to map the change of agriculture expansion and cropping segmentation throughout the national park boundary in Kerinci Mountain, Indonesia. This area studied is located at Kerinci regency, Jambi province, on the island of Sumatra, Indonesia., The mountain is part of Kerinci Seblat National Park (KSNP) which is also known as the home for a range of currently critically endangered species such as Sumatran tiger, orangutan, elephant, and rhinoceros, as listed by UNESCO World Heritage Committee and International Union for Conservation of Nature (IUCN).

The images data used in the analysis were acquired on three dates (1998, 2008 and 2018) and consisted of Landsat 5 Thematic Mapper (TM) and Landsat 7 Enhanced Thematic Mapper Plus (ETM+) with the 30-meter spatial resolution provided by United States Geological Survey (USGS). Additionally, two dates of SPOT-6 images (2013 and 2018) with 1.5-metre (panchromatic) and 6 meters (multispectral) spatial resolution were obtained from LAPAN (National Institute of Aeronautics and Space-Indonesia). These Such images were used to map the segmentation of cropping within the park's boundary.

In the Landsat imagery processing, a supervised classification approach applied to distinguish between forest and the fragmented area around the boundary of the park. On the other hand, the Object-Oriented Image Analysis (OBIA) with machine learning utilizes SPOT-6 imagery to classify the segmentation of crops

throughout the northern section of the Kerinci Seblat National Park. Change in land use/land cover was determined from the multiple dates. By using a series Landsat imagery and classification accuracy around 89 - 90%, the study found that in the last twenty years, forest loss in the park increases significantly from 3379.3 hectares in 1998 to 5685.83 hectares in 2018 (60%).   The classification of SPOT 2013 explained that almost 80% of forest loss within the national park was occupied actively by illegal farmers. It was indicated by the segmentation existence of plastic shade, agriculture, and fallow. Other class/ segmentation such as shrubs and pasture only accounts for 20% or around 749 hectares. The overall classification accuracy in such image achieved 85.29%. The classification of SPOT 2018 enlightened that around 55% of forest loss area within the park was caused by agricultural activities that were signified by the segmentation presence of agriculture, plastic shade and fallow. The class of shrubs contributed around 44% of total deforestation in 2018. The overall classification accuracy in such image attained 85.71% — however, around 50% of the image covered by the cloud. Therefore, the investigation of such activities was not calculated thoroughly.

In conclusion, a series of Landsat imagery can be used to distinguish the trend of forest change due to the availability of images collection throughout the year. On the other hand, OBIA and machine learning are suitable for detecting and mapping small area intensive crops.

DEDICATION

This research is dedicated to all my family's members, teachers, and friends.

ACKNOWLEDGEMENTS

LIST OF FIGURES

LIST OF TABLES

LIST OF EQUATIONS

LIST OF MODELS

LIST OF MAPS

LIST OF APPENDICES

LIST OF ACRONYMS

1. ACORN   Atmospheric Correction Now
2. AI   Artificial Intelligence
3. ALOS   Advanced Land Observing Satellite
4. AOI   Area of Interest
5. ASL   Above Sea Level
6. ATCOR   Atmospheric Correction
7. ATREM   Atmospheric Removal Program
8. AUD   Australian Dollar
9. BIL   Band Interleaved by Line
10. BIP   Band Interleaved by Pixel
11. BPS   Badan Pusat Statistik (Indonesian Central Bureau of Statistics)
12. BSQ   Band Sequential
13. DEM   Digital Elevation Model
14. DEMNAS   Digital Elevation Model Nasional
15. DN   Digital Number
16. ENVI   Environmental for Visualizing Images
17. ERDAS   Earth Resources Data Analysis System
18. FAO   Food Agriculture Organization
19. FFI   Flora Fauna International
20. FLASH   Fast Line-of-sight Atmospheric Analysis of Spectral Hypercubes
21. GCP   Ground Control Point
22. GCS   Geographic Coordinate System
23. GIS   Geographic Information system
24. GDP   Gross Domestic Product
25. ICDP   Integrated Conservation Development Project
26. IFSAR   Interferometric Synthetic Aperture Radar
27. IPBES   Intergovernmental Science-Policy Platform on Biodiversity
                  And Ecosystem Services
28. ISODATA   the Iterative Self-Organizing Technique
29. IUCN   International Union for Conservation of Nature

30.	JM	Jeffries Matusita
31.	JP2	Join Photographic 2
32.	KSNP	Kerinci Seblat National Park
33.	LAPAN	Lembaga Antariksa Nasional (National Institute of Aeronautics and Space)
34.	LiDAR	Light Detection and Ranging
35.	MLC	Maximum Likelihood Classifier
36.	MOA	Ministry of Agriculture
37.	MSS	Multi-Spectral Scanner
38.	OOC	Object-Oriented Classification
39.	PA	Protected Area
40.	PALSAR	Phased Array type L-band Synthetic Aperture Radar
41.	PCA	Principal Component Analysis
42.	RADAR	Radio Detection and Ranging
43.	RGB	Red Green Blue
44.	RS	Remote Sensing
45.	SAR	Synthetic Aperture Radar
46.	SPOT	Satellite Pour l'Observation de la Terre
47.	SVM	Support Vector Machine
48.	TOA	Top of Atmosphere
49.	UAV	Unmanned Aerial Vehicle
50.	UN	United Nations
51.	UNDP	United Nations Development Programme
52.	UNESCO	United Nations Educational, Scientific and Cultural Organization
53.	UTM	Universal Transverse Mercator
54.	WGS	World Geodetic System

I. INTRODUCTION

1.1 BACKGROUND

The Ministry of Agriculture Republic Indonesia (2017) states that in 2016, the total agricultural land in Indonesia had reached 36,764,318 hectares or 19.3% of the entire mainland of the country which has 190.5 million hectares of land. Agricultural land can be found in almost all parts of the Indonesian archipelago. In this state, the agriculture sector was accounted for 14.4% of the total GDP in 2014. This industry employed around 40.12 million people, equal to 35% of the entire Indonesian labour force (Ginting 2015). This percentage is predicted to continue growing compared to other sectors such as the mining, manufacturing and services industries. It is estimated that smallholder or small landowner productivity could result in USD50 billion in revenues by 2030, or around 7% of GDP per annum. Due to the agriculture sector playing such an essential role in growing the Indonesian economy, the country has applied some significant policies to increase agricultural development used for achieving self-sufficiency sufficient in food crops, as was started in the 1980s (Thomas et al. 2004). Such systems consist of escalating and extensive use of agricultural land, generating various types of agricultural products not only for local consumption but also for export. The most important agricultural products presented in Figure 1 is the primary concern for development by the government, such as rice, tropical spices, tea, coffee, cocoa, rubber, palm oil and cassava (Statistics, BPS 2017). Rice, for instance, is the leading staple food that is produced by farmers, the government and private
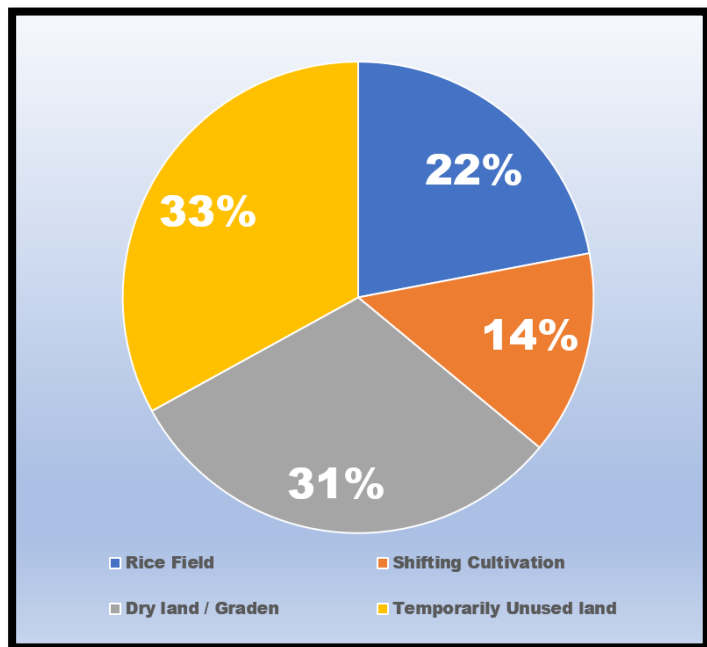
Figure 1: Percentage of Land Utilization in Indonesia 2016

Source: Indonesian's agriculture statistics 2017

companies to meet domestic consumptions needs. The main crops used for domestic consumption are maize, soybean, sweet potato, chilli, peanut, tomato and onion. Due

to land expansion in developing countries, in particular, Indonesia, the development of agricultural land continues to surge annually. Consequently, this has lead to a downward trend in the land available for tropical forests, which decreases every year.

Statistics, BPS (2017) states that land in Indonesia is mostly still covered by tropical rainforest areas at 125, 956,000 ha or 66.1 % of the entire mainland. Globally, Indonesian's tropical forests contribute around 2.3% of the whole world's forested land (FAO-UN 2016). However, tropical rain forests in Indonesia keeps decreasing in size due to human activities such as the expansion of agriculture and settlements. They also affirm that the total loss of forest in Indonesia was around 6.02 million hectares between the years 2000 and 2012, with such damage more massive than deforestation in Brazil over the same period. During that period, most of the tropical deforestation occurred in the western part of Indonesia. Tropical rainforest on Sumatran island has been cleared, and that land has been cultivated for agriculture and state-sponsored crops on a large scale in the globe (Holmes 2000).

Indonesia's deforestation could also be to the broader the environmental change occurring around the globe. Margono et al. (2014) argue that the increase of greenhouses gases such as carbon dioxide are the prime drivers for global warming. Moreover, the IPBES et al. (2019), report that around one million animal and plant species are on the brink of extinction due to human activity . This information was accumulated from the works of around 150 authors, from different countries. The Intergovernmental Science-Policy Platform conducted this work, a compilation on Biodiversity and Ecosystem Services (IPBES), under the supervision of the United Nations, UNESCO and the UNDP.

Currently, the remaining primary forest in Sumatra is only found in Protected Areas (PAs) such as Gunung Leuser, Kerinci Seblat and Bukit Barisan National Parks. Although such clusters of national parks are predominantly still covered by dense trees and vegetation, illegal deforestation activity can still be found adjacent to the human settlements, not only immediately by farms and estates crop areas, but most of the national parks are also encroached upon by the mining industry, gold and coal mining in particular.

Table 1 illustrates that deforestation in Indonesia progressed at a rate of almost 4 million hectares across various types of forests between 2016 and 2017.

Table 1: Deforestation in Indonesia 2016 - 2017

Type of Forest	Legal Status of Forest			Other Areas of Use (B) (Ha)	Total (A+B) (Ha)
	Permanent Forest (Ha)	Conversion Production Forest (Ha)	Total (A) (Ha)		
2	7	8	9	10	11
A. Primary Forest	27,841.10	2,204.70	30,045.80	14,230.10	44,275.90
Primary Dry land Forest	24,578.70	1,508.80	26,087.50	12,344.80	38,432.30
Primary Swamp Forest	1,847.70	636.2	2,483.90	1,175.00	3,658.80
Primary Mangrove Forest	1,414.70	59.7	1,474.40	710.4	2,184.80
B. Secondary Forest	240,437.60	38,116.70	278,554.20	167,188.30	445,742.50
Secondary Dry land Forest	187,916.80	30,270.00	218,186.80	142,575.80	360,762.60
Secondary Swamp Forest	44,208.60	8,048.30	52,256.90	22,274.70	74,531.50
Secondary Mangrove Forest	8,312.20	-202	8,110.60	2,337.80	10,448.30
C. Plantation Forest	-12,808	1,391	-11,417	1,409	-10,008
TOTAL	**255,470.80**	**41,712.40**	**297,183.20**	**182,827.50**	**480,010.80**

Source: STATISTICS (2017)

The available controls to reduce the rate of deforestation are indispensable and include forest patrols, law enforcement and mapping (Bruner et al. 2001). However, the cost to patrol a vast tropical forest is typically high, and most national parks in developing countries are too underfunded for such activities (James et al. 2001). Nevertheless, priority patrolling of the specific forests most threatened with high deforestation rates can still be a practical approach to reduce deforestation rates (Leader-Williams et al. 1988). Another technique to monitor deforestation is using Remote Sensing (RS), a strategy which is applied to recognise forest loss has already taken place (Green et al. 1990).

1.2 OVERVIEW OF INDONESIA

Indonesia is situated between two oceans, the Indian and Pacific Oceans along the equator between Asia and Australia, as depicted in Figure 2. This Southeast Asian country has about 17,000 islands, with five mains islands being Sumatra, Java, Borneo, Celebes and Papua. Indonesia has 34 provinces stretching out from the Indian Ocean in the west to the Pacific Ocean in the East region. Jakarta is the capital city of the state, which is the second-most populous urban area in the world. According to the 2010 census,

Image removed due to copyright restriction.

Figure 2: Map of Indonesia
https://www.countryreports.org/canada/Indonesia.htm

Indonesia's population had reached around 237.6 million people in that year, which means it has the fourth largest population in the world (Siagian et al. 2014). The country also has abundant natural resources including a diverse range of species of flora and fauna. The state also primarily produces a wide range of agricultural products such as rice, tea, coffee, rubber and palm oil. In terms of climate, Indonesia has two main seasons, dry and wet. The dry season runs from April to October and while the wet and season run from November through to March, with the average temperature reasonably constant throughout the year at around 28^0 Celsius.

1.3 STUDY AREA

The studied area revealed with a black rectangle in Figure 3 is part of Kerinci Seblat National Park (KSNP), which is home to the world's most abundant flowers (*Rafflesia sp)* and the most significant habitat for the critically endangered , Sumatran tiger *(Panthera tigris Sumatra).* The park
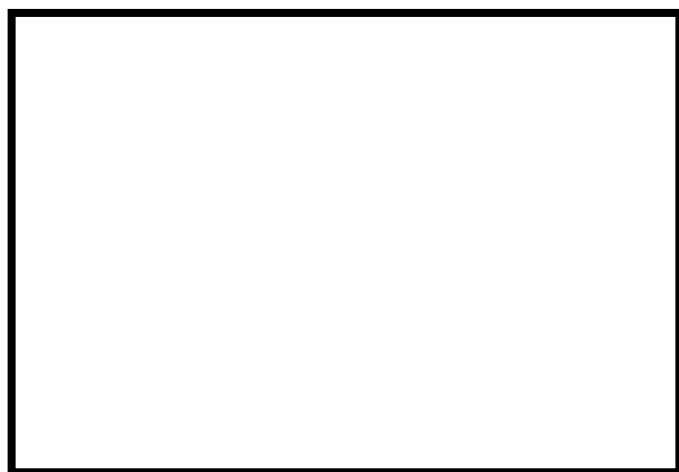
Figure 3: Kerinci Seblat National Park

that shows in Figure 3 is located in four provinces such as Jambi, Bengkulu, West and

South Sumatra province with 14 municipalities and two cities. The total area of the national park is at around 1,389,509.867 ha (KSNP, TS 2018). The park is 345 km long, extending along with the Barisan Mountain range that crosses Sumatra Island. In term of population, the number of people who live around the park is estimated to be around 41,067 people, who occupy around twenty-eight villages. Most of the inhabitant are farmers or agriculturists and workers of tea plantation estates (IBS 2013).

In terms of official status, the research conducted, and findings contained herein pertain specially Kerinci regency, which has 16 sub-districts, stretching from the peak of Mount Kerinci in the north to Lake Kerinci in the south. The total area of the Regency is around 332,000 hectares. The land of the municipal is not only used for human settlement but also used for wildlife conservation and reserves such as Kerinci Seblat National Park (KSNP).

One of the subdistricts of Kerinci Regency used as a study area is Kayu Aro located in the northernmost point of Kerinci. According to Sihotang (2018), Kayu Aro sub-district shown in Figure 4 initially is a dense tropical rain forest and then invaded and opened by a private Dutch company (Namlodse Venotchaaf Vereniging Amsterdam, NV.HVA) to grow tea plantation and other crops started from 1925 to 1928. The area of tea plantation is around 2,500 hectares that currently mostly used to produce tea plantation and coffee as the primary commodity. More than half of the study area is part of Kerinci Seblat National Park (KSNP) that well known as the second-largest protected area in Indonesia.

Figure 4: Kayu aro Landscape
https://www.topsimages.com/images/gunung-kerinci-f4.html

In term of the research area, the total area of the project is around 33,872 hectares demonstrated in MAP 1 that includes national park, settlement, and Kerinci mountain and tea plantation states.
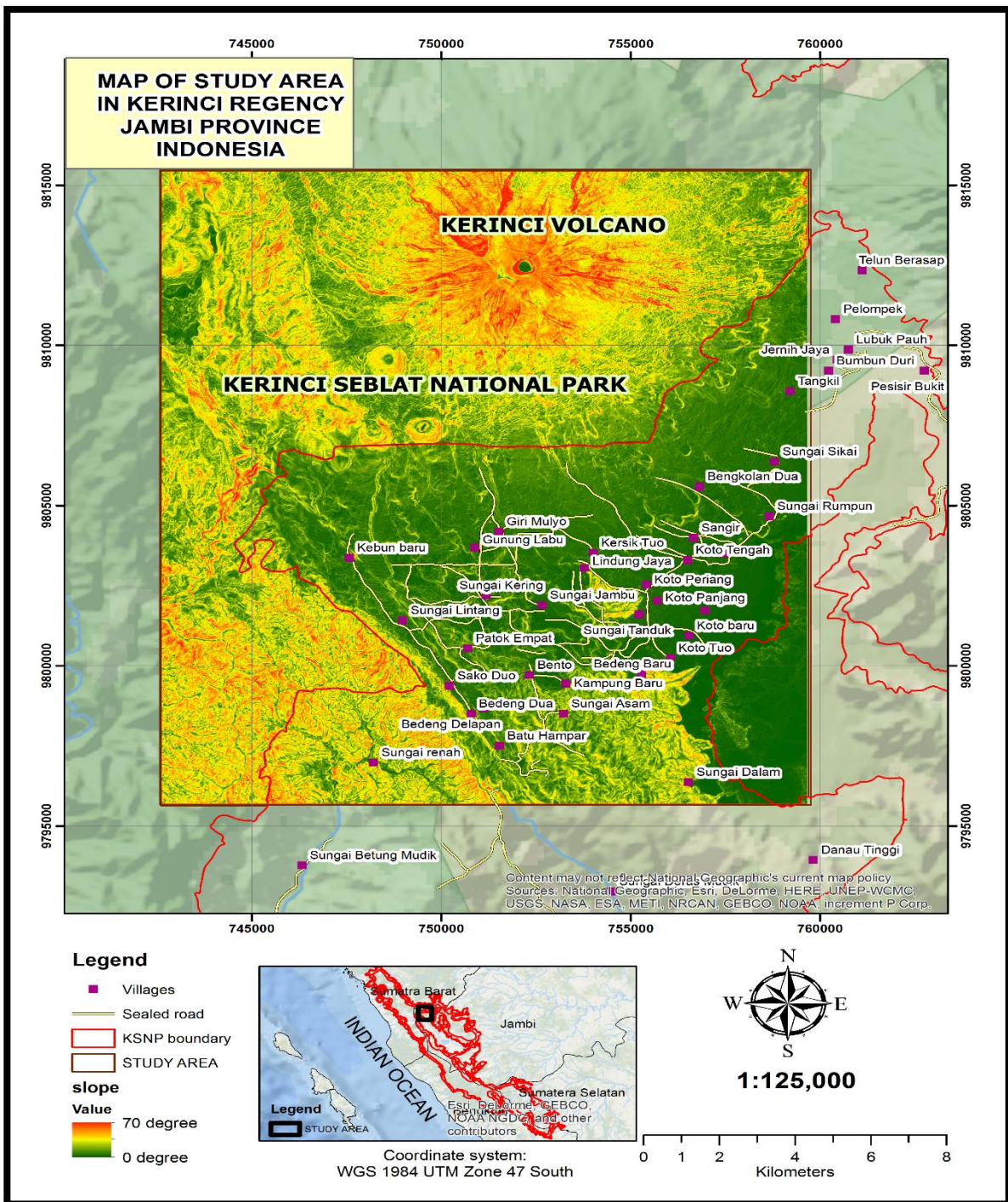
MAP 1: Study Area

1.3.1 Topography

Steep valleys dominate most of Kerinci Seblat National Park topography, and this is especially true within the boundaries of the studied area with slopes as steep as ($\geq$ 60%) and the elevation varying from 1,500 to 3,805 metres above sea level. The peak of geographical is the tallest volcano in Indonesia, Mount Kerinci. The lowest site is at an altitude of 1,500 metres, and this land is mostly used for agriculture, plantations and settlements. The Piedmont of the mountain is around 2,000 metres above sea level, with this land still being used for agriculture.

1.3.2 Climate

In Kerinci Regency, the average temperature varies between 22^0 Celsius in the wet season to 30^0 Celsius in the dry season. While the average precipitation is approximately 150 280 mm^3. However, in the study area of Kayu Aro , the average temperature ranges from 12^0 Celsius to 24^0 Celsius (Statistics, BPS 2017).

1.3.3 Economy and Agriculture

Gross Domestic Product (GDP) of Kerinci is mostly attributed to the agriculture, forestry and fishery sectors. According to Statistics, BPS (2017), Kerinci's GDP reached 9015.4 billion rupiahs or around 9 billion AUD, of which more than 50% is generated by the sectors at 4,708 billion rupiahs or 4.6 billion AUD.   The remaining economic drivers for this regency consist of transportation (7.22% of GDP), communication (10.18%), Social work (7.22%), and manufacturing 2.32 %.

1.4 THE AIM OF THE STUDY

The research aims to provide new information on crop activities throughout the boundary of Kerinci Seblat National Park, with this new information   being available to Park Management in its efforts to overcome unlawful farming activities. The study also aims to reveal the breach of the law taking place within this national park; being farming activities occurred around the adjacent to settlements. The outcome of remote sensing analysis includes the classification of SPOT 6 images into a different type of classification such as cropping area, residential area, shed, barren land, and water body. The initial research question of the study is:

Has there been a change in the cropped areas within Kerinci Seblat National Park in the last 20 years (1998, 2008, and 2018)?

What level of classification hierarchy can be achieved using Object-Oriented Classification (OOC), through machine learning, to understand the structure of cropping activity within the Kerinci Seblat National Park?

1.5   THESIS STRUCTURE

This thesis consists of six chapters. Chapter one describes some aspects that relate to the research. The background of the study provides information about the expansion of agriculture and its influence on deforestation. This chapter also offers general information about Indonesia, including conservation areas, topography, climate and economy of the geographical area studied. Chapter two explores relevant literature that relates to deforestation, starting from global to a local perspective. This section also discusses some approaches used by practitioners and scientists to map and extract information from satellite imagery. The third explains the methodology used to elaborate on the primary data retrieved, the software, and the processing methods used to extrapolate information from satellite images. The resulting findings are provided in chapter four different formats, including descriptions, tables, maps, charts, and graphs. The key or most significant findings of the projects are thoroughly analysed in chapter five. Lastly, chapter six provides recommendations to be considered for further research within the context of a comparable environment. The central conclusion also offered in this chapter to presents a summary of the first results of this research.

II. LITERATURE REVIEW

The literature review in this chapter commences with a background of deforestation and the general drivers of such land transformation both at the global and local levels. It then proceeds to evaluate relevant literature on deforestation, and geospatial techniques applied for mapping deforestation, with a focus on mapping changes in land coverage in the national park and its surrounding spaces.

2.1 GLOBAL DEFORESTATION

Keenan et al. (2015) contended that on a worldwide scale, the total area of forested land covers around thirty per cent (30%) of the Earth's surface. Of the 128 countries reported on, the geographical surface area is estimated to be about 40 million km^2 that can be
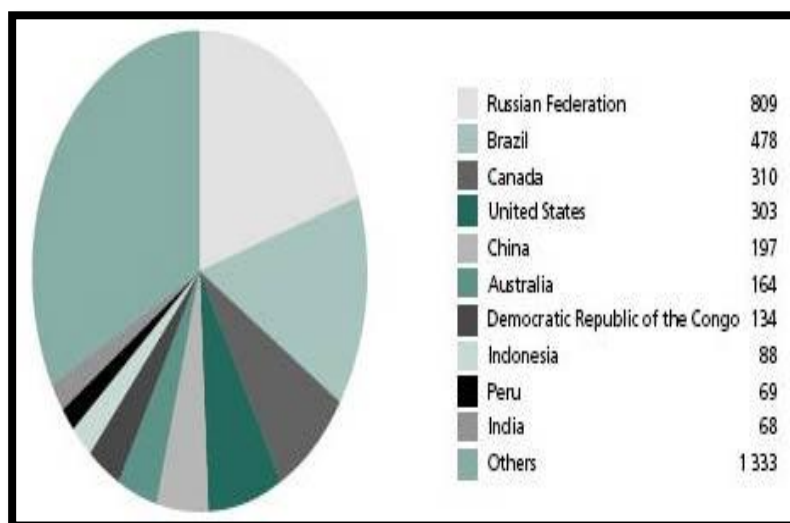
Figure 5: Distribution of forest land by countries
Source: https://www.greenfacts.org

found in the almost main continent in the world such as Europe, Africa, North and South America, Asia and Australia (FAO 2005). It is around 38 % of the world's forest-covered land can be found in the North, Central and South America, especially in Canada, Brazil and Bolivia, as presented in Figure 5. Forest area in Europe, including Russia federation cover approximately 25% of the global forest. Such land in Asia and Africa is around 14% and 16% respectively (FAO 2005). However, the existence of forest area can be affected caused by various factors such as forest fire, disease, pest and human activities such as deforestation. FAO-UN (2016) states that forest loss or deforestation in the tropical areas was at a rate of 6 million hectares over the five years 2010 and 2015.

According to Schuck et al. (2002), deforestation is the act of changing the land's cover by cutting head tree layer to under ten per cent of the original vegetation, which

destructively affects the site. The effect of deforestation, both directly and indirectly, causes the loss of endangered species (Lambin et al. 1999), as well as the decline in the quality of the human environment necessary to meet daily human needs for shelter, freshwater, food and clothing(Kauppi et al. 2006). The other essential impact of deforestation results in enlarged greenhouse gas emissions as the prime driver of global warming (Margono et al. 2014). The pattern of forest loss varies depending on the needs and policies of each country. For example, the rate of forest loss is decreasing in developed countries while in developing countries located in the tropics and subtropics, forest loss or deforestation is still rife (Pendrill, Florence; et al. 2019). Bradford (2015) argues that the most concentrated forest loss ensues in the tropical rainforests such as those in Indonesia in Asia, Brazil, in South America, and the Congo in Africa. The transformation of once-forested areas in such countries can encompass the conversion of forest to building construction, mining, ranches, and agriculture farming (Bradford 2015). Gibbs et al. (2010) argue that the main drivers of deforestation were caused mainly by agricultural expansion. However, Pendrill, Florence et al. (2019) reveal that deforestation in such equatorial countries is associated with three leading causes, namely the development of agriculture, pastures and tree plantations driven by international trade. On the global scale, it can be concluded that deforestation occurs in every part of the hemisphere, but the most significant decreases of forested land can be found mostly in developing countries where rainforests are located.

2.2 INDONESIAN DEFORESTATION

Although having the fourth largest population in the globe, Indonesia is also the most heavily drain-forested land on Earth after a forest in South America (FFI 2018). However, the forest loss continues to undergo a decreasing trend mainly occurred in two islands of, Sumatra and Kalimantan (Borneo) island shown in Figure 6. Margono et al. (2014) find that the loss of forest on the two islands was at 17.63 % and 7.92 % respectively over the period of the years 2000 to 2012. Various islands such as Sulawesi, Java, Bali, and Papua experienced a loss of less than 1% of primary forest over the same periods. Overall, the total loss of forest in Indonesia was around 6.02

million hectares and escalated on average by 47,600 hectares per year between 2000 and 2012.

Rudel et al. (2009) contend that agribusiness companies are the prime causes of deforestation, followed by small farming and illegal logging. Traditional agriculture
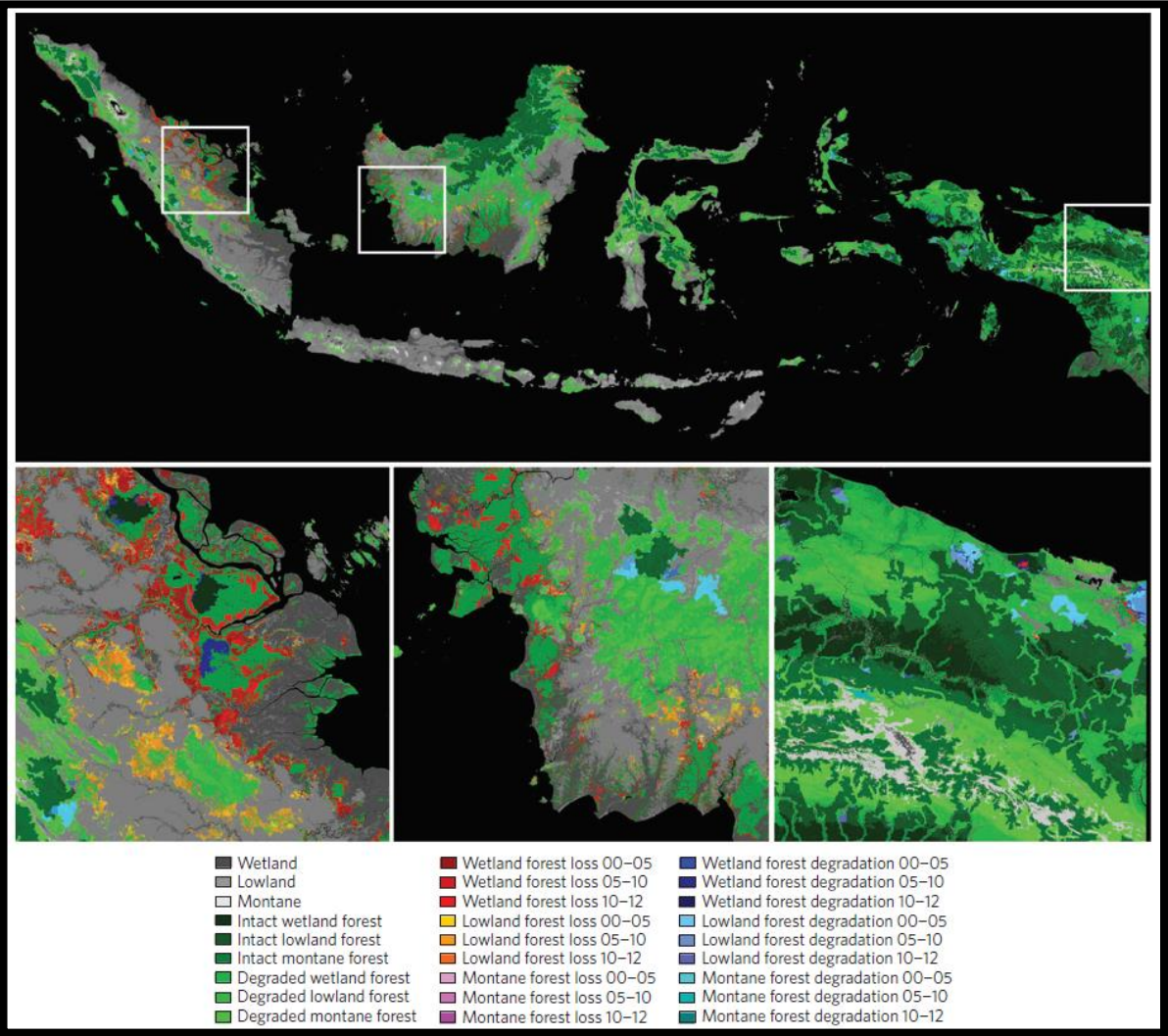
Figure 6: Deforestation in Indonesia

contributes to less than 20% of the deforestation (Lee et al. 2014). Nevertheless, smallholder farming that contributes to deforestation is more problematic to control (Kubitza, Krishna, Alamsyah, et al. 2018). This is because it is difficult to control the illegal activities of individuals, as opposed to organisations, conversely, although large plantation companies contribute significantly more toward forest loss in Indonesia, it is controlled mainly because it operates based on government permission and concessions.

In terms of farmers' lands, Kubitza, Krishna, Urban, et al. (2018) reveals that there are three main problems faced by the government of Indonesia , with these being title deeds, boundaries, and the ambiguous ownership structure of the area. Krishna et al. (2017) dispute the legal status of most farmers' properties as having titles formally, for the cost of obtaining title deeds is relatively high for peasant farmers. Such problems can trigger the ambiguous ownership of the land, and the boundaries of the area with state and private companies are not always clear-cut. Deforestation will prospectively upsurge when farmers have no titles, and it triggers them to penetrate and expand another forest around their land (Kubitza, Krishna, Urban, et al. 2018). To sum up, in the Indonesian context, deforestation can be caused by various factors. The concession to private and large companies that were issued by the government is the primary triggers of forest loss, but it can be handled by changing the regulation and policy. The most challenging is the expansion of forest land that was cultivated by farmers with no title.

2.3   DEFORESTATION IN KERINCI SEBLAT NATIONAL PARK

Kerinci Seblat National Park (KSNP) has been facing many challenges and problems since its establishment in the late 1980s such as illegal logging, mining, poaching, and illegal encroachment. Park officials mainly viewed these activities as opportunistic acts commonly perpetrated by villagers living around the park. According to Bettinger (2014), the number of people who live throughout the boundary of the national park is approximated at 1.7 million inhabitants with unevenly distributed. It is projected that around 70% of the people working in agricultural sectors and approximately 80% of the park boundaries is neighbouring to settlements and farming area. Yusri (2016) states that unlawful encroachment activities within National Park widely caused by the expansion of agriculture and assumed as the primary driver of land-use change in the park. In the local perspective, the drivers of deforestation mostly caused by agricultural expansion and the increasing of population. Bettinger (2014) finds that deforestation is triggered by the growth of inhabitants who live around the park. The linkage between the increases of the population is correlated with deforestation in the national park. However, such a tie was not detrimental when population density is still low. Because of the increase of population and limited

farming land, people expand their farm by cultivating the forest used to meet their daily needs mainly to build their traditional houses. Interestingly, the trigger of deforestation is also contributed by the corruption behaviour of district elites, which supports farmers to cultivate the parking area. Bettinger (2014) also finds that the entanglement of district elites also contributes to the increase of deforestation by inviting many sharecroppers from the outside of district including some local farmers that are working as the producers of forest and agricultural products.

2.4 MAPPING DEFORESTATION IN KSNP

In term of measuring and mapping degraded forest in the national park, the park management has been quantifying such illegal activities by using various methods such as field surveys, direct interview and forest patrols. However, such a conventional manner is not efficient, financial constraint, and time-consuming to monitor and patrols the vast and long unshaped boundary of the park that extends approximately 2,600 kilometres. Therefore, it requires a breakthrough to apply other approaches that can be used to map all vast area of the national park.

Remote sensing and GIS technology can be an alternative solution to portray illegal activities within the vast national park. Numerous studies in detecting cropping area and analysing driving factors in the tropical region have been conducted to predict the variation of cropping using remote sensing and GIS. The research related to deforestation and its variable support such illegal activities also have been performed in the national park. According to Bettinger (2014), ICDP project held in Kerinci Seblat National Park supported by World Bank project determined that forest lost by classifying Landsat imagery between 1995 and 2001 is at 19,199 hectares. Linkie, Smith, Leader-Williams, et al. (2004) applied supervised classification approach of Landsat MSS satellite with two dates, 1985 and 1992. The total forest loss between such two periods is 13.4 km^2. The main result of classification is the forest, rice fields, water, logging roads and farming fields. In Linkie, Smith, Leader-Williams, et al. (2004) study, using a binary logistic regression model as a tool in analysis, it was predicted that in 1999, the risk of deforestation was at 0.630 based on two dates imagery from 1985 to 1992.

Furthermore, in 2017, Kerinci Seblat National Park (KSNP) management also classified the forest using Landsat imagery 2016 used to determine the zone of forest restoration and rehabilitation. KSNP (2018) states that forest loss in the national park is at 1087.6 km^2 in 2017. Such damage was obtained through via visual interpretation technique. In conclusion, by using a different approach of classification, the trend of deforestation in Kerinci Seblat National Park continues to increase over time by comparing the dates between 1985 and 2017.

2.5 THE APPLICATION OF REMOTE SENSING

According to Jensen, J (1996), Remote sensing (RS) is the science to obtain and interpret information from a distance without physical interaction with the object using particular platform that includes airborne and space borne. The role of remote sensing provides biophysical information that can be utilized in various applications. In bio-geographical studies, Millington et al. (2011) state that remote sensing is used to map and monitor land cover to obtain specific information on habitat and species. It is also used to support conservation and biodiversity evaluation and robust and cost-effective tools for evaluating the spatial and temporal dynamic land cover/ land-use change (Lambin et al. 2003). Moreover, remote sensing using space borne platform has enormous advantages in revealing the information in the remote and inaccessible area and also obtaining information with large geographical areas (Jensen, J 1996). Due to its reliability to capture the vast region, currently, such platform is a one of commonly paramount tool used to obtain Earth surface information in supporting various purposes such as military, research, agriculture, and other applications.

The quality of information which is generated by remote sensing technology varies depending on the spatial, spectral, temporal, and radiometric resolution. Presently, Remote sensing technology has various type of improvement such as high spatial resolution which can capture Earth surface information in submeter (Oza et al. 2008). Satellite imagery with high spatial resolution also has commercially provided the data for public used to observe and study the information of the surface. For example, Quick Bird satellite imagery with 60 cm resolution (Panchromatic) is accessible for finding agriculture and civilian (Liaghat et al. 2010). IKONOS imagery can be applied to extract information of the structure plant attributes that include the volume of plant, diameter,

stems per area, the plant height (Gebreslasie et al. 2011). RADAR and LiDAR can also provide information and map structure type of vegetation (Levick et al. 2008).

The application of remote sensing can be applied in various studies such as agriculture, forest, marine, urban area, etc. In agriculture study, Liaghat et al. (2010) argue that RS technology is a cost-effective way to interpret physical parameters such as crop (broccoli, corn, paddy rice, apple and other types of agriculture products), soil moisture, and nutrient contents. Such technology is also possible to combine with precision crop management structure (Waheed et al. 2006). RS application even able to assess and crop condition a harvest forecasting, detecting crops pest, diseases, water supply, weather supply information and livestock surveys.

Remote sensing has been applied in many countries to map land cover and vegetation at a different stage from local to the national level (Rosenqvist et al. 2003). By considering and applying temporal resolution of the specific sensor, RS also can be used to map the forest change over time (Hansen et al. 2008). In deforestation study, Landsat imagery is an example of a sensor that has been widely utilised to determine deforestation in the tropical region (Lambin, EFJGe et al. 1999).

In conclusion, remote sensing technology application in mapping deforestation cropping has an essential role in providing information for decision-maker on a different level of policy (Liaghat et al. 2010).

2.6 MAPPING CROPPING USING REMOTE SENSING

Various approaches have been applied to attain cropping system classification utilising remotely sensed imagery. In general, the classification method can be divided into two methods, spectral-based classification and object-based classification (OOC).

2.6.1 Feature Extraction using Spectral -based Classification

Spectral-based interpretation applies the spectral information of each pixel to distinguish the object on the Earth's surface using pattern recognition approaches (Zhang 2013). This type of analysis is a standard method that applies spectral as a leading information and ignoring the other information such as spatial and a group of the pixel that is required to be contemplated as an object (Myint et al. 2011). The standard algorithms used in classification based on spectral are supervised

interpretation using training samples and unsupervised classification with no training samples.

Supervised classification is a simple application with widely used in the classification of the image, and such an approach is easy to recognise and interpret the objects in a particular image (Radoux et al. 2014). The pattern of clustering pixel in classification process can be analysed using some spectral similarity method such as Spectral Euclidian Distance (SED), City Block/ Interpoint Distance, Sum Squared Error (SSE), Jeffries Matusita (JM) distance, and Mahalanobis Distance. These approaches mostly used to distinguish the distribution and spectral distance between a pixel to other pixels and also between a pixel and the mean of clustering pixels. In term of the algorithm of classification, in parametric supervised approach, the most common method used in the classification of the image is Maximum Likelihood Classifier (MLC) that is applied to assign each pixel with the highest probability of being a particular class. MLC applies Bayes decision rule in predicting the probability of class membership via the utilisation of training data. The Decision in determining the class is based on the highest probability, which ranges from 0 to 1. The technique of such classification is not only MLC, but the other approaches also had been developed such as Parallelepiped classifier, Mahalanobis Distance Classifier, Support Vector Machine, Neural Network classifier, Fisher classification, Minimum Distance-to-Means Classifier and multinomial logistic regression (Borra et al. 2019).

According to Vogelmann et al. (2012), unsupervised Classification is also part of the spectral-based method by which the grouping of the pixel into a particular cluster class is performed by computer/software so that the human error can be minimalized. This method is also not applying training samples in classification. Thus, the process is easy and fast to perform. Moreover, the prior knowledge of the image is not required; the analyst's work presents after the classification process is done. ISODATA method is the prominent approach used in an unsupervised classification approach (Dhodhi et al. 1999). The minimum Euclidian distance and the spectral mean of the pixel is the main parameter to classify and group the pixel into a specific class. The iteration is performed to recalculate the mean and reclassify pixel to generate the new mean. The splitting, merging, grouping and deleting process is performed depends on

the value of determined threshold parameters. The new cluster of pixels combine with the nearest class except the distance and variability is distinctive. The unclassified level can be formed if the pixels do not meet the determined criteria. According to Jensen, J (1996), the other parameters required in this approach are a minimum distance between clusters, the maximum number of pixels in the specific group, and maximum standard deviation. The application of the ISODATA method is appropriate to classify a homogenous landscape in which the number of the land cover class is limited, and it is also able to provide the information of remote area with no sample training data. The process of classification using the unsupervised method is often used in before delivering the general cluster of the image, and then such an approach is combined with supervised classification to obtain the excellent result of classification. The other spectral-based classification methods include Bayesian network, sub-pixel and fuzzy classification.

2.6.2 Feature Extraction using Object-based Classification (OOC)

According to Blaschke et al. (2010), Object-based classification (OOC) approach is appropriately used to classify the image with high spatial resolution. OOC method not only relies on spectral information, but the OOC also applies other elements such as texture, colour, size and shape. Such methods attempt to imitate the ability of human in interpreting the object through visual interpretation. OOC method classifies the pixels based on the spatial relationship with neighbouring pixels and image segmentation by which such an image is the main component in classification using objects. Segmentation is a procedure to group an image into segments that have a spectral similarity. In general, the segmentation algorithm can be separated into fourth types: Point-based, region-based, edge-based, and the combination of all the classes (Schiewe et al. 2002). It is also a primary function that isolated an image into separated regions based on parameters specified (Myint et al. 2011). In term of application, segmentation is also appropriate in classifying high spatial panchromatic images over as urban and agriculture fields (Mueller et al. 2004).

Object-based classification (OOC) can be performed through machine learning. In remote sensing machine learning can be divided into two categories: traditional and new trend classification (Camps-Valls 2009). The traditional machine learning

classification includes supervised, unsupervised, and temporal classification. The new type of machine learning classification includes manifold, semi-supervised, transfer, active and structure learning. According to Friedl et al. (1999), the classification of land cover can obtain high accuracy by operating a decision tree approach as a base of the classifier. This type of classification as known as the non-parametric algorithm that it does not mean that such an algorithm has no parameters. It requires many parameters to define the amount of data. The algorithm such as K-nearest neighbour and decision trees are counted as a non-parametric algorithm since the number of parameters upsurges with the extent of the training data. This algorithm does not create any hypotheses on the underlying data distribution (non-statistical approach). The other tree-based classifier includes Initialize CART, Initialize Neighbours, Initialize Naïve Bayes, Initialize SVM and Initialize Random Forest (RF).

One type of decision trees classifier used in classification agriculture and urban areas is the RF algorithm that was proposed by Breiman (1999). It selects the features by chance and generating a classifier with a bootstrapped sample of training data. By comparing with other machine learning, Novack et al. (2011) argued that the RF approach is more appropriate and accurate in classifying urban area with an overall accuracy of 95%. RF is one of the flexible machine learning and easy to be performed (Blaschke et al. 2010). However, Pal (2005) argued that RF is comparable to Support Vector Machine (SVM) in term of classification the landscape using Landsat Enhanced Thematic Mapper Plus (TEM+). Nevertheless, RF is appropriate to be used due to its simplicity and dual functionality for image classification and regression analysis (Brodský et al. 2006).

Ok et al. (2012) examine two types of classification, Random Forest (RF) as parcel-based method and Maximum Likelihood Classifier (MLC) as a pixel-based method in classifying agricultural crop using SPOT 5 imagery. The study found that the overall accuracy of RF is better than MLC, where the overall accuracy is 85.89% or around 8% better than using unsupervised classification, MLC. Therefore, in this research, the random forest was used as the primary classifier to map the distribution of agriculture and cropping segmentation.

2.7 SUMMARY

In conclusion, both Object-Oriented Classification (OOC) and spectral-based classification are appropriately applied in the classification of the image with low spatial resolution (Mitri et al. 2004)However, in analysing high spatial resolution, SPOT-6 images, for instance, OOC is appropriate to be applied to get a better classification than spectrally based approaches. In answering the first research question where classification focus on determining two modest classes, forest and non-forest, spectral-based classification is recommended to utilise due to its simplicity. In solving the second research question that relates to higher spatial resolution imagery, object-oriented classification is endorsed to be utilised in determining segmentation of agricultural land and other the complexity of segments (Geneletti et al. 2003). Therefore, both approaches, either Object or Spectral-based classification, were performed in this project to determining forest/non-forest and cropping segmentation.

III. METHODS AND MATERIALS

This study applies two types of classifiers used to extract information from remotely sensed images. These are Spectral-based Classification using Maximum Likelihood as an algorithm and Object-Oriented Classification using the Random Forest as the main algorithm. The processing of both Landsat and SPOT-6 images is divided into three-part stages with these being, Pre-processing, processing, and Post-processing. The flowchart in Figure 7 below demonstrates the processing stages, which is describing in as follows:
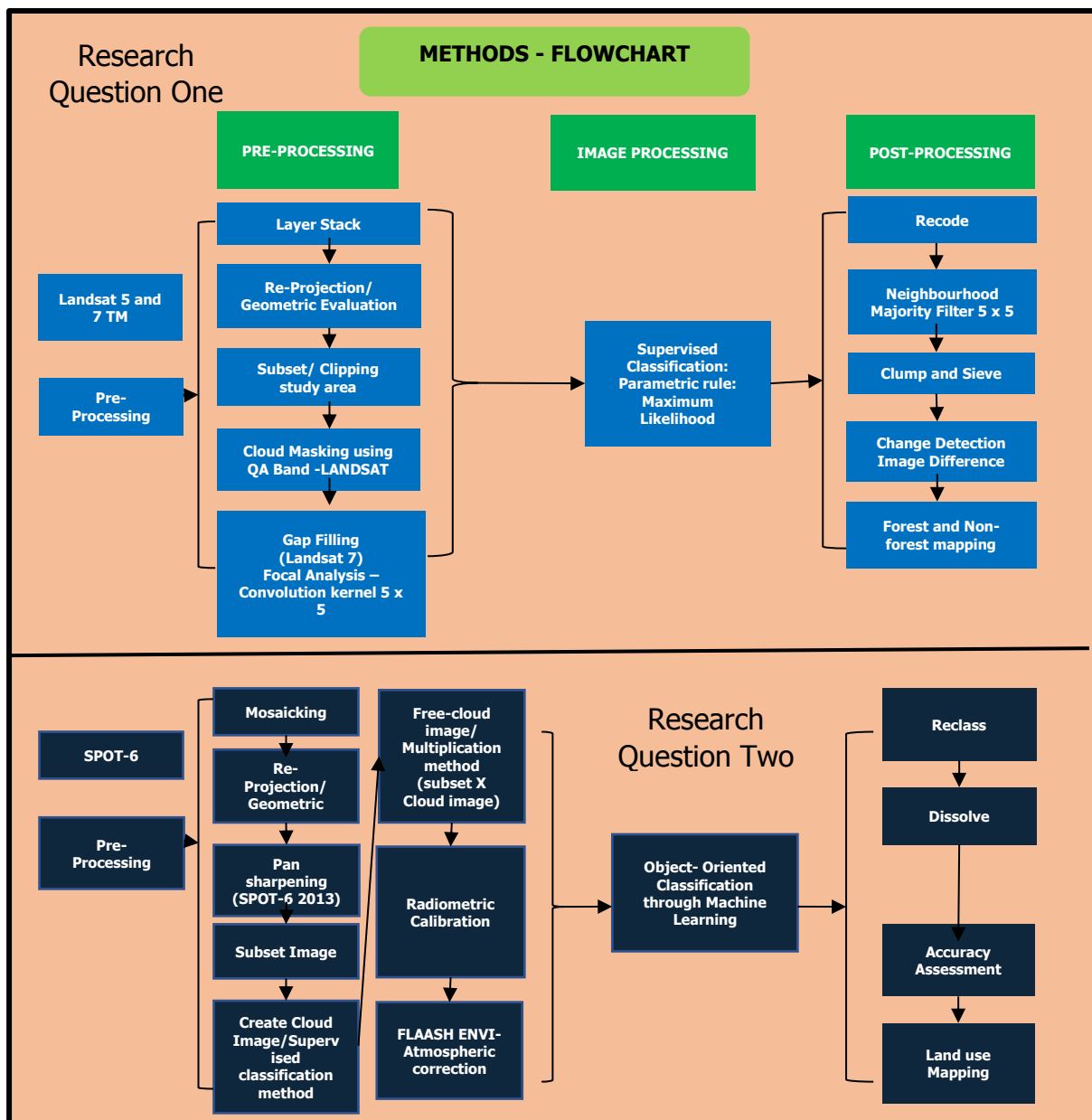
Figure 7: Flowchart /methods of research

The processing of Landsat images was performed using a Spectral-based Classification approach, while SPOT-6 images were processed using Object-oriented Classification (OOC). This latter approach was performed via machine learning, which was run in Spatial Model Editor, a tool within ERDAS IMAGINE software. There are three input files in this process, which are Training, Segmentation Vector Data, and
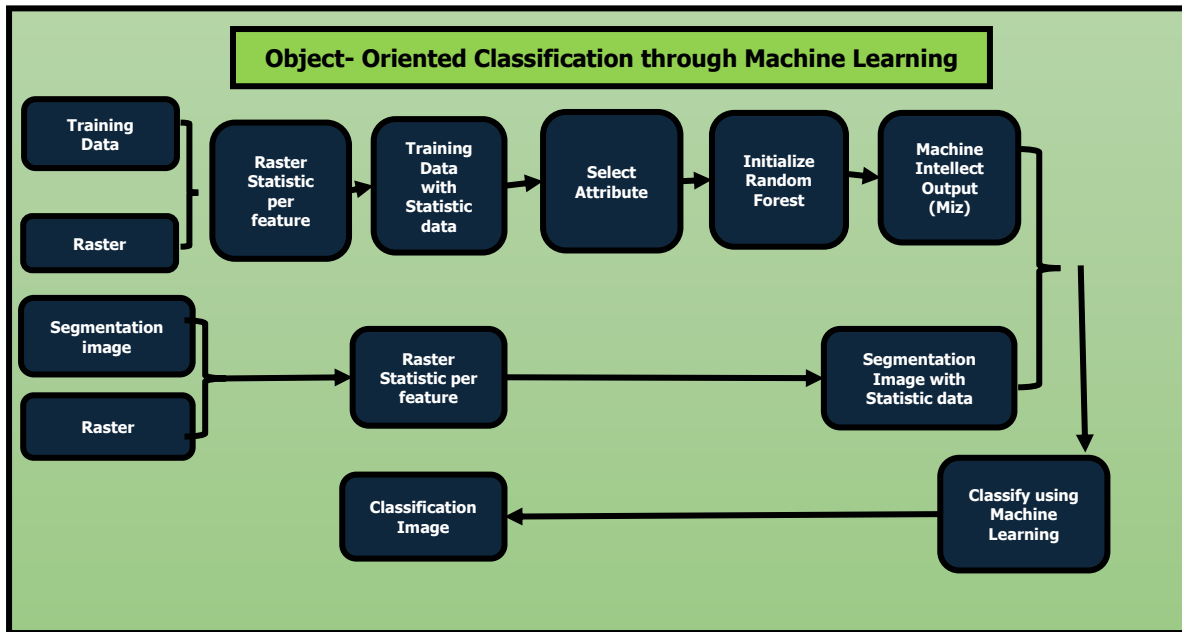
Figure 8: Object-Oriented Classification through Machine Learning

surface reflectance stored in raster format. Figure 8 shows the processing stages in generating a classification image through machine learning. It can be seen that there are three inputs in this process. Information such as mean and standard deviation of the vector data (training and segmentation) is derived from raster input by using statistics operator provided by ERDAS IMAGINE.

3.1 PRIMARY DATA (LANDSAT AND SPOT-6)

According to Homer et al. (2004), Landsat provides a long record of historical data with a no-cost policy that is widely used for various applications such as detecting changes including change in land cover. Therefore, to obtain continuity of data availability for the twenty years period, Landsat images are considered as primary analysis material to detect the change in Kerinci Mountain. The Landsat images used in this study consist of two dates of imagery from Landsat-5 Thematic Mapper (1998, 2008) and one date of imagery from Landsat-7 Enhanced Thematic Mapper Plus (2018). LANDSAT images were derived from the United States Geological Survey (https://earthexplorer.usgs.gov/.

Landsat 5 TM and 7 ETM+ cover seven spectral bands with a spatial resolution of 30 meters. Landsat 7 ETM+ also has one panchromatic with a spatial resolution of 15 metres shown in Table 2 and Table 3, respectively. Operational imaging of Landsat 5 begun from 1 March 1984 to 30 November 2011 and Landsat 7 launched on 15 April 1999 where such satellite is still operating until the present day. The Landsat imagery used in this study is Landsat image level 2 ordered via the web portal of the United States Geological Survey (USGS). The Level 2 terrain product data was already radiometrically and geometrically corrected with coordinates system called World Geodetic System 84 (WGS 84). The USGS provided Level 2 Landsat data formed on Surface Reflectance images that were already processed operating Landsat Ecosystem Disturbance Adaptive System (LEDAPS).

Table 2: The Outline of Landsat-5 Bands with Wavelength and Spatial Resolution

	Bands	Wavelength (nanometres)			Resolution (Metres)
LANDSAT 5 Thematic Mapper ™	Band 1 - Blue	450	-	520	30
	Band 2 - Green	520	-	600	30
	Band 3 - Red	630	-	690	30
	Band 4 - Near Infrared	770	-	900	30
	Band 5 - Short-wave Infrared	1550	-	1750	30
	Band 6 - Thermal Infrared	10400	-	12500	120* (30)
	Band 7 - Short-wave Infrared	2090	-	2350	30

* Band 6 was acquired at the 120-meter spatial resolution, it was resampled to 30-meter pixels.

Table 3: The Outline of Landsat-7 Bands with Wavelength and Spatial Resolution

	Bands	Wavelength (nanometres)			Resolution (Metres)
LANDSAT 7 Thematic Mapper Plus (ETM+)	Band 1 - Blue	450	-	520	30
	Band 2 - Green	520	-	600	30
	Band 3 - Red	630	-	690	30
	Band 4 - Near Infrared	770	-	900	30
	Band 5 - Short-wave Infrared	1550	-	1750	30
	Band 6 - Thermal Infrared	10400	-	12500	60* (30)
	Band 7 - Short-wave Infrared	2090	-	2350	30
	Band 8 - Panchromatic	520	-	900	15

* Band 6 was acquired at the 60-meter spatial resolution, it was resampled to 30-meter pixels.

To obtain data about crop activities within the studied area, two dates of SPOT-6 images were applied to extract information of the crops. Such images were acquired from LAPAN (Lembaga Penerbangan dan Antariksa Nasional - National Institute of Aeronautics and Space – Indonesia) and obtained with limited access through http://bpdjn-catalog.lapan.go.id/catalog/index.php.

Spectra-based Specification of SPOT-6 images consists of four band ranges (multispectral at 6 metres spatial resolution) ranging from 455 nanometres at the visible band to 890 nanometres in the infrared channel. Panchromatic images also provide a range from blue to the infrared red band with a high spatial resolution (1.5 metres spatial resolution). The details of the spectral specification band shown in Table 4:

Table 4: Spot-6 bands with wavelength and spatial resolution

Bands	Wavelength (μm)	Spatial resolution (m)
Band 0 – Visible Blue	0.455 - 0.525	6
Band 1 – Visible Green	0.530 - 0.590	6
Band 2 – Visible Red	0.625 - 0.695	6
Band 3 - Near Infrared (NIR)	0.760 - 0.890	6
Band PAN – Panchromatic	0.4.50 – 0.745	1.50

The SPOT of 2013 was supplied in the orthorectification format, which is geometrically corrected. Such an image is stored using projection UTM Zone 47 South, Datum of WGS 1984, and metres as the unit of the image. However, the SPOT image of 2018 is provided with no projection and datum. Therefore, for further analysis, such the image was evaluated geometrically using Google Earth images used as the source of projection reference. Such data also was converted to UTM zone 47 South with WGS 84 datum used to obtain a similar projection with 2013 image. The type of data is stored in JP2 compressed bitmap extensions and rescaled into unsigned 12-bit, which range from 0 to 4096 (2^{12}).

3.2 SECONDARY DATA

Secondary data is used to support further analysis. The information of a road, settlement, waterbody, regency and province boundary stored in shapefile extension were acquired from manual digitising held by Kerinci Seblat National Park in the year 2000. Different social information such as population, agriculture products were derived from field survey held by the bureau statistic of Indonesia conducted in 2017 and 2018. This data also includes a Digital Elevation Model (DEM) obtained from DEMNAS (http://tides.big.go.id/DEMNAS/). The application of DEM is used to distinguish and classify the different type of deforestation by elevation zones. Such data are compiled from various sources such as IFSAR, TERRASAR-X, and ALOS PALSAR. The spatial resolution of the data is 0.27-arcsecond or 8.1 metres.

3.3 SOFTWARE

A range of software was used to process the image data for this research. These tools were as follows:

a. Earth Resources Data Analysis System (ERDAS) Imagine 2018 (64 bit)

Most of the processing of classifications of forests and the non-forested area was performed using this software, which included Pre-processing, Processing and Post-processing. The processing of SPOT-6 imagery was also conducted using this software, in particular, determining the agricultural segmentation. The classification of the image with a random forest as the algorithm was performed using machine learning that runs through spatial model editor attached in the software.

b. Environment for Visualizing Images (ENVI 64 bit and ENVI Classic)

The software mostly used to perform Pre-processing of SPOT-6 satellite imagery such as reprojecting, pan sharpening, subset image, radiometric calibration, and atmospheric correction (FLAASH). The output of such a process generates surface images that can be used to extract information throughout the images.

c. ArcGIS Version 10.6

The output of Objected-Oriented Classification generated through machine learning is a classified image stored in vector format. ArcGIS/ ArcMap software was applied to produce training samples vector and image segmentation trough

Full Lambda Schedule (FLS) segmentation as one of the processing tools in ERDAS Imagine software.

d. Google Earth Pro

The primary purposes of utilisation of Google Earth are used to evaluate the geometric of the image, and in the study, such software was applied mostly for the evaluation of geometric and accuracy assessment.

3.4   LANDSAT - IMAGE PRE-PROCESSING

3.4.1 Layer Stack

The original image of Landsat imagery was obtained from the USGS website, and it was provided in a single separating band. The fusion of the separated band required to obtain multispectral images. Layer stack tool is used to stack multiple bands into a single multi-band image file.

3.4.2 Reprojection

The original coordinate system of Landsat images in the region of the study area is projected into Universal Transverse Mercator (UTM) Zone 47 **North**. Therefore, to maintain projection consistency across all datasets, the reproject tool in ERDAS Imagine is used to convert to the original position of the study area into UTM zone 47 **South**.

3.4.3 Geometric Evaluation

Wolf et al. (2000) state that geometrically corrected images can be utilised to obtain exact distance, polygon size, and precise bearing information. The geometric distortions potentially consist of scan skew, scanning system, the altitude of variation of the sensor, non-linear scanning system and earth rotation (Netanyahu et al. 2004). According to Jensen, J (1996), geometric errors can be divided into two common faults; internal and external. Internal means that the errors introduced by its system combine with earth rotation. This type of error is skew and scanning system. External issues presented by natural phenomena through time and space such as altitude and attitude changes.

Control point coordinates (GCP) and polynomial equations can be applied to scale, rotate, balance, warp bend the images and fit the image into the coordinate

system on the surface of the earth. The highest polynomial controls the degree in the transformation process. The first order is linear, and the second and so forth is non-linear. The order more than one such as cubic polynomial can correct distortion (Aber et al. 2010). The formula to find the minimum number of GCP is given by in Equation 1:

$$Min\ GCP = \frac{(t+1)(t+2)}{2}$$

Equation 1: Minimal Ground Control Point

Where t: Order of transformation

The orders of polynomials used in this project are two orders, with minimum GCP 6 points. The equation applied to Calculate Root Mean Square Error (RMS) or distance between the actual location and desired output coordinate shown in Equation 2 as follows (ERDAS-IMAGINE 2013):

$$RMS\ error = \sqrt{(\mathrm{xi}-xr)^2 + (yi-yr)^2}$$

Equation 2: Root Mean Square Error (RMS)

Where:
X_i and Y_i are the input source coordinates; X_r and Y_r are the referenced coordinates.

In this research, the evaluation of geometric was conducting in two approaches, geometric verification using Landsat metadata, and verification using fieldwork data and Google Erath coordinates.

3.4.4 Subset / Clipping

The focus of the study was mainly located in the southern part of Kerinci Mountain, which is both parts of Kerinci Seblat National park and Kerinci municipal area. All the Landsat imagery of 1998, 2008, and 2018 were clipped into the same size as the study area.

3.4.5 Noise reduction using Principal Component Analysis

Figure 9 shows the relationship between Band A and B that creates an ellipse shape result. The major axis of the ellipse is called the first principal component (PC1) and the orthogonal to the first principal component as the second principal component (PC2). The direction of the PCI axes describes the

Figure 9: Two-band scatterplot (ERDAS 1999

eigenvector and the length of the PC1 axes define the eigenvalue of the data. PC1 usually demonstrates the most significant variability of the data (Taylor 1977).

According to Jensen, J (1996), Principal Component Analysis (PCA) is a method of image transformation that is applied to decrease the dimensionality of the interrelated band into a fewer band that are more interpretable than the original image. The transformation of image results in the new axes that paralleled to the axes of the ellipse shape of data can be interpreted as the variability and relationship among the variables.

There are three main stages in generating Principal Component transformation (Eklundh et al. 1993). These are (1) calculating the covariance and correlation of the data, (2) computing eigenvalues and eigenvectors (3) computing Principal Components.

$$V = \begin{bmatrix} v_1 & 0 & 0 & \cdots & 0 \\ 0 & v_2 & 0 & \cdots & 0 \\ & & \cdots & & \\ 0 & 0 & 0 & \cdots & v_n \end{bmatrix}$$

$$E \; Cov \; E^T = V$$

Equation 3: Linear Transformation

Equation 3 obtained from Faust et al. (1989) shows the linear transformation of the matrix process to generate V value or diagonal matrix of eigenvalues where Cov is the covariance matrix, and E is the matrix of eigenvectors. T is the transposition function, and V is the diagonal matrix of eigenvalues where non-diagonal is zero. The V value is also ordered from highest to the least (V1 value > other V values).

Equation 4 describe the process to convert original data file values into principal component values as follows (ERDAS 1999).

Where *e is* the number of principal components, and P*e* is the output of PC value. Moreover, K is the input band, and n is the total number of bands. Lastly, d_k represents the input data file (in-band k), and E is the eigenvector matrix.

$$P_e = \sum_{k=1}^{n} d_k E_{ke}$$

Equation 4: Transformation into PCA

In the classification of the image, the reducing number of PC Axes (dimension) can be used to diminish noise throughout the image. Johnson et al. (2002) argue that the Principal Component (PC) that contributes less than 20% to the total data that it can be explained as noise.

In this study, the image that can be used to classify forest and non-forest has transformed into a first component image. By considering the number of components desired and the noise band, then such an image is inserted into the original image space. The final image has the same number of bands and stored as float data to allow negative to a positive value, and such data was expected to have less noise compared to the original image.

3.4.6 Cloud Masking

Kerinci Mountain is typically covered by dense cloud throughout the years due to its location in a tropical zone and its elevation that reaches almost 4000 metres above sea level. Therefore, it is a big task to acquire a series of cloud-free optical images in this study area, and most images exhibit some amount of cloud. The masking of the cloud is applied by using a particular band called QA band (Quality Assessment) provided by USGS who applied LEDAPS software (Landsat Ecosystem Disturbance Adaptive Processing System's) to generate cloud image band. QA band is a single band image that is encoded with different pixel attribute and values that are used to differentiate a particular attribute such as cloud and non-cloud. Table 5 shows the bit value that represents a particular attribute in such image.

Attribute	Bit Value
Dark Dense Vegetation	1
Cloud	2
Cloud Shadow	4
Adjacent to cloud	8
Snow	16
Water	32

Source:https://www.usgs.gov/land-resources/nli/landsat/landsat-4-7-surface-reflectance-quality-assessment?qt-

The cloud masking processing was performed for two images, Landsat-5 1998 and 2008. It was conducted because, in the northern and the middle part of the study area, the cloud with its shadows was still detected. Moreover, the Landsat-7 image of 2018 was moderately covered by cloud, but most of the study site within such image was relatively free of cloud cover. Therefore, masking cloud was not conducted for such an image.
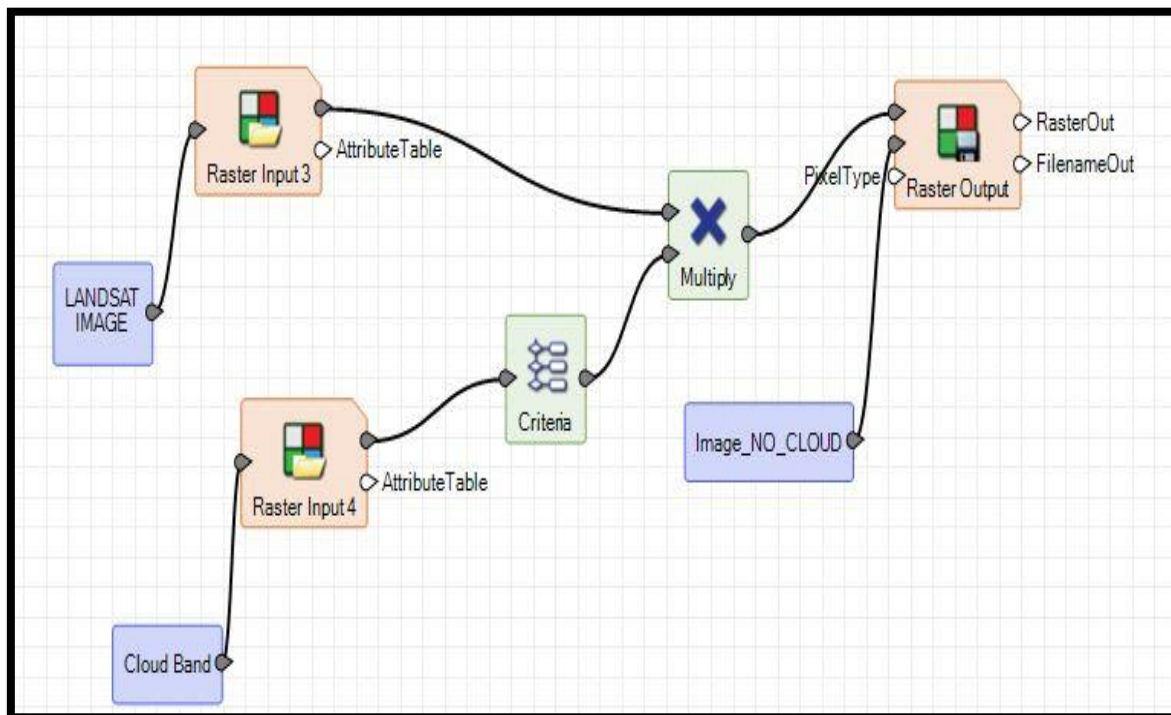
Model 1: Cloud masking model

Model 1 depicts the process of removing cloud by utilising matrix multiplication calculation that was applied to eradicate cloud and shadow. Such computation multiplies the original image of Landsat image covered with cloud and Quality Assessment (QA) single band which contained the information of cloud and shadow.

Figure 10 portrays the distribution of cloud (white colour) and shadow (grey colour) for Landsat image of 2008. The histogram of cloud and shadow varies from 1 to 248464 and other with zero values. Before running this model, the recode function was performed to change the value of cloud and shadow mask into 0, and other attributes were converted into 1 to which was then multiplied by the original image to generate an image with zeros for cloud and cloud shadow.
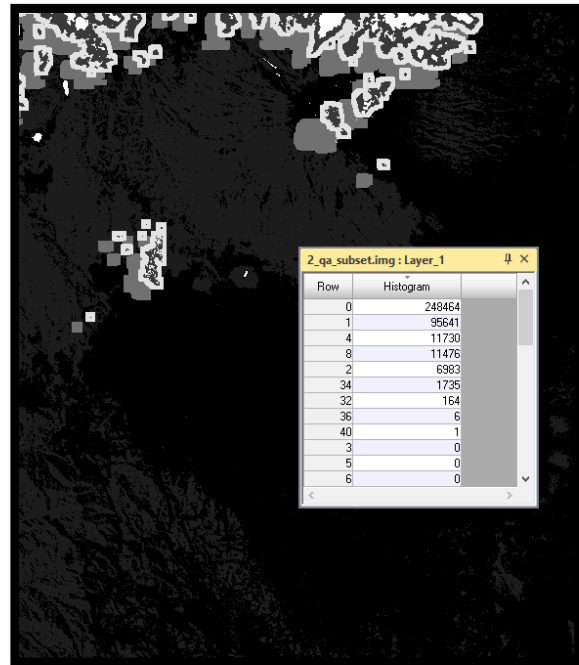
Figure 10: Quality Assessment Band

By applying noise reduction through Principal Component Analysis (PCA), the final result of images was stored into the float type file that varies from negative to positive value. Therefore, multiplication approached used in Model 1 was applied to obtain a new image with not include cloud cover.

3.4.7 Gap Filling

The Scan-Line Corrector small mirrors associated with Landsat 7 experience failure on 31 May 2003. Consequently, many gaps or stripes can be found throughout the Landsat 7 imageries. Therefore, to overcome such issues, spatial enhancement process is performed to fill in the gaps. There are various techniques to overcome such an issue. However, in this research, a focal analysis tool with the mean function was applied to fill in the gaps. The recode function was operated towards the affected line into Digital number (DN) zero. Then, the kernel size 5 x 5 was run to obtain a new centre value used to fill in the gaps.

3.5 LANDSAT - DIGITAL IMAGE PROCESSING

In this study, the primary classifier used to classify forest and non-forest is Maximum Likelihood Classification assumed as the common baseline for extraction of remotely sensed data. This part consists of four-part, the introduction of Maximum Likelihood Classification, evaluating signatures and classification, and accuracy assessment discussed as follows:

3.5.1 Band Combination

According to Singh (1988), there are four bands in Landsat TM that is suitable to display information of vegetation such as band 2,3,4, and 5. The combination of false colour composite 4, 5, 3 in RGB (Red/Green/Blue) sequence is the most suitable for presenting information on forest and land uses classes. In term of contrasting health vegetation, Meng et al. (2009) argue that the band combination 543 can reveal the information of healthy vegetation with bright green. In this study, the band combination 5, 4, 3 is used to display information of forest and non-forest class. It is because visually, the discrepancy of agriculture and tea plantation class can be seen clearly throughout the image.

3.5.2 Spectral signature collection

In ERDAS IMAGINE, the first tool used before running supervised classification-Maximum Likelihood is the signature editor that was applied to create, manage, and classify specific area within the images. The number of signatures consists of around 50 – 100 signatures for each class used to obtain a good result. A signature is a set of data that identifies various type of training samples such as Area of interest (AOI) and cluster. A specific algorithm uses such a data set as the input in the classification process. Type of signature can be divided into two types, parametric signature (statistical parameter) and nonparametric (location or object) (ERDAS 1999).

3.5.3 Evaluating Signatures

Different approaches can evaluate signatures. In this study, there are two main methods used to evaluate the significance of the image that is contingency and separability. Contingency can describe the information of the actual classified as expected generated from the training sample. This method is created in the matrix

calculation called the contingency matrix. This matrix can be applied only for supervised classification with some sample training polygons (ERDAS 1999).

There are multiple approaches used to compute similarity and Separability, with these being Euclidean, Divergence, Transformed Divergence, and Jefferies-Matusita (JM). According to Jensen, J (1996), the JM distance has an overwhelming behaviour to separate the class compared to divergence, but it is not efficient as transformed divergence. In this research, Jeffries Matusita distance used to distinguish the distance among the classes by determining the threshold. The range of JM distance is between 0 and 1414 that can be explained as follows (Jensen, J 1996).

a. Classes are separable when the JM value surpasses 1,380
b. Classes are not separate when the JM value less than 1,300
c. There is uncertainty when the JM value between 1,350 and 1,380

Equation 5 was applied to compute an alpha value that then used for computing

$$\alpha = \frac{1}{8}(\mu_i - \mu_j)^T \left(\frac{C_i + C_j}{2}\right)^{-1} (\mu_i - \mu_j) + \frac{1}{2}ln\left(\frac{|(C_i + C_j)/2|}{\sqrt{|C_i| \times |C_j|}}\right)$$

Equation 5 Computing Alpha for Jeffries Matusita Distance

C_i= The covariance matrix of signature i

C_j= The covariance matrix of signature j

μ_i= The mean vector of signature i

μ_j= The mean vector of signature j

Jeffries-Matusita distance provided by ERDAS (1999) is given Where:

After obtaining alpha value, Equation 6 was utilised to compute JM distance as follows:

$$JM = 1000 \{2(1 - e^{-\alpha})\}^{0.5}$$

Equation 6: JM Distance equation

3.5.4 Supervised-Maximum Likelihood Classification (MLC)

There are two standard decision rules for the supervised classification, parametric (maximum likelihood, Mahalanobis distance, minimum distance) and non-parametric (parallelepiped, feature space). In this case, the maximum likelihood that known as Bayesian decision rules is used maximum probability (likelihood) to allocate pixels to classes. It also uses statistical criteria (covariance matrix) and has the availability of weighting factors (ERDAS-IMAGINE 2013).

The formula for the maximum likelihood classifier is as follows (Richards 1999) shown in Equation 7:

$$D = \ln(a_c) - [0.5 \ln(|Cov_c|)] - [0.5\ (X\text{-}M_c)T\ (Cov_c\text{-}1)\ (X\text{-}M_c)]$$

Equation 7: Maximum likelihood Classification

Where D is the weighted distance, C is a particular class, and X is the candidate pixel. Moreover, M_c is described as the mean vector, a_s is the per cent probability of pixel to be a member of class c. Cov_c can be named as the covariance matrix in the sample of class c. Furthermore, Cov_c is determinant, and Covc-1 is the inverse of Covc. Lastly, Ln is termed as natural logarithm function, and T is the Transposition function.

In term of the number of classes, the image initially was classified into various type of classification determined based on the majority of class throughout the image. Then, such classes recoded into two new classes, forest and non-forest. The first classes that were created consist of some classes. Recode function then used to categorise all different classes into two new classes, forest and non-forest.

Table 6 below describes the type of classes generated from the Maximum Likelihood Classification (MLC) method. These classes were then are converted into two main classes, Forest and Non-forest.

Table 6: The number of classes created through MLC Classifier

Id	Classes	Recode
1	Old Forest	Forest
2	Tea Plantation / Shrubs/ Agriculture	Non- Forest
3	Volcanic Rock	
4	Built-up/Road	

3.5.5 Accuracy Assessment of Landsat Imagery

The classified image must be assessed to determine the classification process is satisfactory. This evaluation is known as Accuracy Assessment, which is used by evaluating the detailed scenes with a reference image or data (Campbell et al. 2011).

Accuracy assessment report creates some critical information such as overall classification accuracy and overall Kappa statistics. This two information provides the overall accuracy of the classification computation. The report also differentiates between producer's and user's accuracy that deliver different information. Sketchily, producer's accuracy is the comparison between accurate pixels and total pixels in a particular column. Conversely, user's accuracy is the comparison between accurate pixels and total pixels in a particular row. Both accuracies were provided in percentage unit. Another term for the accuracy report was an error of omission and commission and the omission is the error pixel in a row of matrix table and commission is the error in a column of matrix table.

According to Jensen, JR (2009) the cause of error in remote sensing is derived from different sources such as an error in data acquisition, pre-processing, information extraction, data conversation, error assessment, and decision making. This circumstance causes the classification cannot obtain a complete classification. For instance, Kim et al. (2014) applied reliable reference data to classify forest cover change in the United States from 10 years period, from 1990 to 2000. Such classification obtained the highest overall accuracy is around 93%. However, in other cases, the other Accuracy Assessment varied from 77% to 88%.

In terms of evaluation of error matrices, the *Kappa Coefficient* is a measure of accuracy between classification map and truth values (reference). A kappa value of 1 denotes strong agreement, while a value of 0 shows no agreement. The kappa coefficient is calculated shown in Equation 10 as follows:

Where:

i is the class number

$$\kappa = \frac{N \sum_{i=1}^{n} m_{i,i} - \sum_{i=1}^{n}(G_i \, C_i)}{N^2 - \sum_{i=1}^{n}(G_i \, C_i)}$$

Equation 10: Kappa Coefficient

N is the total number of classified values

$m_{i,i}$ is the number of values belonging to the truth class

C_i is the total number of predicted values belonging to class **i**

G_i is the total number of truth values belonging to class **i**

The threshold of K values used in this research is provided by (Landis et al. 1977) as follows:

K values > 0.8 is defined as strong agreement

K values between 0.61 and 0.80 are substantial agreement

K values between 0.41 and 0.6 are moderate agreement

K values between 0.21 and 0.40 are a fair agreement

K values < 0.2 is poor agreement.

According to Congalton et al. (1991), the number of the reference data is crucial in defining the classification with the

$$N = \frac{2^2(85)(15)}{5^2} = 203 \; points$$

Equation 11: Sample size (error 5%)

minimum number of samples being more than 250 to predict the mean accuracy of a class with an allowed error of around 5%. However, for a sample with a predicted accuracy of 85% with error 5%, the minimum sample size can be calculated shown in Equation 12

Moreover, the expected accuracy of 85% with a permissible error of 10%, the sample size would be 51 that computed as follows shown in Equation 12.

$$N = \frac{2^2(85)(15)}{10^2} = 51 \; points$$

Equation 12: Sample size (error 10%)

Furthermore, the minimum number of samples points used to assess the accuracy of classification for forest and non-forest is 50 samples that were recommended by Congalton et al. (2008). Therefore, this project applies 50 samples for the forest class and 50 samples for non-forest samples points. The ground truth points were not provided for three images with different date (1998, 2008 and 2018).

Consequently, the number of samples points were chosen randomly using equalised random distribution parameter. Such parameter used to choose points as a reference which has an equal number of random points both in the forest and non-forest class. Such points then were converted to shapefile and KML (Keyhole Mark-up Language) used to evaluate such points into particular class using ArcGIS 10.6.1 and Google Earth Pro. History images provided in Google Earth Pro was used to compare between classified image and samples points as a reference in particular dates.

3.6 LANDSAT - POST-PROCESSING

3.6.1 Recode

Recoding process is applied to decide class to new class values. Such a process causes the number of classes decreasing due to combining the class process. This function has a crucial role in determining forest and forest, the unsupervised classification using maximum Likelihood algorithm generates different types of classes, and then recode function is used to group some classes into a particular class.

3.6.2 Neighbourhood

The raw output of classification product occasionally consists of small clumps that are evenly distributed in the thematic image. This technique chooses surrounding pixels value into consideration to define the pixel value. A statistical approach was used in this function, such as the majority function used to combine the small pixel to the majority pixel that was adjacent to such pixel. Convolution filtering with a different type of kernel size also into consideration to obtain good results such as 3 x 3 or 5 x 5 size window. In this study, the pixel windows used to merge small clumps into the majority of the class is 7 x 7 window used to obtain the maximum function of merging the smaller class into the larger class.

3.6.3 Clump

This function is applied to agglomerate a contiguous group of pixels into one independent class or polygon. The size of the clump can be detected from the attribute table of the image by observing the histogram value. A threshold value of histogram (i.e. clump size) was used to sieve or eliminate the particular value of clumps.

3.6.4 Sieve

The function of the sieve is utilised to recode or remove the small clumps to a certain class or grouping into the majority of neighbouring values. In ERDAS IMAGINE, there is four types minimum size unit of that can use to remove or group clumps into
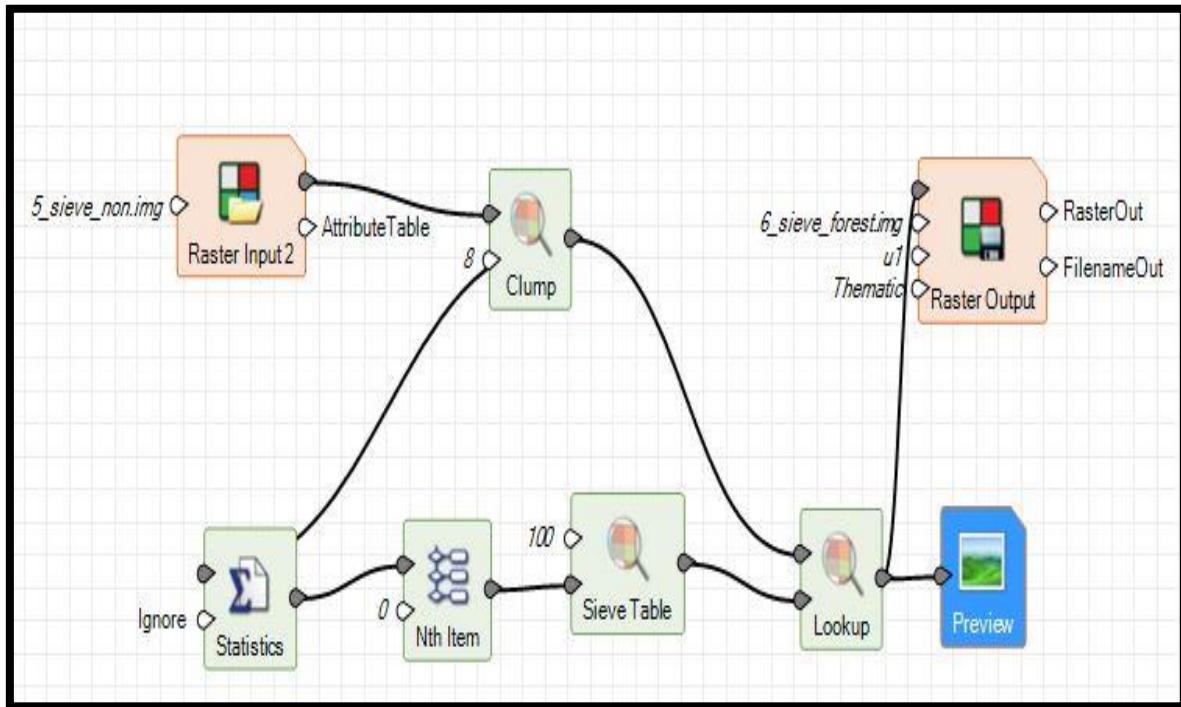
Figure 11: Clump and Sieve using Spatial model Editor

particular class or value such as pixels, hectares, acres, and square miles.

In ERDAS Imagine, the processing of clump and sieve can be performed using spatial modeller as follows:

Figure 11 describes the processing of remove small clumps and then converted to the majority class. The size of the histogram was calculated using statistics tool. The threshold value of clumps size is 50 pixel that means above such value remains.

3.6.5 Change detection

The Landsat images with a different date are classified individually. Then the three thematic images are compared, pixel-by-pixel, to obtain the changing image. The function of the image difference tool in ERDAS IMAGINE generates two outputs images, image difference and highlight difference file. This last type can be used to compute the change (increase/decrease change) between two images. In observing

change detection National Park, the boundary of National park is included in this process to detect the change of deforestation over the year.

3.7 SPOT-6 - IMAGE PRE-PROCESSING

The aim of pre-processing steps is used to enhance the remotely sensed imagery, to remove undesirable distortion and improves a significant feature of images for advance processing. In this study, the image pre-processing was applied using ENVI software that includes reprojection, subsetting, pan sharpening, radiance calibration, and computing Surface Reflectance. ERDAS IMAGINE software was used to remove Cloud and to evaluate geometric correction.

SPOT-6 image of 2018 and 2013 that were obtained from LAPAN was provided in different parameters shown in Table 7. Therefore, the pre-processing was applied to create a new image with similar parameter.

Table 7: Metadata of SPOT-6 images (2018 and 2013)

Data	2018	2013	Processing tool
Coordinate System	Latitude longitude	UTM Zone 47 South	Projection (ENVI)
Pan-sharpening	Complete (PMS*)	Incomplete (MS*, P*)	Gram-Schmidt Pan-sharpening (ENVI)
Cloud	Cover by cloud (around 40%)	Free cloud	Supervised Classification/ Cloud, Non-Cloud (ERDAS)

PMS* = Panchromatic Multispectral, MS*= Multispectral, P*= Panchromatic

3.7.1 Mosaicking/ fusion

Mosaicking is the process of merging various images into a single image. Such a process requires all the images to combine with the same datum, projection and interpolation resampling method.

Metadata of SPOT-6 imagery can be used to save a seamless image that stored is inextensible Mark-up Language (XML). This file can be used to load all images of SPOT-6 in ENVI software. The total number of scenes stored in metadata is 34 scenes, and two scenes of 34 (R2C2, R2C3) is used as the study are shown in Table 8.

Table 8: Number of SPOT-6 scenes (2013)

ID	Scene Code	ID	Scene Code	ID	Scene Code
1	R10C1	17	R4C1	29	R8C1
2	R10C2	18	R4C2	30	R8C2
3	R10C3	19	R4C3	31	R8C3
4	R1C1	20	R5C1	32	R9C1
5	R1C2	21	R5C2	33	R9C2
6	R1C3	22	R5C3	34	R9C3
7	R2C1	23	R6C1		
8	**R2C2***	24	R6C2		
9	**R2C3**	25	R6C3		
10	R3C1	26	R7C1		
11	R3C2	27	R7C2		
12	R3C3	28	R7C3		

R= Row; C=Column

Table 9 presents the number of images in the XML file, and these images consist of 28 images stored in JP2 (JPEG2000). All the images can be loaded into ENVI through XML file. It creates a seamless image, so it does not require mosaic processing. The list of images as follows:

Table 9: Number of Spot-6 scenes (2018)

ID	Scene Code	ID	Scene Code
1	R1C1	17	R4C1
2	R1C2	18	R4C2
3	R1C3	19	R4C3
4	R1C4	20	R4C4
5	R2C1	21	R5C1
6	R2C2	22	R5C2
7	R2C3	23	R5C3
8	R2C4	24	R5C5
9	R3C1	25	R6C1
10	R3C2	26	R6C2
11	R3C3	27	R6C3
12	R3C4	28	R6C6

3.7.2 Projection and subset image

Satellite image SPOT-6 is obtained and downloaded from LAPAN server in Indonesia with Geographic Coordinate System (GCS) with a three-dimensional
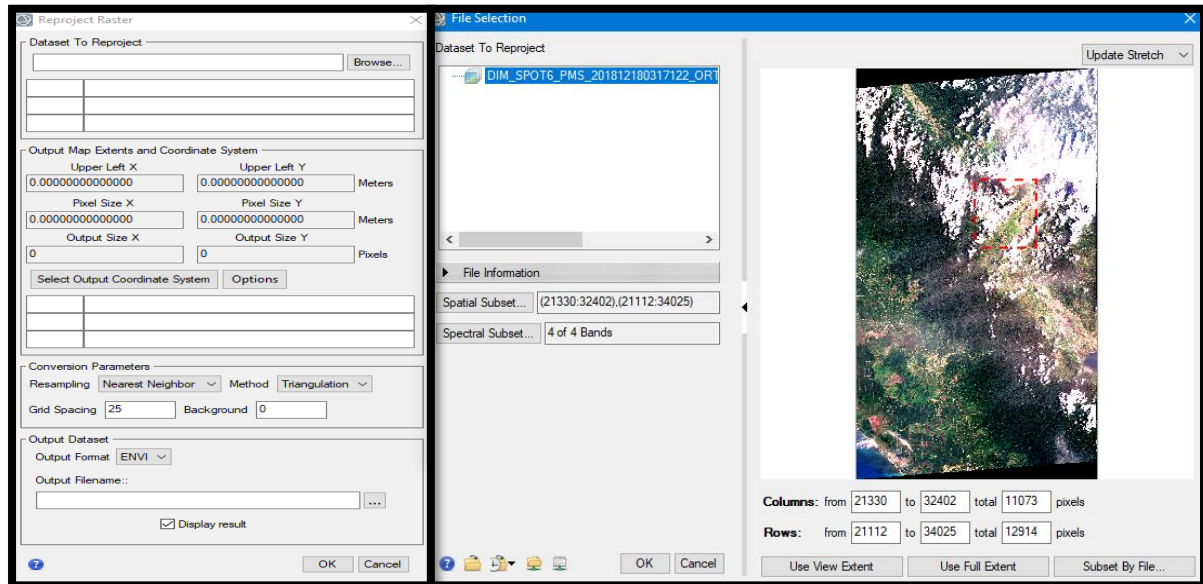
Figure 12: Reproject and subset image using ENVI version 5.6

ellipsoidal surface in determining the location on the Earth. Such a system consists of three main part, such as prime meridian, datum (with ellipsoidal parameters), and angular unit. Satellite images from 2013 were formatted and projected into Universal Transverse Mercator (UTM). The details in Figure 12 presented using ENVI software version 5.6 as follows:

Unit   : Metre

Datum   : World Geodetic System (WGS) 1984

Prime meridian   : Greenwich

Ellipsoid   : WGS 84

Projection   : UTM Zone 47 South

Axis order: E, N

EPSG Code   : 32747

However, 2018 image was formatted in Geographic Coordinate System (GCS) with datum WGS 84 (World Geodetic System 84). The unit used in this format is degree (latitude/longitude) while the Spot-6 image of 2013 in projected in metres. Therefore, to avoid technical error in further analysis of the images, the coordinate

system for all images are transformed into one system, Universal Transverse Mercator (UTM) Zone 47 South, WGS84.

The clipping process also applied the similar polygon used in Landsat image as a study area to clip the SPOT-6 image. Therefore, the images have a similar extent to the previous processing using Landsat images.

3.7.3 Image Pansharpening

The multispectral and panchromatic image of 2018 that was obtained from LAPAN has been fused and merged into a new image with a high spatial resolution image. However, the image of 2013 was obtained with separate multispectral and panchromatic image. According to Dong et al. (2009), there are hundreds of methods used to fuse between multispectral and panchromatic image. However, some techniques provide lower difficulty and faster processing time. Such techniques include Intensity-hue-saturation (HIS), Principal Component Analysis (PCA), Brovey transform, wavelet transform, and Artificial Neural Network (ANN). According to Laben et al. (2000), the Gram-Schmidt method is more precise compared to another approach, such as Principal Component method. This technique is recommended for most application because it applies spectral response used to predict the display of panchromatic data. Maurer (2013) argues that Gram-Schmidt is one of the most well-known algorithms used to pan-sharpen multispectral images. Such a technique can maximise image sharpness and reducing colour alteration. However, this method is more complicated compared to other methods because it needs forward and backward, transforming the whole scenes. In this study, Gram-Schmidt is used as a fusion technique to colourise lower spatial resolution.

3.7.4 Radiance Calibration

In general, some sensors such as Landsat, Spot-6, and other sensors generate a small signal out. It creates bias or offset when no radiation detected, and a skewed called Gain shown in Figure 13. Therefore, the calibration is required to correct such sensor error.
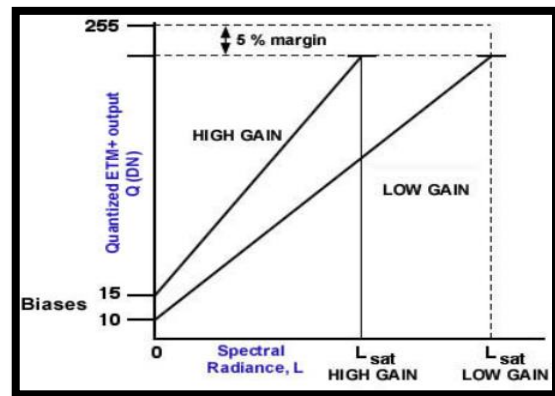
Figure 13: Gain and Bias

According to Jensen, J (1996), radiometric resolution commonly intensifies the probability of phenomena remotely sensed images more correctly. SPOT-6 sensor stored information in 12 bits (values from 0 to 4096) and such imageries were provided as raw digital number (DN) amounts of encoded radiance.

$$Lb\,(p) = \frac{\text{Digital Number (DN)}(p)}{\text{GAIN (b)}} + \text{BIAS (b)}$$

Figure 14: Conversion DN to Radiance (SPOT-6)

Figure 14 describes the equation used to obtain radiance image by calculating three parameters such as digital number, Gain, and Bias value. Due to all the images in this study obtained on different dates, it is required to correct the radiometry across all images that are standardised for sun elevation and Earth-sun distance used to generate uniform composite scenes in the analysis.

By using ENVI Software, the conversion of the original image into reflectance consist of two main stages shown in Figure 15.

The process calibration provides two output radiance and TOA reflectance, while FLAASH processing generates surface reflectance.
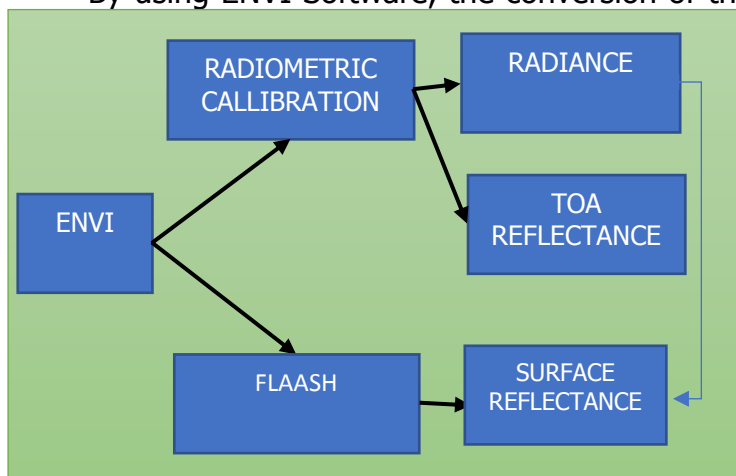
Figure 15: Radiometric Calibration and Surface reflectance

The final output of radiometric correction is

surface reflectance, and the input image in such a process is the radiance image. Therefore, in this study performs radiance conversion and computing surface reflectance.

In computing radiance, GAIN and BIAS parameter are applied to convert Digital Number (DN) into physical units of Top-of-Atmosphere (TOA) radiance. SPOT-6 imagery applied difference equation to obtain radiance value. Nevertheless, ENVI software can adjust such equation as long the data loaded through metadata. The formula of SPOT-6 radiance conversion is given:

Where:
$L_b (p)$ = TOA radiance in $W.sr^{-1}.m^{-2}. \mu m^{-1}$;

b　　= Respective band;

DC (p) = Raw digital number (DN);

If the radiance is used for FLAASH processing, the equation result will be divided with 10 to obtain units of $\mu W/ (cm^2 * sr * nm)$

Table 10 displays the list of Gain and Bias value for the image of 2013. The Gain value is quite similar that varies from 8.5 (Blue band) to 13.73 (Infrared band). The Bias values are zero for all band in the image of 2013. The details of the value can be seen as follows:

Table 10: Gain and Bias of SPOT-6 imagery recorded on 15 April 2013

BAND	GAIN	BIAS
B0 (Blue)	8.51	0
B1 (Green)	9.52	0
B2 (Red)	10.44	0
B3 (Infrared)	14	0

Table 11 illustrates the Gain and Bias value for the image of 2018. The range of the gain varies from 7.75 for the Blue band to 13.88 for the infrared band. It can be detected that Bias value is zero for all band of SPOT-6 imagery recorded in 2018.

Table 11: Gain and Bias of SPOT-6 Imagery recorded on 18 December 2018

BAND	GAIN	BIAS
B0 (Blue)	7.75	0
B1 (Green)	9.25	0
B2 (Red)	10.34	0
B3 (Infrared)	13.88	0

ENVI Software generates a radiance image by using Gain and Offset values derived from metadata of SPOT-6 imagery shown in Figure 16. Such values should be in units of (W/ (m2 * sr * μm)). By loading metadata is stored in Extensible Mark-up Language (XML) data file, ENVI will adjust

$$L_\lambda = Gain * Pixel\ value + Offset$$

Figure 16: Conversion formula DN to radiance - ENVI

and compute the radiance calibration using SPOT-6 conversion formula. However, without defining the type of images through metadata, the default conversion of the image uses the original equation provided by ENVI software to compute radiance value.

3.7.5 Surface reflectance

In general, there are two types of reflectance on the top of the atmosphere, planetary radiance and planetary reflectance. In obtaining an explicit scene, a reduction in between-scene variability can be obtained through the normalisation process. The parameter values used in this normalisation are incoming solar irradiance and solar elevation. In ENVI software, the proportion of surface and atmospheric reflectance of the Earth is calculated using the default equations that shown in Figure 17, and the formula is given:

$$\rho_\lambda = \frac{\pi L_\lambda d^2}{ESUN_\lambda \sin \theta}$$

Figure 17: Default equation of TOA and surface reflectance

Where:

L_λ = Radiance in units of W/ (m2 * sr * μm)

d = Earth-sun distance, in astronomical units (1 unit~149.6 x 10^6 km).

$ESUN_\lambda$ = Solar irradiance in units of W/ (m2 * μm)

θ = Sun elevation in degrees

ENVI involves not only Gain and Bias/Offset values, but it also uses other value to generate Top-Of-Atmosphere (TOA) and surface reflectance. Such element consists of irradiance, sun elevation, and acquired time that was provided in the metadata.

Table 12 depicts the list of parameters used to compute surfaces reflectance images. This information was derived from metadata of the SPOT-6 image of 2013

Table 12: Metadata of SPOT-6 imagery required on 15 April 2013

Date	15/04/2013
Time	03:15:34
Projection	WGS 84 UTM 47M
TOA solar irradiance for the band	
Solar Irradiance B0	1982.672
Solar Irradiance B1	1826.087
Solar Irradiance B2	1540.494
Solar Irradiance B3	1094.747
Incidence Angle	23.77032
Sun Azimuth	130.10279
Sun Elevation	55.21976
Distance to Earth	0.966684

Table 13 portrays the parameter values used to generate radiance and surface image. It can be seen that the value of irradiance for each band is similar to solar provided in the previous image (SPOT-6 image of 2013). The parameter below was derived from metadata of SPOT-imagery recorded in 2018.

Table 13: Metadata of SPOT-6 imagery required on 18 December 2018

Date	18/12/2018
Time	03:17:20
Projection	WGS 84 UTM 47M
TOA solar irradiance for the band	
Solar Irradiance B0	1982.672
Solar Irradiance B1	1826.087
Solar Irradiance B2	1540.494
Solar Irradiance B3	1094.747
Incidence Angle	20.32
Sun Azimuth	130.102
Sun Elevation	55.21976
Distance to Earth	0.966684

The other parameters values used to generate surface reflectance is the information of wavelength value that includes the centre and Lists full-width-half-

maximum (FWHM) value that is illustrated in Table 14 where both scenes (Images of 2013 and 2018) has the same range wavelength value.

Table 14: Wavelength value of SPOt-6 images

BAND	Wavelength(µm)		Centre (µm)	FWHM (µm)
B0	0.455	0.525	0.49	0.263
B1	0.53	0.59	0.56	0.295
B2	0.625	0.695	0.66	0.348
B3	0.76	0.89	0.825	0.445

Fast Line-of-sight Atmospheric Analysis of Spectral Hypercubes (FLAASH) is one tool that can be used to correct wavelengths, particularly in the range of near-infrared and shortwave infrared sections. According to Jensen, J (1996), FLAASH showed in Figure
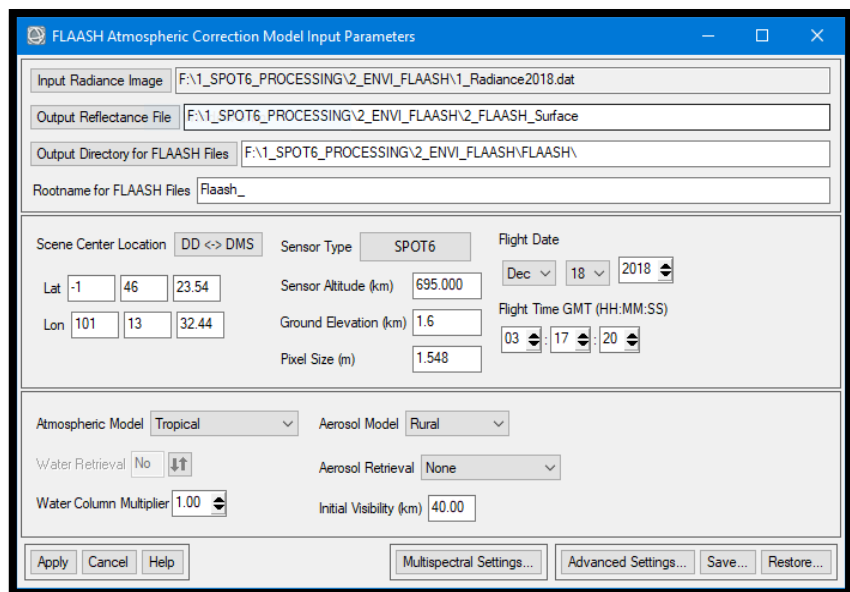
Figure 18: FLAASH Atmospheric correction tool using ENVI version 5.6

18 is used to improve images quality for atmospheric water vapour, oxygen, carbon dioxide, ozone, methane, aerosol and molecular scattering. Moreover, according to Cooley et al. (2002), one of the main aims of FLAASH processing is to invert radiance at detector into reflectance at the surface. FLAASH require input data in float format with units of µW/ (cm2 * sr * µm). However, the input image used in this study has unit W/ (m2 * sr * µm). Therefore, it does not meet these criteria. In converting radiance data, scale factor has to consider in this stage. The single factor with a default value of 1.00 is used where the input image is generated from Radiometric Calibration in ENVI software. Otherwise, the single scale factor value used is 10.

FLAASH is also one of the approaches to perform correct Atmospheric correction. It is a process to eradicate the absorption and scattering properties from the atmosphere to acquire the surface reflectance. There is various type of

atmospheric correction algorithm used based on radiative transfer modelling such as ATCOR, ACORN, ATREM and FLAASH. This algorithm can be found in ENVI software.

In term of generating surface reflectance, the transformation of the original image into surface reflectance image consists of four stages; (1) Converting DN to at-sensor-radiance (2) to apparent reflectance (3) to scaled-surface-reflectance- (4) to real-surface-reflectance.

The output of the radiometric calibration process using ENVI software as follows:

a. Interleave BIL (Band sequential), BIL (Band Interleaved by Line), and BIP (Band Interleaved by Pixel).
b. Data Type: Floating point, Double, and 16-bit unsigned integer
c. The default scale factor in generating radiance in-unit W/ (m2 * sr * μm is one (1.00). However, if the image used as FLAASH input, the default format of the image are as follows: BIL interleave, Floating-point, Scale factor= 0.1, and the unit of μW/ (cm2 * sr * nm).
d. Surface reflectance image. The image will be used as the main image in the classification process.

3.7.6 Cloud Masking
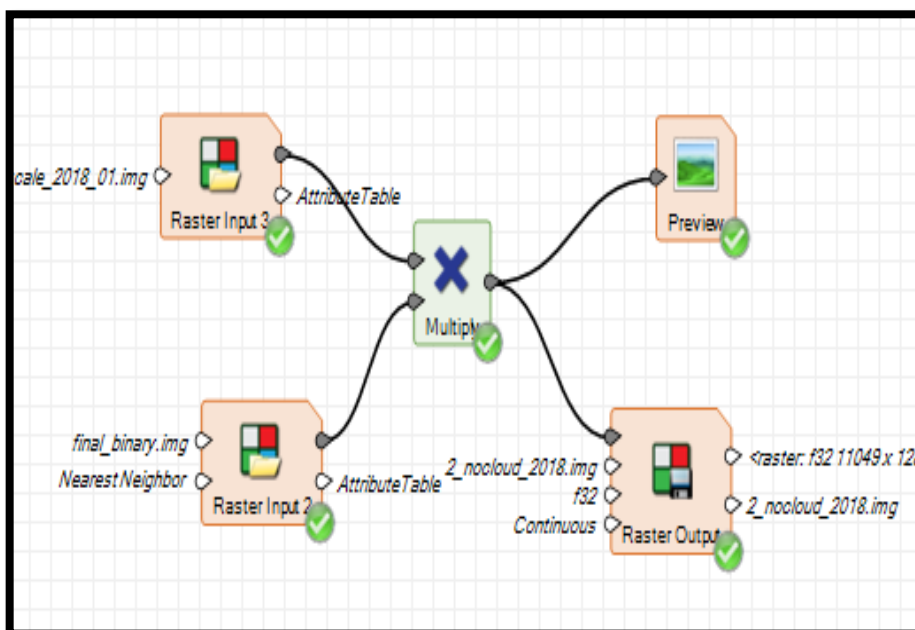
Model 2: Remove Cloud model

The image of 2018 mostly covered by cloud at around 40% of cloud. SPOT-6 image was not only provided with the satellite imagery, but it was also equipped with cloud data stored in Geography Mark-up Language (GML) format. However, such a file cannot cover all

the clouds in the study area. Therefore, the supervised classification was used to extract information on the cloud. The final process of this will generate the new image that consists of two attributes, cloud and non-cloud. Then such binary image multiplies with the original image to obtain a free-cloud image as shown in Model 2.

3.7.7   Geometric Evaluation

The geometric evaluation process in SPOT-6 image has the same procedure with geometric evaluation in Landsat 5 and Landsat 7. The primary software used to evaluate geometric of SPOT-6 of 2013 and 2018 are Google Earth, and ERDAS IMAGINE. The ground truth data were collected from fieldwork using Garmin GPS and Google Earth Pro. The Ground Control Point (GCP) chosen is the points that are easy to distinguish in the field, such as statues, village gates, and the intersection of roads.

3.8   SPOT-6 - DIGITAL IMAGE PROCESSING

Model 3 displays the comprehensive stages in computing training data and FLS segmentation through machine learning. The Random forest (RF) classifier was applied to compute training data and then stored within machine learning output. Such file then was classified together with FLS segmentation to generate a vector file of classification.
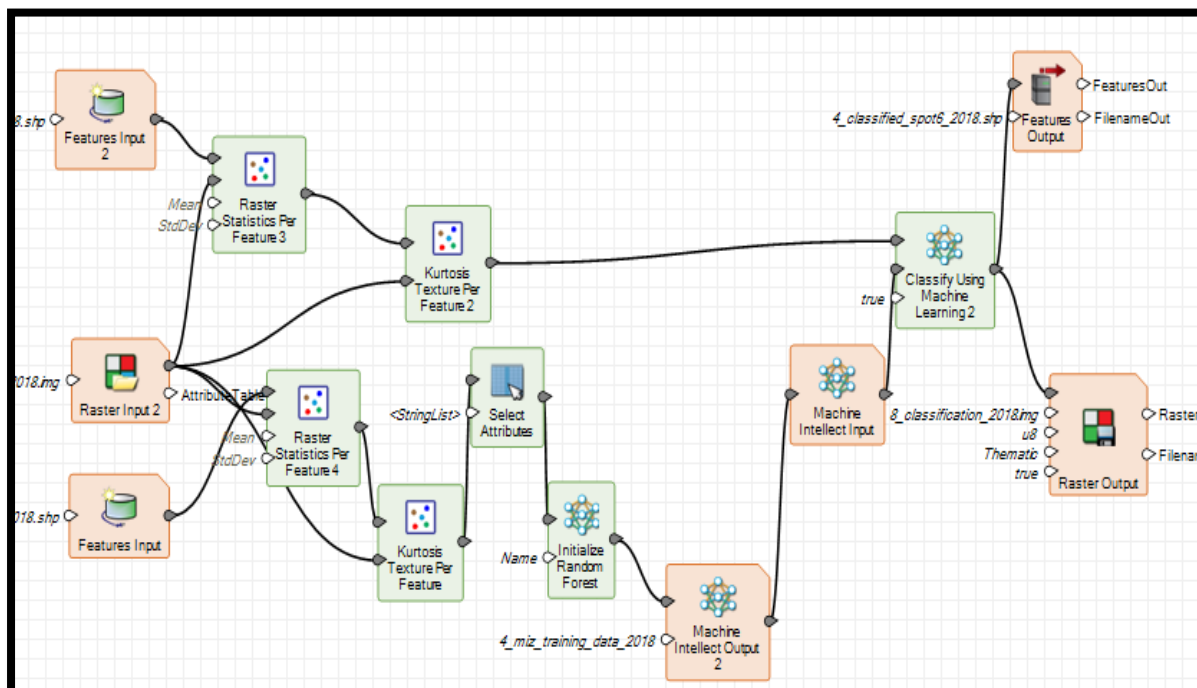
Model 3: Classification using machine learning

3.8.1 Creating segmentation file

Object-oriented Classification (OOC) was performed based on segmentation of the image into objects, not single pixels, which is known to be used in spectral-based classification. The objects or physical features on the surface of the earth can be defined by considering properties such as size, shape, spectral and texture. The general calculation using OOC is performed in two main stages: Segmenting the image using polygon features which are created by respecting spectral, size, shape, and texture. In this study, the segmentation was performed by using Full Lambda Schedule (FLS) segmentation provided in ERDAS IMAGINE software. This tool can be found at ERDAS IMAGINE –> Raster –
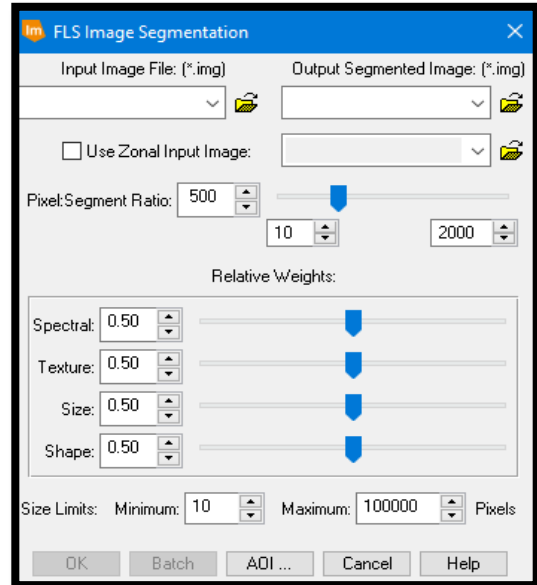
Figure 19: FLS Segmentation

> Unsupervised -> FLS Image Segmentation. Algorithm of FLS creates segmentation based on pixels and the spatial (location) within the image. Some parameters can be utilised to generate segmentation from the image that shown in Figure 19 as follows:

(1) Segment ratio: The average number of pixels within segmentation features where the size is the critical parameter.

(2) Relative Weights: Such parameter manages the merge cost function. The high value of relative weights weight implies the homogeneity of the weights and the same value of the results of the relative importance in the same segmentation. In this study, the parameters used for segmentation were:

Pixel segmentation ratio: 2000

Spectral   : 0.50

Texture   : 0.90

Size   : 0.80

Shape   : 0.90

Minimum size limit: 20

Maximum size limit: 100000

(3) Spectral: is measured using **the mean** of DN values of pixels. Within segments, **Standard deviation** is calculated for texture segments. The number of pixels within segmentation is applied for the size weights. **Boundary complexity** is utilised for the shape weights, and **pixel count** method is used for the size limits.

a. The users assign the segmented objects to particular classes by the attribute values determining while computing training samples.

3.8.2 Adding the mean and standard deviation value into a training data attribute

Training samples polygon were derived from FLS segmentation process. The new attributes called "class" then created through ArcGIS software. The statistical
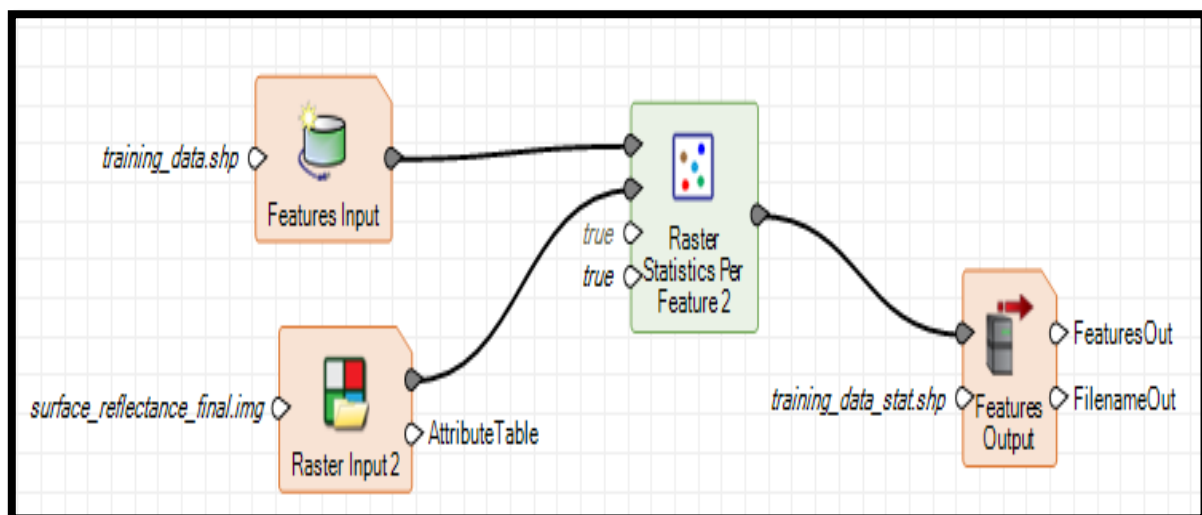
Model 4: Adding statistical information into training data

information within the class then was computed to generate information such as the mean, and standard deviation. Such statistics value was derived from SPOT-6 raster. Raster Statistics per feature tools was used to transfer the information from raster to training samples performed using model shown in Model 4.

3.8.3 Adding the Mean and Std deviation value into an unclassified data attribute

Model 5 displays a similar process shown in model 3 (above). However, in this process, the Raster Statistic tool adds statistical information into all segmentation attribute generated from FLS segmentation tool. Therefore, in the same segment, this polygon has similar statistical value with sample training polygon.
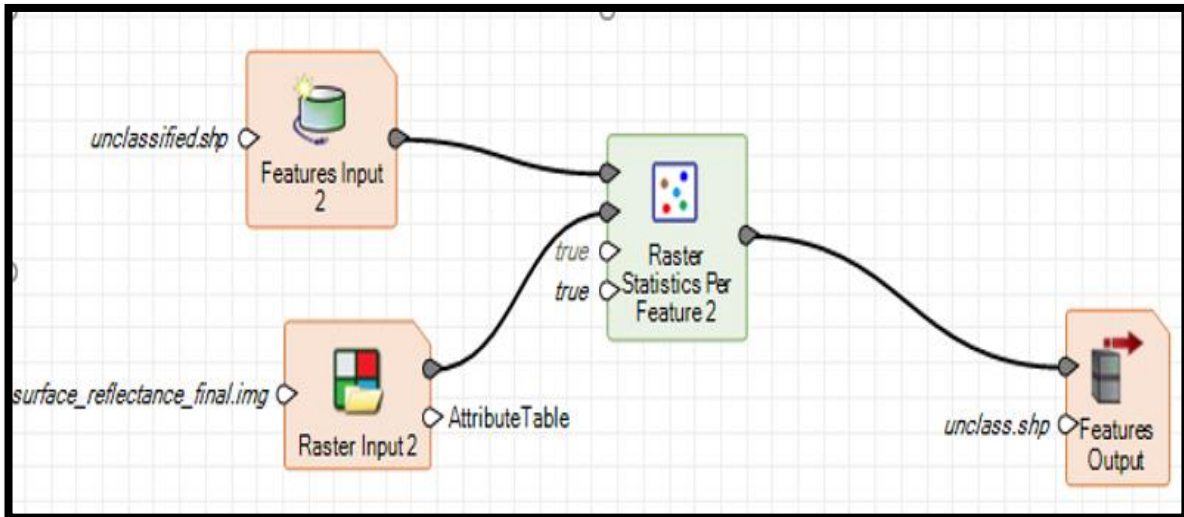
Model 5: Adding statistical information into classified image

3.8.4 Converting training data to Machine Intellect Output

ERDAS Imagine software provided five supervised machine learning algorithm which can be performed in Spatial Model Editor and Model Maker.
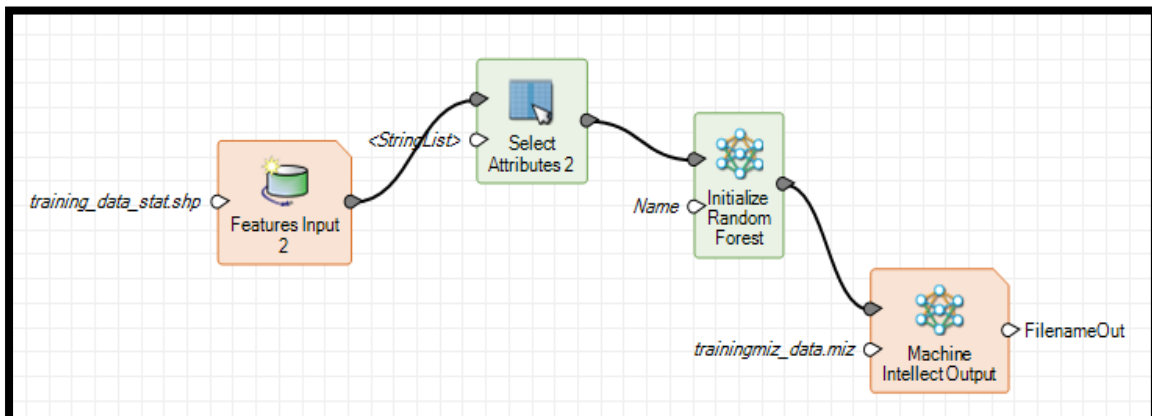
Model 6: Initialize Random Forest

Such classifiers are Initialize CART, K-Nearest Neighbours, Naïve Bayes, Random Forest, and Initialize SVM. The classifier approach used in this thesis is Initialize Random Forest (RF). According to Novack et al. (2011), RF is a powerful method used to classify urban land cover with accuracy achieving 95% compared to

other classifiers. Blaschke et al. (2010) argued that the Random Forest method has high predictive accuracy in the classification of the object compared to the others. The final output in this stage produces a new file called Machine Intellect Output stored in the MIZ extension shown in Model 6.

3.8.5 Classifying features input using Classify Using Machine Learning
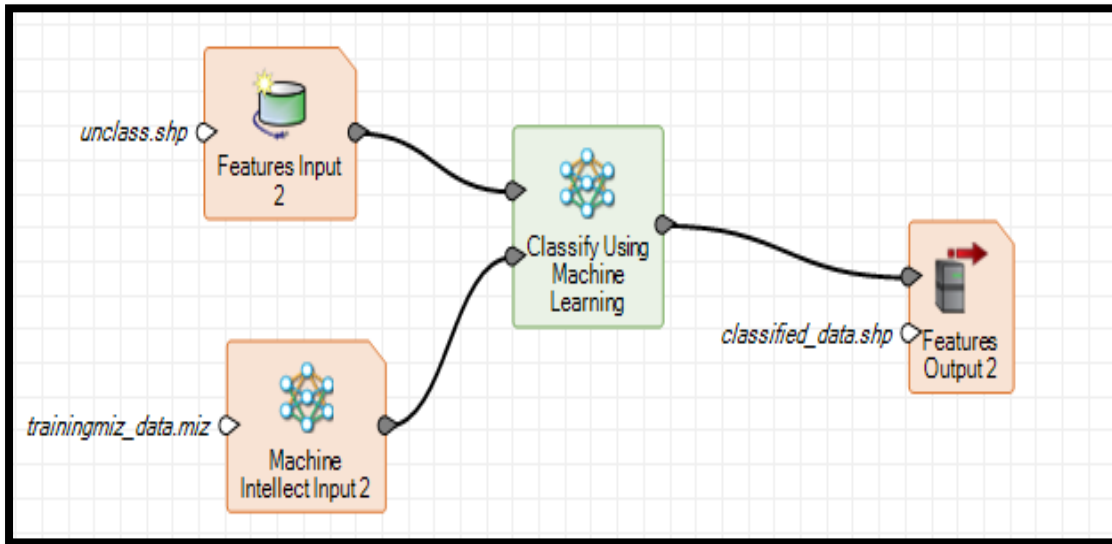
Model 7: Classify using Machine Learning

This final stage generates a new polygon with a different type of classification. Each segment has some extra information such as class, mean, and standard deviation value. Model 7 demonstrates the computation classified image using MIZ extension and machine learning classification.

3.8.6 Accuracy Assessment of SPOT-6 Imagery

This final process is used to evaluate the accuracy of the classification using object-based oriented (OBIA) classification through machine learning. Due to the final product of OBIA was stored in a vector, such data then was converted to a raster map. According to Stehman et al. (2011), pixel per pixel approach is a simple method to assess the classification that provides area-based accuracy. The method used to create reference data is equalised random sampling with total sampling is 357, where each point has 51 points. Such a number point is appropriate to generate a good accuracy proposed by Congalton et al. (1991). The authors also argued that the sample points around 250 or more are suitable to be applied to obtain good accuracy and avoid the complexity of evaluation. In term of reference evaluation, this study utilised fieldwork data, the daily park report, and Google Earth imagery.

3.8.7 SPOT-6 – POST IMAGE PROCESSING

The final product of the classification using machine learning is a vector file stored in the polygon file. Such a new image was still intricate with many segmentations. According to Novack et al. (2011), dissolve operator can be used to merge adjacent features that share similar class value. Therefore, in this study, such operation was performed on the remove and merge such segmentation into one classification group and generate a simple classification image.

3.8.8 Dissolve
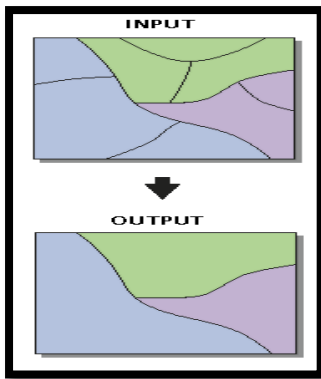
Figure 20: Dissolve processing

The dissolve tool provided by ArcGIS software is used to aggregates the adjacent polygons or features based on similar attributes or class (Novack et al. 2011). The process of dissolve can be seen in Figure 20. In this study, the dissolve tool is used to simplify the number of segmentation and calculate the extent of similar attributes.

IV. RESULTS

4.1 LANDSAT - PRE-PROCESSING

4.1.1 Geometric evaluation

All Landsat imageries used in this study are categorised as Level 2 images. It means that such data is radiometric and geometric corrected. The previous geometric verification of Landsat imagery was done by comparing to fieldwork data collected by USGS. Table 15 shows the results of the geometric correction of Landsat imagery of 1998 and 2008 that was performed and calculated by USGS. It is clear that the average error of the Landsat image of 1998 and 2008 is relatively small at 0.185 and 0.173 pixels respectively, where the number of GCP is 960 and 507 separately. However, the Landsat 7 imagery 2018 was not applied many ground truths points. Therefore, it requires to evaluate by using minimum GCP points.

Table 15: The Root Mean Square Error (RMSE) produced by USGS

TM LANDSAT	RMSE (Pixels)					Number of GCP
	Quad_UL	Quad_UR	Quad_LL	Quad_LR	Average	
1998	0.228	0.194	0.169	0.147	0.185	960
2008	0.215	0.200	0.143	0.132	0.173	507

The further geometric evaluation was conducted in this study by using fieldwork data and Google Earth imageries in which the number of sample points used is ten points. Such points relatively can be recognised well in the field, such as the village gate, statues, and intersection roads.

Table 16 presents that the overall error for the image of 1998 (Landsat-5) is around 4.90 meter. Such error is below the spatial resolution of Landsat 5 and 7 at 30 meters. Visual checking using Swipe tool in ERDAS IMAGINE software presented that all Landsat image 1998, 2008, and 2018 were well co-registered.

Table 16: Geometric correction of Landsat-5 1998

ID	X_i	Y_i	Xr	Yr	RMSE	Name
1	755559	9804365	755565.1	9804366	6.16	Sim. Teh Sangir
2	754005	9803566	754010.3	9803566	5.30	Tugu Macan
3	752580	9804350	752573.4	9804350	6.66	Teh Giri Mulyo
4	748685	9803159	748686.9	9803165	6.07	Teh Kebun Baru
5	751152	9802147	751151.9	9802145	2.15	Simp. Sungai Kering
6	750556	9800460	750559.6	9800460	3.63	Gate Patok Empat
7	752796	9801593	752795.7	9801594	1.28	Ujung Sungai Jambu
8	752921	9801144	752925.3	9801150	7.44	Jambu - Bento
9	755785	9801170	755783.1	9801175	5.41	Simp. Sei Tanduk
10	749544	9807563	749540	9807560	4.86	Belibis
				RMSE	**4.90**	

4.1.2 Noise reduction using Principal Component Analysis

Figure 21 and Figure 22 below display the result of the image transformation of Landsat-5 and Landsat-7 (1998, 2008, and 2018) using ERDAS IMAGINE software. The pixel value of such images was stored into float type that varies from negative to positive value. Such images were displayed using the first three axes, PC1, PC2, and PC3.
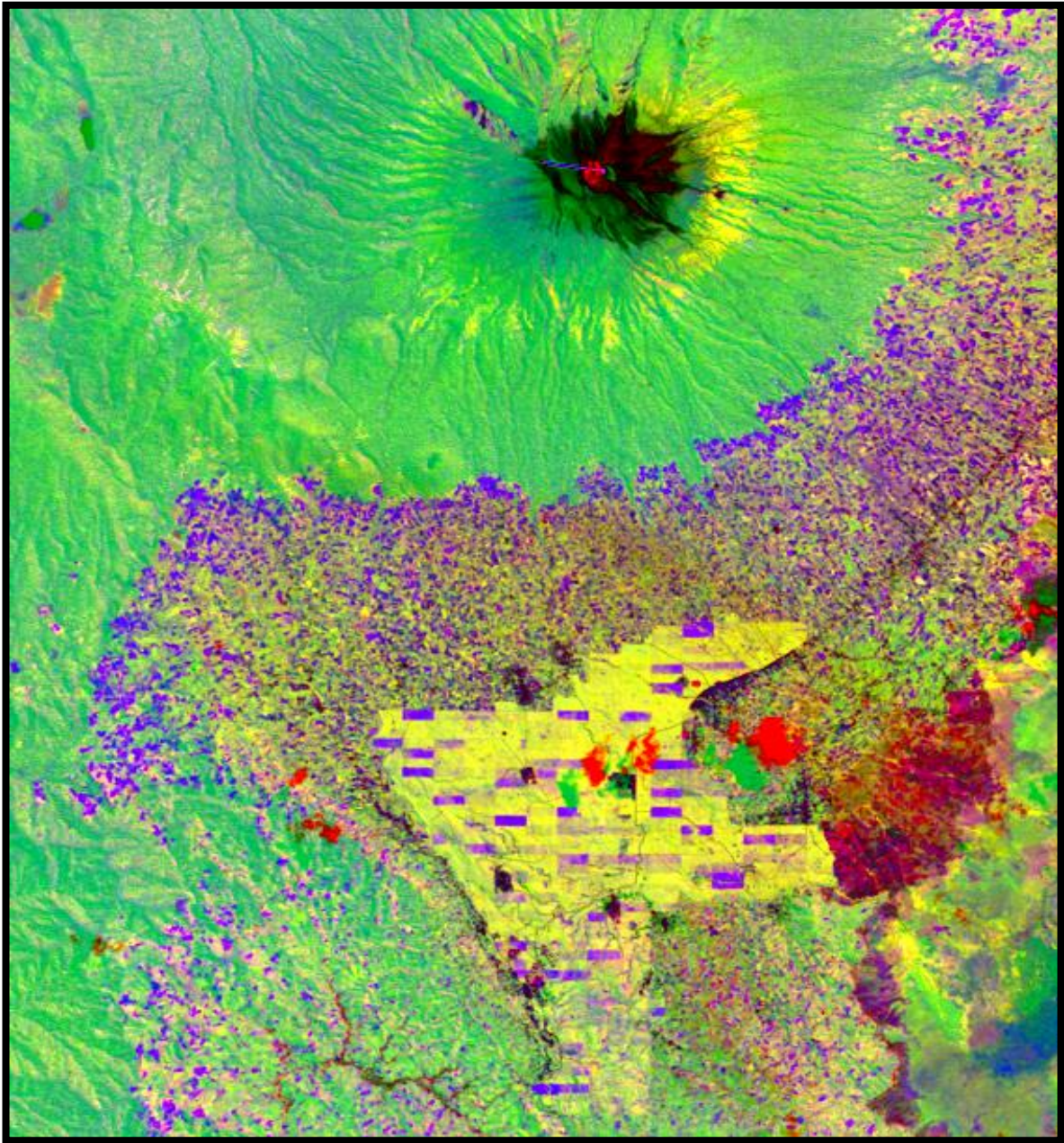
Figure 21: PCA 1998
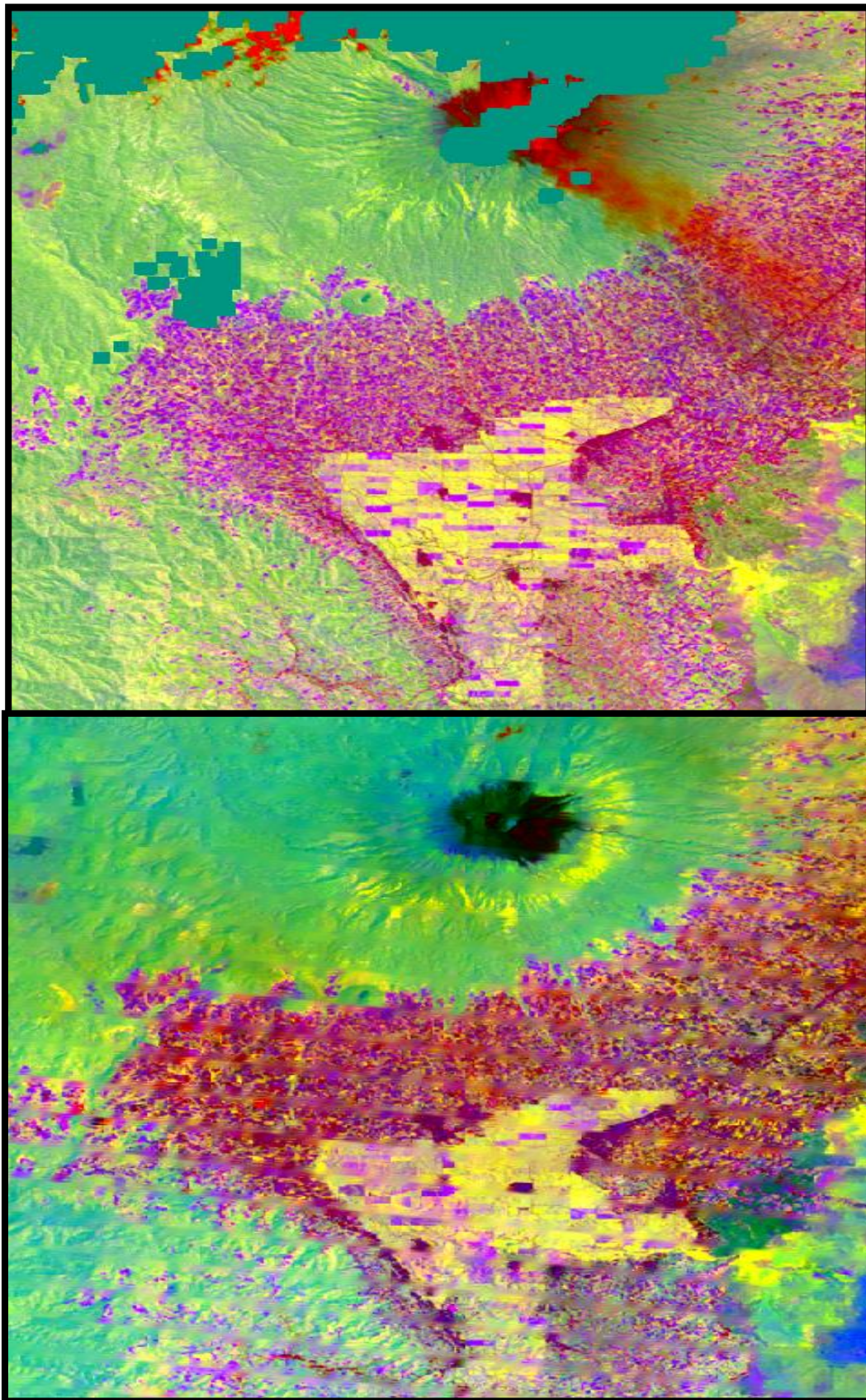
Figure 22: PCA 2008 and 2018

Table 17 explains the contribution of each band for total eigenvalues of Landsat-5 image of 1998. It can be seen that first to third component (PC1, PC2, and PC3) explains 98.14 % of the variability of the image data and rest of them can be supposed to be noises that explain around 1.8% of image variability. Figure 23 compares the contribution of each PCA axis in a line plot. It is clear that from the fourth to the sixth component is located close to X-axis means that such component is less contribution to the total variability of the data.

Table 17: The cumulative of eigenvalues in each band (1998)

Band	Eigenvalues	Percentage (%)	Cumulative (%)
Band 1	786556.0	79.62	79.62
Band 2	152494.1	15.44	95.05
Band 3	**30529.2**	**3.09**	**98.14**
Band 4	13575.9	1.37	99.51
Band 5	3955.4	0.40	99.92
Band 6	837.5	0.08	100.00
Total	987948.1		
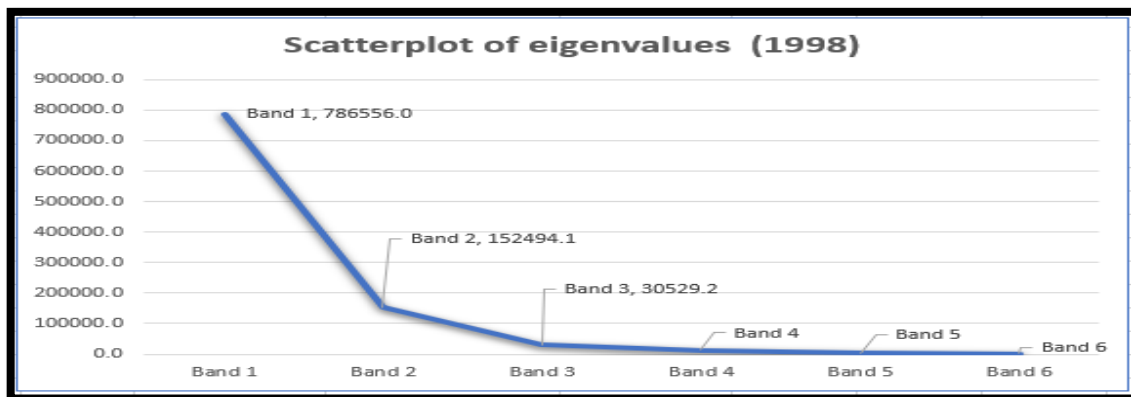
Figure 23: Line plot of eigenvalues image of 1998

Table 18 illustrates the cumulative of eigenvalues in the Landsat-5 image of 2008. It is evident that the first three bands provide 97% of the total variability of the data. It is around 3% of the total fusion of variability contributed from the fourth to the sixth band.

Table 18: The cumulative of eigenvalues in each band (2008)

Band	Eigenvalues	Percentage (%)	Cumulative (%)
Band 1	5415930.7	82.42	82.42
Band 2	628153.3	9.56	91.98
Band 3	**330491.3**	**5.03**	**97.01**
Band 4	153534.4	2.34	99.35
Band 5	32484.2	0.49	99.84
Band 6	10250.3	0.16	100.00
	6570844.1		

Figure 24 describes such cumulative eigenvalues in the line plot. It is apparent that the last three band value almost coincides to the X-axis of the plot that indicates their less contribution to the total variability of the data.
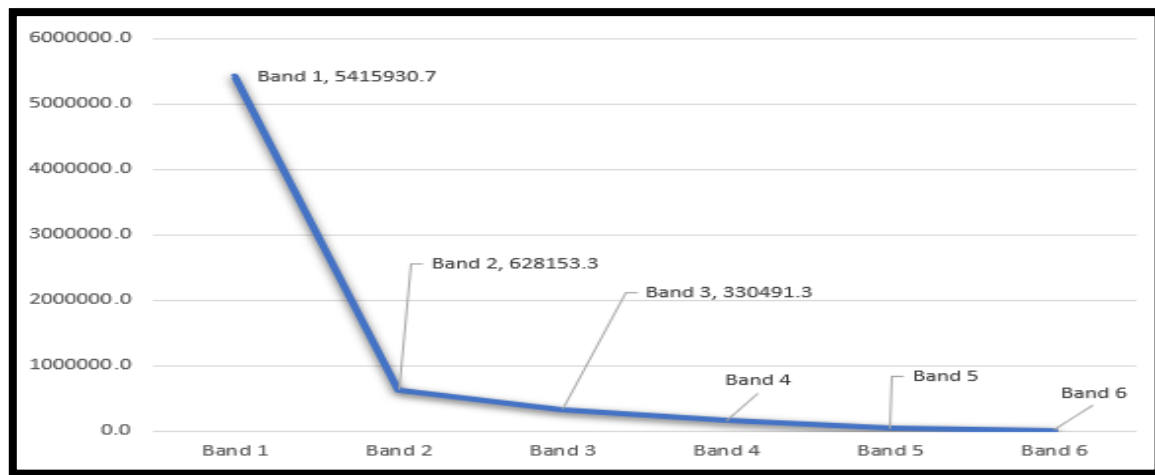
Figure 24: Line plot of eigenvalues (2008)

Table *19* depicts the eigenvalues and percentage of Landsat image of 2018 bands. Such data determined that the first three bands denote 99.48% of the total variability of the image and the last three bands only denotes 0.5% of the total variability of the image of 2018.

Table 19: The cumulative of eigenvalues in each band (2018)

Band	Eigenvalues	Percentage (%)	Cumulative (%)
Band 1	503249.96	67.11	67.11
band 2	222743.16	29.70	96.81
Band 3	**20064.96**	**2.68**	**99.48**
Band 4	2460.42	0.33	99.81
Band 5	890.60	0.12	99.93
Band 6	526.53	0.07	100.00
Total	749935.63		

By applying the line plot in Figure 25, it can be seen that the setting of bands four to six is almost similar to X-axis. It can be concluded that such a band group denotes less contribution to the total variability of the image. The line and point of the first three bands can be ascertained obviously from the plot where the first three bands have more contribution to the total variability of the scene.
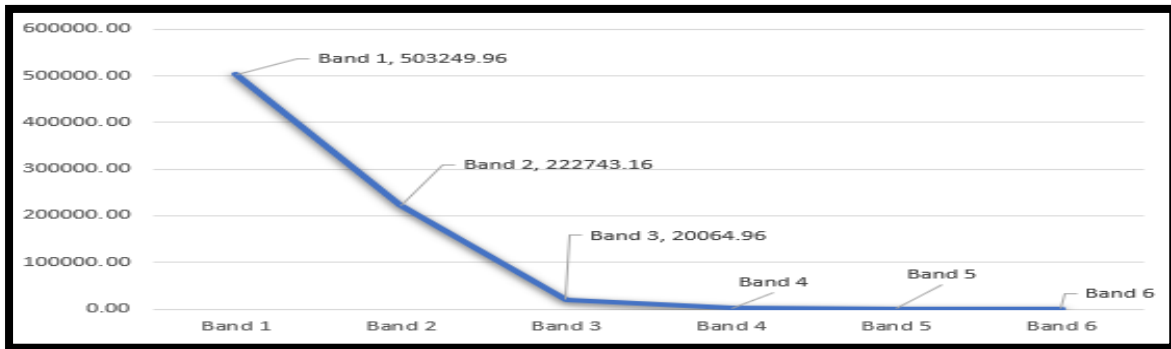
Figure 25: Line plot of eigenvalues (2018)

4.1.3 Cloud Masking

The red marks in Figure 26 illustrate the presence of the cloud and its shadows both in the Landsat-5 image 1998 and 2008. Landsat-7 2018 also cover by cloud, particularly in the northern part of the study area shown in the yellow circle. However, the cloud masking processing was not performed for such image due to less of cloud cover in the study area shown in the white circle.
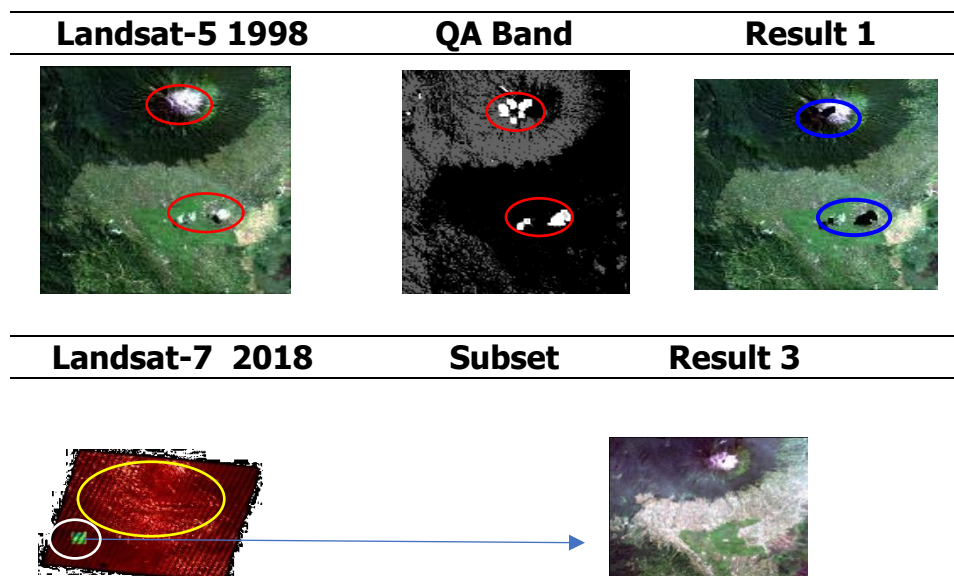
Figure 26: Cloud masking process

4.1.4 Gap Filling

Landsat-7 2018 (A)	Result (B)
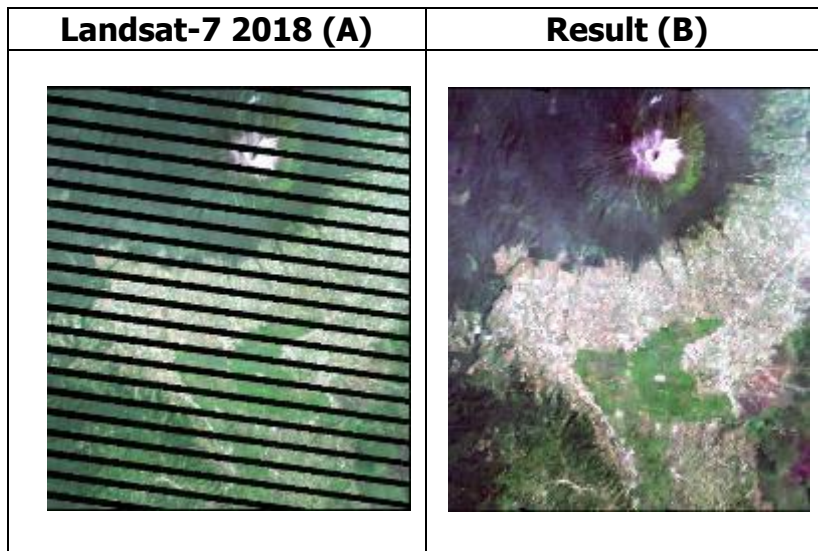
Figure 28: Focal Analysis (Gap)

Figure 27: Focal Analysis (No line/Gap)

Figure 27 and 28 Figure 28 depict the comparison of the Landsat-7 image and unstripped image. It can be seen that there are many gaps or stripping that evenly distributed throughout the image shown in column A.

To fill in the gaps, the kernel size 5 x 5-pixel window used to obtain the suitable result presented in Column B. Every pixel analysed spatially, and then the neighbourhood pixel value around the gap was computed statistically using Mean which is applied to replace the centre pixel using the mean of the pixels in the window.

By using the measurement tool in ERDAS IMAGINE, it can be found that the magnitude of the gap within the image is 11 pixels or around 330 in length metres shown in Figure 29.
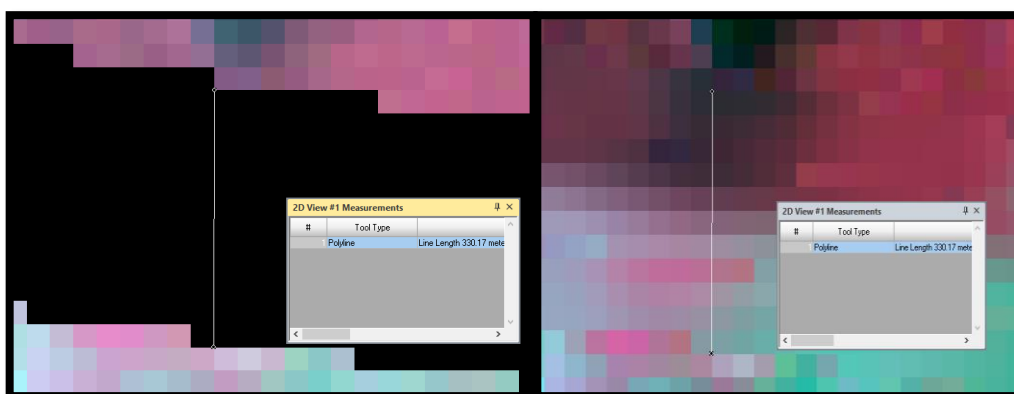
Figure 29: Gaps in Landsat-7 imagery

Figure 30 portrays the comparison between two images that are located at 748979.34, 9808046.19.   Part A shows the gaps with zero value that can be determined no data. However, part B describes the image with a non-zero value that all the values obtained using the mean function.
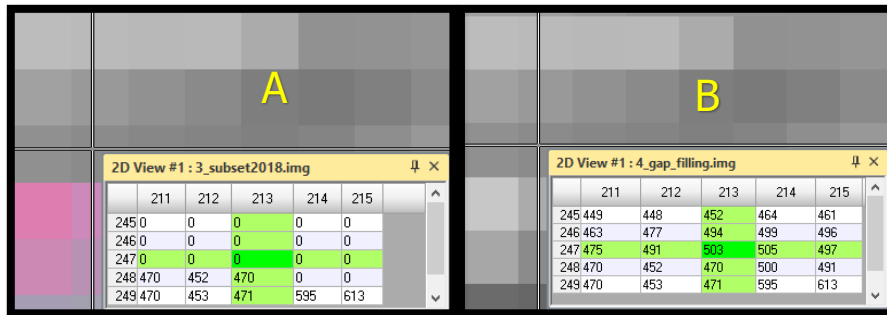
Figure 30: 5 x 5 Kernel size

The statistical process creates the image becomes blurred shown in Figure 31.
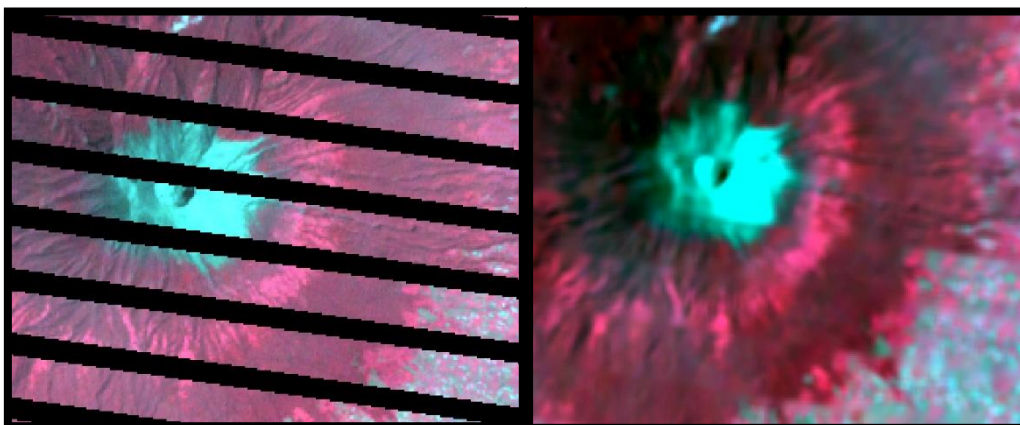
Figure 31: Gap filling constrain

4.2 LANDSAT - DIGITAL IMAGE PROCESSING

In this study, the primary classifier used to classify forest and forest was Maximum Likelihood Classification (MLC) which is the common baseline for extraction of remotely sensed data. This part consists of four sections, Spectral signature collection, evaluating signatures, classification, and evaluating the classification results through accuracy assessment discussed as follows:

4.2.1   Band Combination

Figure 32 and Figure 33 portray the difference between band combination 543, 453 and 451 in Landsat-5 Multispectral recorded in 1998. It can be seen clearly that the combination of 543 bands has various colour that assigns to specific classes. In term of forest and non-forest classification, such combination can assist the interpreter in distinguishing the various classes throughout the image.

Conversely, band combination 453 can differentiate visually between forest and non-forest class. Such combination was also applied in image 2008 and 2018. However, it was entirely tasked to distinguish the class that has similar spectral such as agriculture class and tea plantation. Then, the collection of spectra was applied to differentiate the spectra of the classes.

RGB: 451

RGB: 453
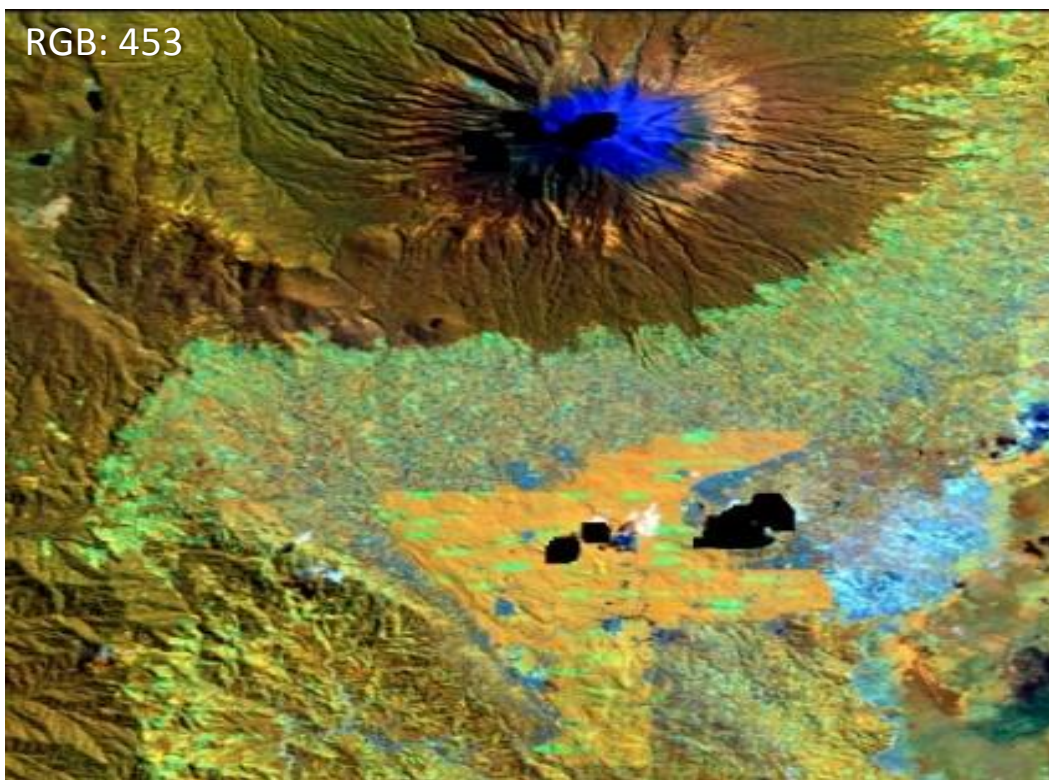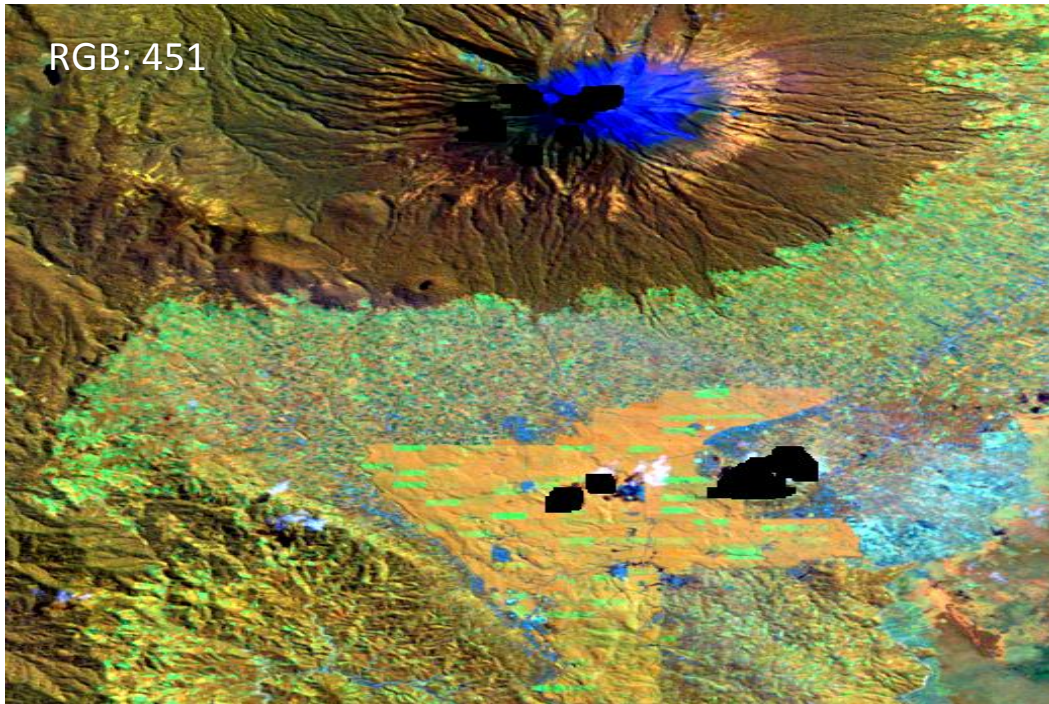
Figure 32: Band Combination 453 and 451
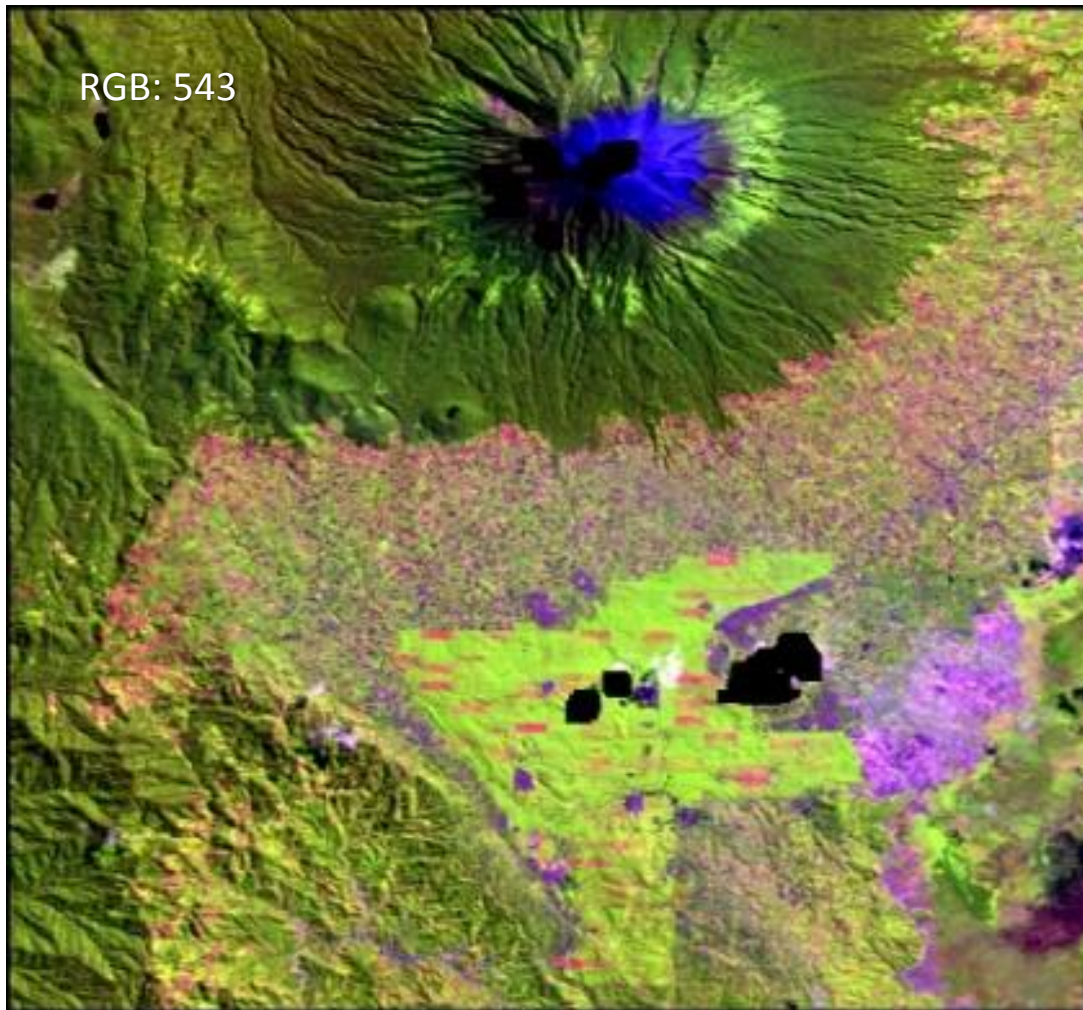
Figure 33: Band Combination of 543

4.2.2 Spectral signature collection
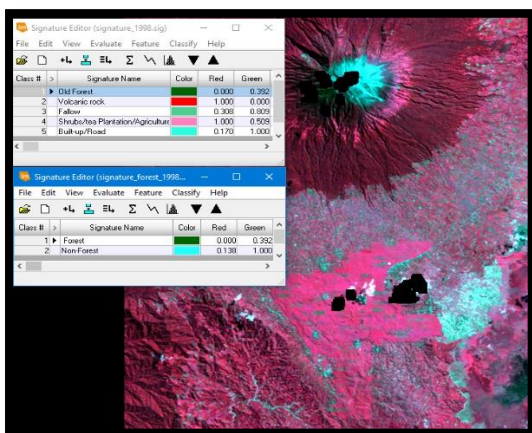
Figure 34: Spectral signature (Landsat of 1998)

Figure 34 describes the process of collecting spectral information where the first spectral consist of 5 classes and then non-forest class was combined into one class, non-forest class. In this study, this stage was also applied for the other images such as Landsat 2008 and 2018.

4.2.3 Evaluating signatures
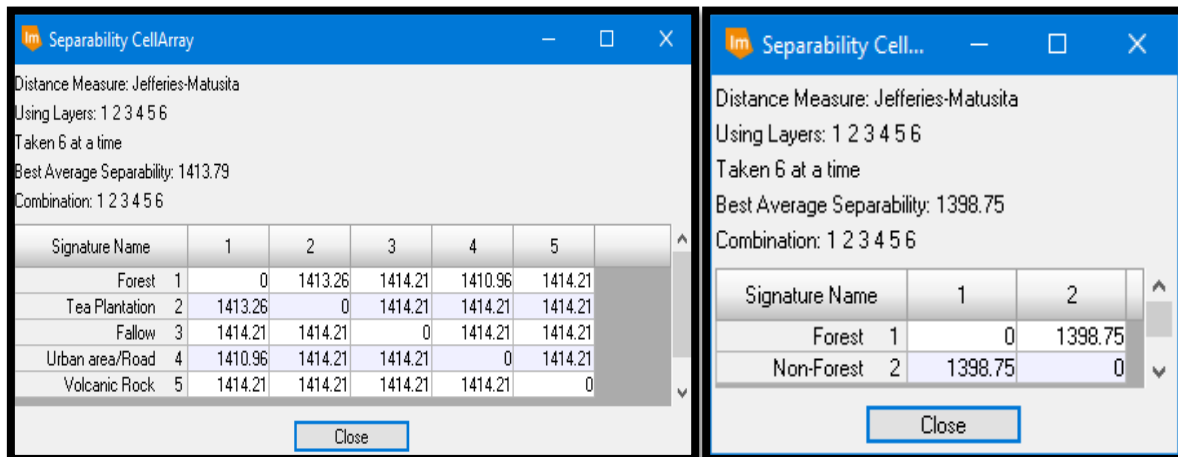
Figure 35: Jeffries Matusita Distance Classification image of 1998

Figure 35 describes the evaluation of signatures using Jefferies-Matusita distance for image Landsat-5 of 1998. In general, all the classes are separated from each other that shown with best average separability at 1413.79. The highest value of separability at 1414.21 that describes the average separability between among the classes except for separability value between old forest and plantation at 1413.74. As all such classes merge into two classes (forest and non-forest), the best average separability decreases into 1385.16. Nevertheless, such value is still categorised as good separability (minimum value at 1380).

```
ERROR MATRIX - 1998
-------------

                              Reference Data
                              --------------
Classified
     Data          Forest       Non-Forest      Row Total
----------         ----------   ----------      ----------
     Forest          10892              3           10895
Non-Forest              44           1948            1992

Column Total         10936           1951           12887

               ----- End of Error Matrix -----


ERROR MATRIX
-------------

                              Reference Data
                              --------------
Classified
     Data          Forest       Non-Forest      Row Total
----------         ----------   ----------      ----------
     Forest          99.60           0.15           10895
Non-Forest            0.40          99.85            1992

Column Total         10936           1951           12887

               ----- End of Error Matrix -----
```

Figure 36: Contingency error matrix (Image if 1998)

Figure 36 explains the relationship between the classified image and reference data Landsat image of 1998. It is observable that the contingency matrix presented in the table informs that there is no error matrix can be found both for forest class and non-forest class. There is 10936, and 1951 column total for forest and non-forest class respectively. It can be seen that the error of forest is around 0.15 % or 3 pixel and 0.40 % or 44 pixels for non-forest.

Figure 37: Jeffries Matusita Distance Classification image of 2008

Figure 37 illustrates the separability of the Landsat image of 2008. It is distinguishable that the best average separability for four classes is 1413.15. After such classes were combined into two classes, the best average decrease into 14012.93, but such value is still above the lower threshold separability at 1380.

Figure 38 express the contingency matrix between forest and non-forest class for the image of 2008. The column total of forest class is 827 for forest and 461 for non-forest class. It can be seen that the error pixels for the forest is 3 pixel or 0.65% and there is no pixel as an error for forest class.

Figure 38: Contingency error matrix (Image of 2008)
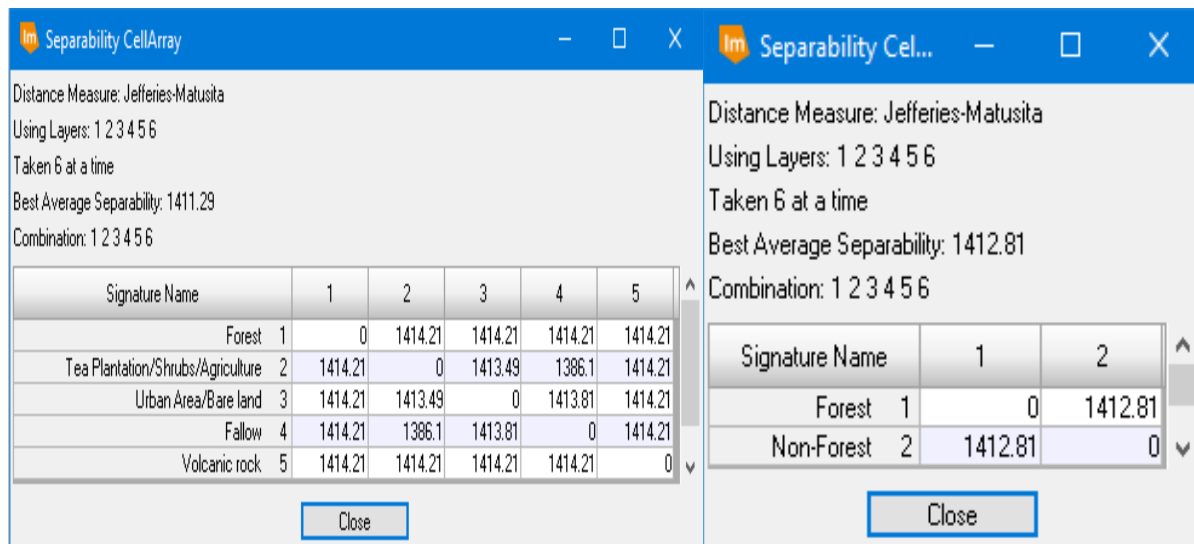
Figure 39: Jeffries Matusita Distance Classification image of 2018

Figure 39 represents the distance of each class of image classification of Landsat-7 2018. It can be detectable that the best average separability is for the fourth classification is 1411.29 and the 1412.81 for forest and non-forest class.

```
ERROR MATRIX - 2018
-------------

                              Reference Data
                              --------------
Classified
     Data          Forest        Non-Forest       Row Total
----------       ----------     ----------       ----------
    Forest          2533              1              2534
Non-Forest            20           2920              2940

Column Total        2553           2921              5474

              ----- End of Error Matrix -----

ERROR MATRIX
-------------

                              Reference Data
                              --------------
Classified
     Data          Forest        Non-Forest       Row Total
----------       ----------     ----------       ----------
    Forest          99.22           0.03             2534
Non-Forest           0.78          99.97             2940

Column Total        2553           2921              5474

              ----- End of Error Matrix -----
```

Figure 40: Contingency error matrix image of 2018

Figure 40 portrays the contingency error matrix of Landsat-7 image of 2018. It is recognisable that the error for the forest is 1 pixel or 0.03 % and 20 pixels for non-forest. The total column total of forest class is 2553 and 2921 for non-forest class.

4.2.4 Maximum Likelihood Classification (MLC)

Figure 41 represents the result of classification using MLC classifier that consists of Landsat-5 of 1998,2008 and 2018. It is clear that the edge between two classes, forest and non-forest can be seen visually for three images shown underneath. The dark green colour represents the class of forest, and the green colour portrays the class of non-forest. The details of the map can be shown in Appendix one to three in the chapter of appendices.
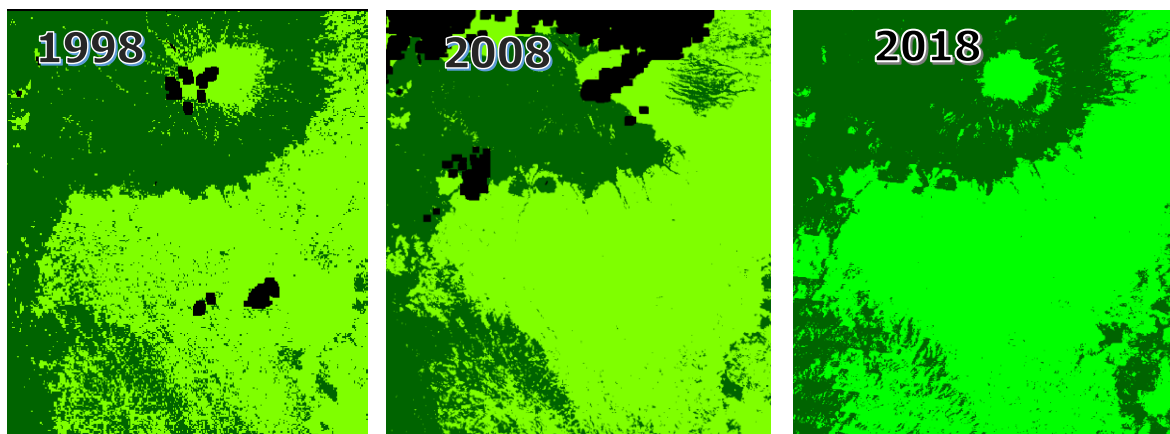
Figure 41: The result of MLC

Table 20 describes the comparison between forest and forest from 1998 to 2018. It can view that the percentage of the forest is 51% in 1998. Such trend moderately decreased around 35% and 36% in 2008 and 2018. Conversely, there was a substantial increase of non-forest area at around 63.5 % in 2008 and 2018. However, the image of 1998 and 2008 had the area that categorised as zero value due to cloud cover. It creates the total area was not similar to the image of 2018 (free cloud).

Table 20: Forest and non-forest from 1998 to 2018

Year	Forest (Hectares)	%	Non-forest (Hectares)	%	Total
1998	17102.7	51.22	16288.4	48.78	33391.1
2008	11332.9	36.58	19644.9	63.42	30977.8
2018	12071.4	35.65	21793.5	64.35	33864.9

4.2.5 Accuracy Assessment of Landsat Imagery

```
ERROR MATRIX - Landsat5 (1998)
-------------

                    Reference Data
                    --------------
Classified Data              Forest Non-Forest
--------------  ---------- ---------- ---------- ----------

       Forest          0         45          6          0
   Non-Forest          0          5         46          0

Column Total           0         50         52          0

            ---- End of Error Matrix -----


ACCURACY TOTALS
---------------

       Class   Reference Classified Number     Producers  Users
        Name      Totals     Totals Correct     Accuracy
     Accuracy
   ---------- ---------- ---------- ------- --------- -----

       Forest         50         51      45  90.00%     88.24%
   Non-Forest         52         51      46  88.46%     90.20%

       Totals        102        102      91

Overall Classification Accuracy =      89.22%

        ----- End of Accuracy Totals -----


KAPPA (K^) STATISTICS
--------------------

Overall Kappa Statistics = 0.7843
```

Figure 42: Accuracy Assessment image of 1998

Figure 42 shows an accuracy assessment report for Landsat images of 1998. It can be seen that the overall classification accuracy of the image is 89.22%, with a Kappa statistic of approximately 0.78. The number of classified and reference point is 102, with 11 points identified as incorrect pixels. The omission and commission errors vary from 10 % to 12% that generated from producer and user's accuracy shown in figure 25. In general, the classification accuracy is quite high due to the modest /high-level type of classification (forest and non-forest).

Figure 43 represents the accuracy assessment report for the image of 2008. Such classification obtained overall accuracy at 88.24% with pixels error varies from around 5% to 8%. It is clear that the producer's accuracy reaches 91.49% and 85% for non-forest and forest class respectively. Conversely, the user's accuracy is around 92% and 84% for forest and non-forest class. By using the Kappa statistic approach, the overall Kappa Statistic is 0.76 that can be categorised as substantial agreement.

```
ERROR MATRIX
-------------

                              Reference Data
                              --------------
Classified Data                 Forest      Non-Forest
---------------  ----------    ----------   ----------      ----------
                      0            0            0               0
         Forest       0           47            4               0
     Non-Forest       0            8           43               0
                      0            0            0               0

Column Total          0           55           47               0

          ----- End of Error Matrix -----


ACCURACY TOTALS
---------------

         Class   Reference      Classified    Number  Producers     Users
         Name      Totals          Totals     Correct Accuracy      Accuracy
        ---------- ----------    ----------   ------- ----------    -----
                      0            0             0      ---          ---
         Forest      55           51            47     85.45%       92.16%
     Non-Forest      47           51            43     91.49%       84.31%
                      0            0             0      ---          ---

         Totals     102          102            90

Overall Classification Accuracy =     88.24%

            ----- End of Accuracy Totals -----



KAPPA (K^) STATISTICS
---------------------

Overall Kappa Statistics = 0.7647
```

Figure 43: Accuracy Assessment image of 2008

```
ERROR MATRIX
------------

                    Reference Data
                    --------------
Classified Data           Forest Non-Forest
--------------- ---------- ---------- ---------- ----------

        Forest          0         46          5          0
    Non-Forest          0          5         46          0


Column Total            0         51         51          0

              ---- End of Error Matrix -----

ACCURACY TOTALS
---------------

        Class  Reference Classified Number    Producers   Users
        Name     Totals    Totals Correct      Accuracy
    Accuracy
        ---------- ---------- ---------- -------   ---------- -----
                        0          0        0        ---      ---
        Forest         51         51       46      90.20% 90.20%
    Non-Forest         51         51       46      90.20% 90.20%


        Totals        102        102       92

Overall Classification Accuracy =      90.20%

        ----- End of Accuracy Totals -----



KAPPA (K^) STATISTICS
---------------------

Overall Kappa Statistics = 0.8039
```

Figure 44: Accuracy Assessment image of 2018

Figure 44 portrays the accuracy assessment report for the image of 2018. The overall classification accuracy reaches 90.20% with Kappa statistics at 0.8 (strong agreement). The producer and user's accuracy for both forest and non-forest class are around 90%. The omission and commission error matrix for both classes are around 10%. In general, this classification can separate two different, forest and non-forest classes suitably.

4.3 LANDSAT - POST-PROCESSING

4.3.1 The final result of Post Processing

Figure 45 shows the classified images that have modified through post-processing. Small clumps (above) which were found both in the forest and non-forest class has been generated to the majority of class through neighbourhood function tool, and the rest of them afterwards processed using sieve function tool provided by ERDAS IMAGINE software. Due to this study focus on the area around the boundary of National Park, the classified image then clipped with the boundary vector to generate an area of interest (AOI) around the boundary.
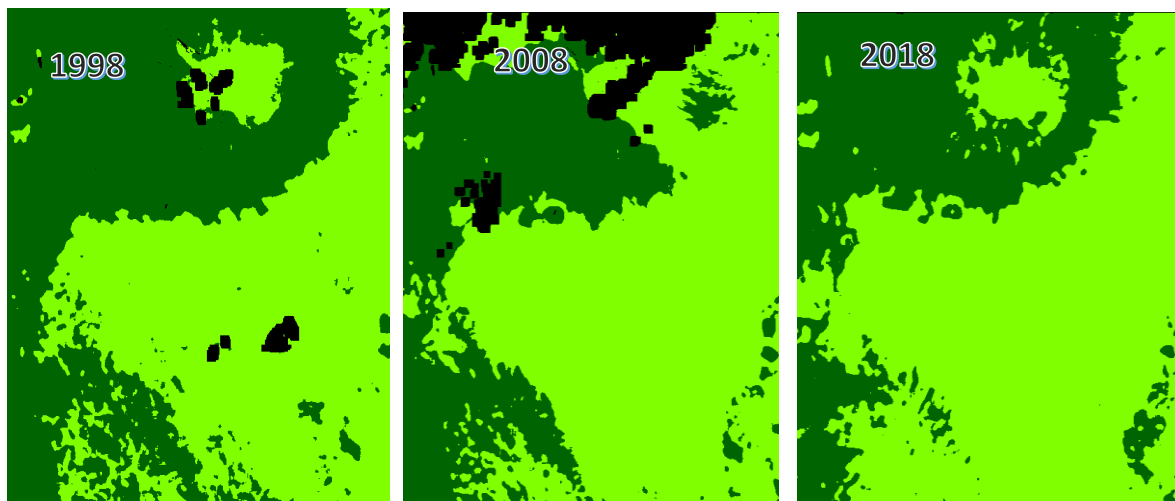
Figure 45: Final processing- Neighbourhood function

Table 21 shows the new calculation derived from neighbourhood processing. It can be compared that the calculation of percentage and the area changed for Landsat 1998. However, Landsat 2008 and 2018 relatively the same with the image without applying neighbourhood function.

Table 21: The final classification through neighbourhood function

Year	Forest (Hectares)	%	Non-forest (Hectares)	%	Total
1998	15906.8	47.64	17484.4	52.36	33391
2008	11155.4	36.01	19822.5	63.99	30978
2018	12032.8	35.53	21832.1	64.47	33865

By using the clip tool in Arc Map, the classified image then clipped into a smaller area which was located around the boundary of the national park shown in MAP 2. It can be compared that there is a significant change between forest loss in 1998 and 2018. However, the image of 2008 cannot be compared to the other image due to the existence of the cloud shown in the red rectangle. QA band provided by USGS did not include such area as cloud or shadow. In this classification, such area was categorised non-forest. Therefore, this image cannot be contrasted to other images due to a different size. Such cloud and shadow cover were estimated at around 400 − 500 hectares shown in MAP 3 (black rectangle).The investigation through other images (image of 2008) provided by Google Earth with the same date shows that some area was categorised as non-forest in particular area around the centre of the boundary of the park. Otherwise, in the northeast part, such area was classified as forest.

MAP 2 and MAP 4 displays that there is considerable change between the image of 1998 and 2018. Deforestation size is at 3379.34 and 5685.83 hectares respectively. The fixed forest loss in 2008 is estimated around 2495 hectares where around 400 − 500 can be categorised as forest loss or forest area.

Table 22: Forest and Non-forest throughout the boundary of the national park

Year	Non-forest / Deforestation (Hectares)
1998	3379.34
2008	4544.34
2018	5685.83
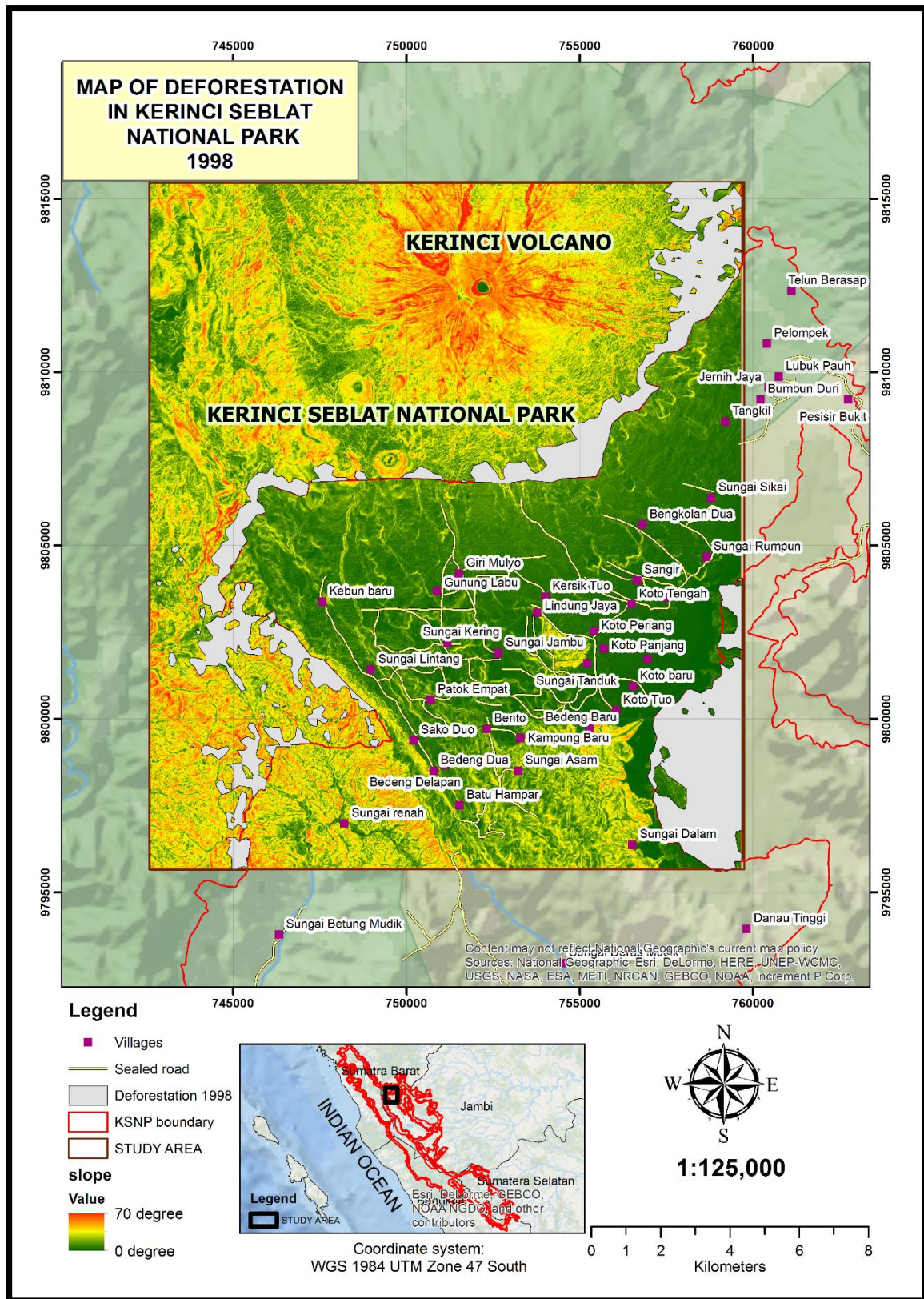
MAP 2: Deforestation within National Park in 1998
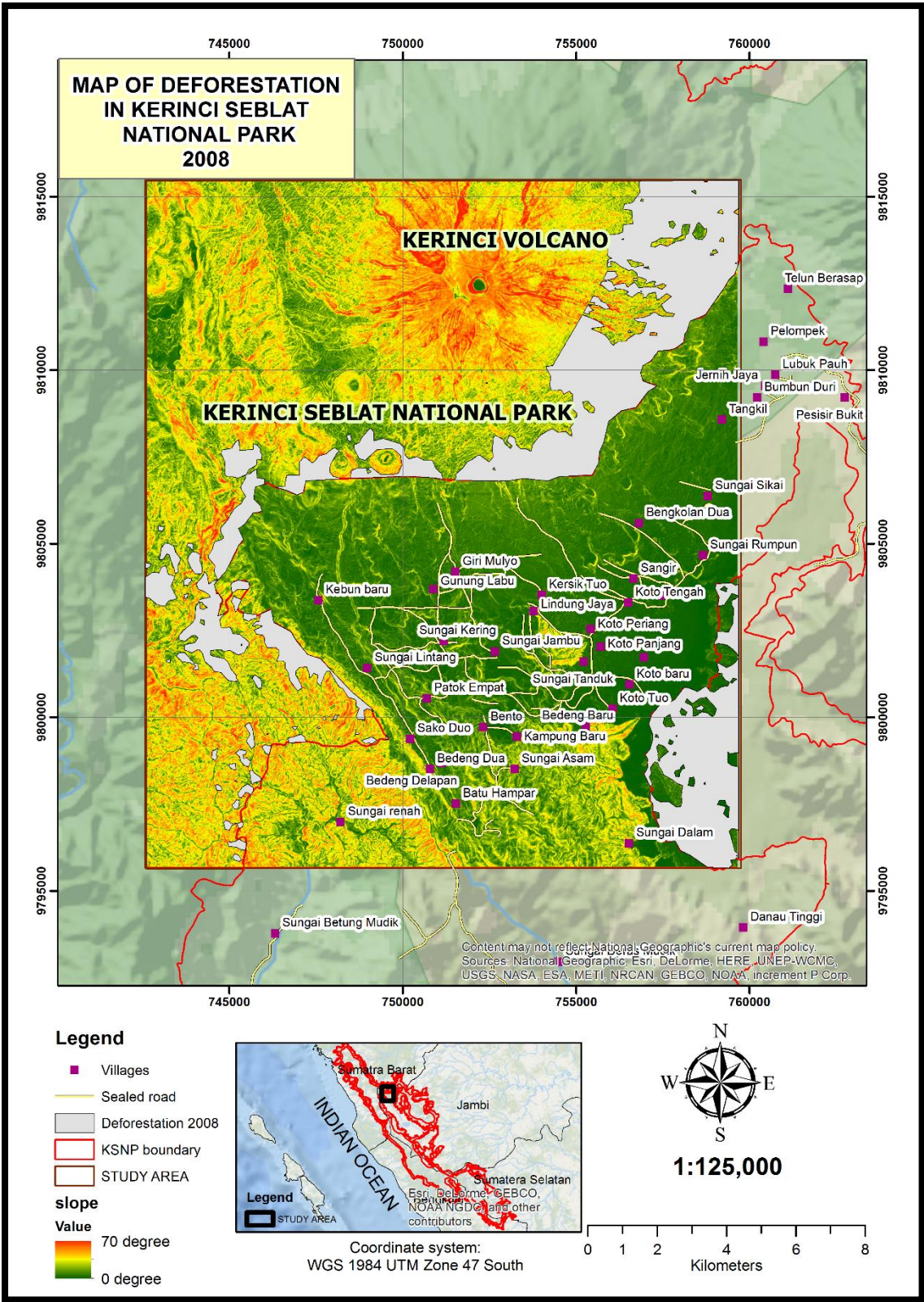
MAP 3: Deforestation within National Park in 2008
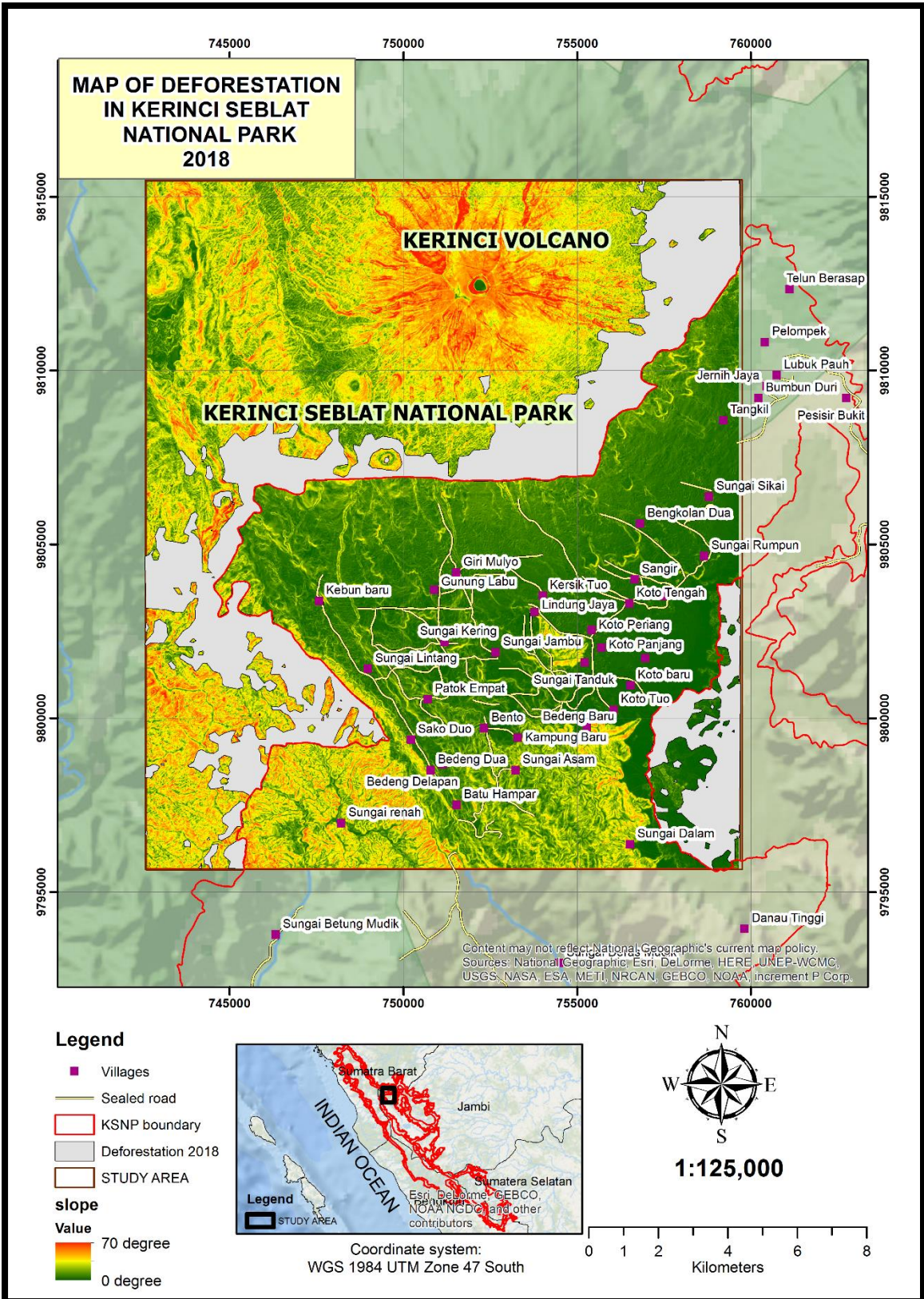
MAP 4: Deforestation within National Park in 2018

4.3.2 Change detection

By applying the change detection tool in ERDAS IMAGINE, the increased and decreased forest loss can be investigated by comparing two different date images. Table 23 shows that there is a significant change between the image of 1998 and image of 2018 (20 years period). It can be seen that the forest loss increases around 2700 hectares and decreased at around 393 hectares. Such loss occurred throughout the boundary of the national park that can be detected in MAP 5.

Table 23: Deforestation change from 1998 to 2018

1998 - 2018	Area (Hectares)
Increased	2700.27
Decreased	393.77

KERINCI VOLCANO

KERINCI SEBLAT NATIONAL PARK

Telun Berasap

Pelompek

Lubuk Pauh

Jernih Jaya
Bumbun Duri

Tangkil

Pesisir Bukit

Sungai Sikai

Bengkolan Dua

Sungai Rumpun

Giri Mulyo

Sangir

Gunung Labu

Kersik Tuo

Koto Tengah

Kebun baru

Lindung Jaya

Koto Periang

Sungai Kering

Sungai Jambu

Koto Panjang

Sungai Lintang

Koto baru

Patok Empat

Sungai Tanduk

Koto Tuo

Bento

Bedeng Baru

Sako Duo

Kampung Baru

Bedeng Dua

Sungai Asam

Bedeng Delapan

Batu Hampar

Sungai renah

Sungai Dalam

Sungai Betung Mudik

Danau Tinggi

Content may not reflect National Geographic's current map policy.
Sources: National Geographic, Esri, DeLorme, HERE, UNEP-WCMC,
USGS, NASA, ESA, METI, NRCAN, GEBCO, NOAA, increment P Corp.

Legend

- Villages
- Sealed road
- KSNP boundary
- STUDY AREA

Deforestation trend

- Decreased
- Increased
- Unchanged

slope

Value

70 degree

0 degree

INDIAN OCEAN

Sumatra Barat

Jambi

Sumatera Selatan

Bengkulu

Esri, DeLorme, GEBCO,
NOAA NGDC, and other
contributors

Legend
STUDY AREA

N
W E
S

1:125,000

Coordinate system:
WGS 1984 UTM Zone 47 South

0 1 2 4 6 8
Kilometers

MAP 5: Change detection 1998 to 2018

4.4 SPOT-6 IMAGE PRE-PROCESSING

4.4.1 Mosaicking
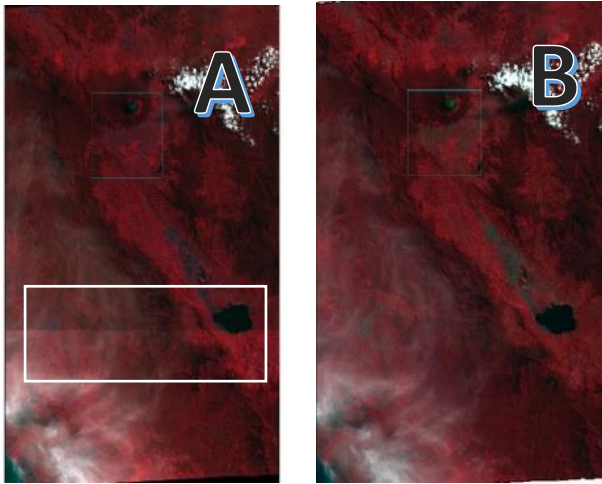
Figure 46: Mosaic images

Figure 46 displays the discrepancy between the loading process through metadata and separate loading between two images. Part B shows a seamless image from two images. However, in Part A, it can be detected that there is a seam between two images shown in the white rectangle. Two images in Part requires mosaic processing to merge between the images.

Not only two or more images, but ENVI software can also load all separated images into one file through a metadata file (XML extension). Therefore, by using ENVI software, mosaic processing is not required in this study.

4.4.2 Radiance Calibration

This step was utilised to calibrate the image by turning the digital number of pixel data to radiance unit (Wµm-1 m-2 sr-1). ENVI software can detect automatically the original equation used to convert digital number to radiance unit, but it requires to load metadata file. Otherwise, ENVI applies a default formula for the radiance conversion. Figure 47 shows the location in the SPOT-6 image of 2013 that was used to detect the pixel value change between the original and radiance image. Table 24 (below) displays the change of pixel value between the original value and the

Figure 47: Radiance Image

radiance image. It can be seen that the value of the pixel of the radiance image is

lower than the original image. In this case, ENVI divided the digital number with a gain value of each to generate a new pixel value of radiance image (DN/Gain value)/10. The value often is used as a scale factor for the subsequent processing through the FLAASH tool. Otherwise, such value can be removed.

Table 24: Digital number image of 2013

Before	After
Band 4: 1002 (Gain: 14)	Band 4: 7.1
Band 3: 256 (Gain:10.44)	Band 3: 2.4
Band 2: 351(Gain:9.6)	Band 2: 3.6

4.4.3 Surface reflectance

The Surface reflectance value obtained from FLAASH processing is unitless and ranges between $0 - 1$. Visually, there is a significant discrepancy between the original images with surface reflectance image, which is brighter than the original scenes. By using spectral profile and vegetation index (NDVI), it can be seen that the surface reflectance image value is higher than the original scenes shown in Figure 48. In part A, the NDVI value original image of 2013 is 0.65, and in part, B shows that the surface reflectance image is 0.81 (sample location located at X: 750702, Y: 980624, UTM Zone 47S). While, the NDVI value original image of 2018 in part C is 0.58, and the NDVI value of the surface image is at 0.67 in part D. The Spectral profile also has a slight difference between the original image and surface reflectance image shown in Figure 48.
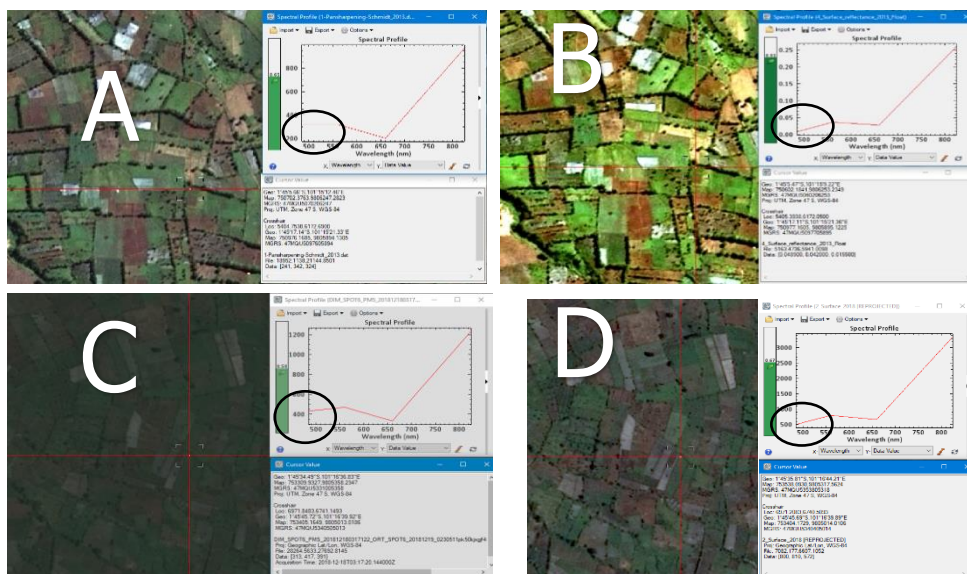
Figure 48: Spectral Profile image of 2013 and 2018

4.4.4 Projection

The geographic coordinate system of all of the vectors and raster data in this study was formatted into Universal Transverse Mercator (UTM) Zone 47 projection that be used to simplify the subsequent image processing. However, SPOT-6 image of 2018 is stored in latitude and longitude geographic coordinate system (Lat/long). Therefore, the conversion of the system was applied to obtain a new projection. Table 25 portrays the difference between Lat/long coordinate system and a new image with UTM as a coordinate system. Such coordinate value was obtained from the SPOT-6 image of 2018.

Table 25: Coordinate position before and after converting projection

	Original Image		The image with new projection	
Image Code (2018)	Longitude (UL*: X)	Latitude UL: Y	UTM Easting	UTM Northing
R2C2	101.0550	-1.57406944	728633.62	9825904.98
R2C3	101.2256	-1.5740694	747623.34	9825885.48
R3C2	101.0550	-1.7731805	728610.54	9803882.70
R3C3	101.2256	-1.7731805	747598.34	9803860.74
Projection	Geographic (Lat/Lon)		UTM Zone 47 South	
Units	Degrees		Meter	

*UL: Upper Left of image

4.4.5 Image Pansharpening
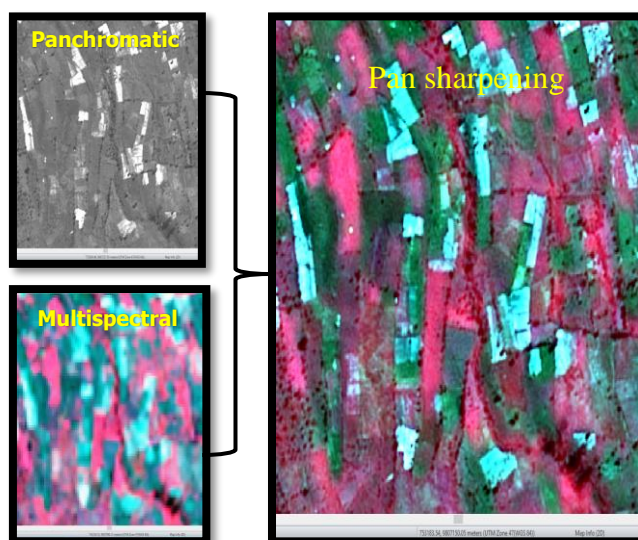
Figure 49: Pan-Sharpening

Figure 49 exhibits the visual comparison between a panchromatic image with high spatial resolution and multispectral image with low spatial resolution. By using ENVI version 5.2, these two images can be sharpened using Gram-Schmidt Pan sharpening. This approach is suitable sharpening process to obtain good results (Laben et al. 2000).It can be seen

that the computation of two different resolution can generate a new image with the spatial resolution with various of colour.

4.4.6 Cloud Masking

The study area is located in the foothill of the mountain. The cloud mostly covers this area throughout the year due to its location at high altitude and tropical region. Therefore, there is less collection that provides free-cloud images. The image recorded in December 2018 was mostly covered by thick cloud. Thus, such clouds mostly impede the information throughout the boundary of the national park. Supervised classification approach is used to generate binary classification with two classes; cloud and non-cloud. Multiplication method between the study area and binary non-cloud image creates an image with no cloud shown in *Table 26*. It can be observed that the free-cloud image is brighter than the original image. It is because of the change of distribution and the range of pixel value within the image.

Table 26: Cloud masking result

Before (Image of 2018)	After (Image of 2018)
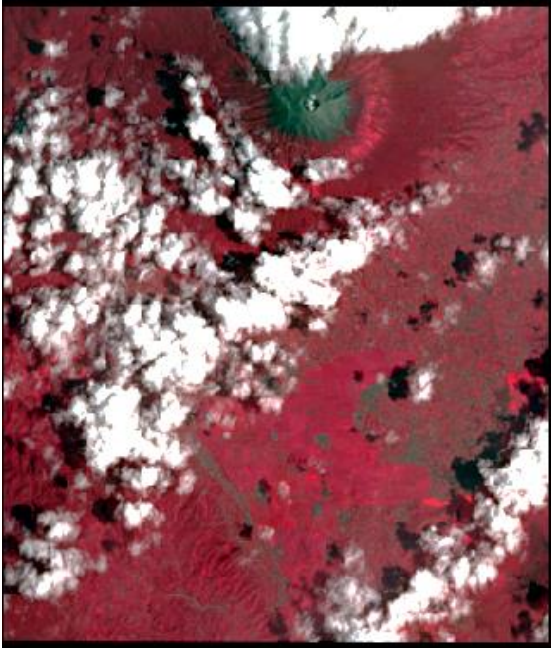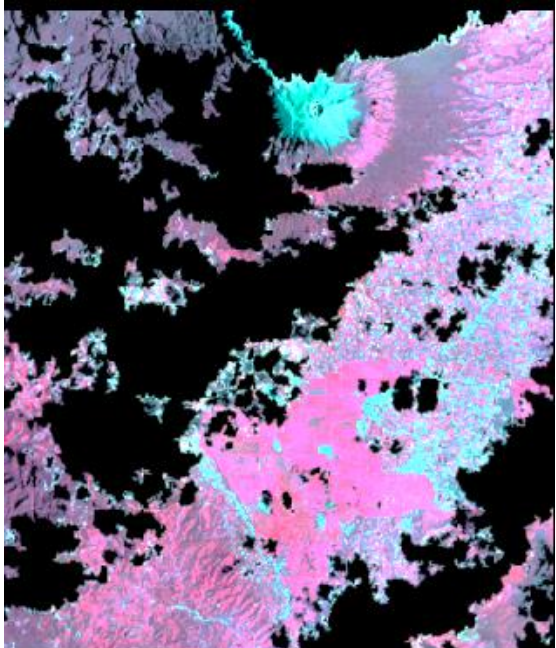
4.4.7 Geometric evaluation

The process of geometric evaluation was operated to confirm that the satellite image has the right position on the surface of the Earth. In general, the result of the geometric assessment was revealed in Table 27 and Table 28 implies no geometrically

significant differences between GCPs data and SPOt-6 2018 Image. The average of RMSE is 1.49 m and 1.46, where such value is below the spatial resolution of the image at 1.54 metre.

Table 27: Geometric Evaluation image of 2018

ID	X_i	$Y_{i.}$	X_r	$Y_{r.}$	RMSE
1	755533.19	9801179.45	755532.91	9801181.2	1.77
2	753040.14	9801149.05	753040.66	9801149.33	0.59
3	754058.33	9803581.86	754056.94	9803580.93	1.67
4	751552.94	9802824.29	751552.33	9802822.8	1.61
5	752253.36	9803138.49	752253.88	9803136.6	1.96
6	756725.09	9801744.09	756724.33	9801742.45	1.81
7	757025.15	9802024.52	757025.44	9802022.85	1.69
8	757208.59	9802364.16	757208.12	9802364.35	0.51
9	756424.27	9803224.16	756423.43	9803222.97	1.46
10	754316.91	9803019.69	754315.17	9803019.2	1.81
RMSE (Average)					**1.49**

Table 28: Geometric Evaluation image of 2013

ID	X_i	$Y_{i.}$	X_r	$Y_{r.}$	RMSE
1	755533.15	9801179.3	755532.91	9801181.2	1.92
2	753040.11	9801149.05	753040.66	9801149.33	0.62
3	754058.43	9803581.83	754056.94	9803580.93	1.74
4	751552.44	9802824.29	751552.33	9802822.8	1.49
5	752253.37	9803138.27	752253.88	9803136.6	1.75
6	756725.09	9801744.09	756724.33	9801742.45	1.81
7	757025.12	9802024.52	757025.44	9802022.85	1.70
8	757207.85	9802364.16	757208.12	9802364.35	0.33
9	756424.27	9803224.14	756423.43	9803222.97	1.44
10	754316.91	9803019.61	754315.17	9803019.2	1.79
RMSE (Average)					**1.46**

4.5 SPOT-6 - DIGITAL IMAGE PROCESSING

This chapter describes the results gained from various steps of image processing performed in the previous chapter. It is organised into four-six main stages: 3. Accuracy assessment; and 4. Change detection

4.5.1 Creating Segmentation file

FLS segmentation parameters used to generate segmentation image as follows; Segment ratio 1500, Spectral 0.5, Texture 0.8, Size 0.9, Shape 0.8, Minimum 20 and Maximum 100000. Figure 50 informs the result of creating a segmentation image through FLS segmentation tool provided by ERDAS IMAGINE software. It can be seen that both image 2013 and 2018 segmentation can create a general pattern of land use in the study area.
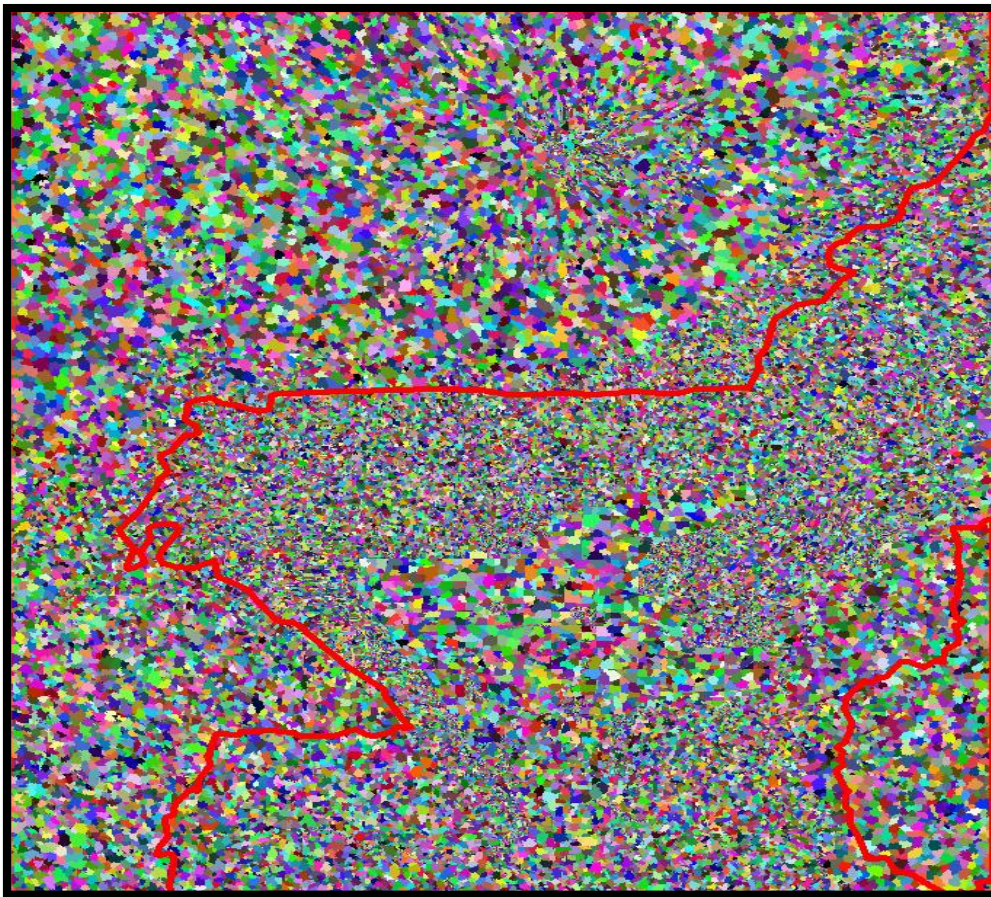
Figure 50: Segmentation of 2013

4.5.2 Classification using Machine Learning (Image of 2013)

The final result of image classification of 2013 using machine learning generated segmentation with eight types of classification. Such classification consists of forest, agriculture, fallow, pasture, rocks/ settlement/plastic shade, shrubs, tea plantation, and water body. The result of classification can be found in

Table 29, and the details of the map can be seen in Appendix 4.

Table 29: Classification image of 2013

Id	Class	Area (hectares)	%
	No data	7.56	0.02
1	**Forest**	**18993.40**	**56.0**
2	Agriculture	3818.52	11.3
3	Fallow	4844.15	14.3
4	Pasture	682.77	2.0
5	Rocks/Plastic/built-up/road	1693.42	5.0
6	Shrubs	1156.76	3.4
7	Tea	2444.52	7.2
8	Water Body	280.37	0.8
	Total	33921.47	100.00

4.5.3 Crops/ Agriculture Activities in Kerinci Seblat National Park (2013)

Inside the national park, there is the fourth type of classification that can be detected using machine learning classification. Such classes were derived from the detailed image of 2013 through machine learning. The tool used to separate the boundary of the park is the clip provided by Arc Map software. There is four class within the national park that consists of agriculture, plastic shade, fallow and pasture. The total of classification inside the park is around 4033.72 hectares, which can be categorised as the number of forest loss. While the total number of segmentations is 10501, which is used by the owner of the land to farm in such area shown in *Table 30*.

Table 30: The segmentation of deforestation throughout the boundary of the national park (Image of 2013)

Class	Number of segmentations	Area (Hectares)	Percentage (%)
Agriculture	1677	687.69	17.05
Plastic shade	4930	1298.43	32.19
Fallow	2579	1298.43	32.19
Pasture	83	37.55	0.93
Shrubs	1235	711.62	17.64
TOTAL	10501	4033.72	

Figure 51: Segmentation of farming area (Drone recorded on February 2019)

The number of farming owner inside the national park can be detected through the existence of a combination of such classes. Figure 51 (yellow polygon) obtained from fieldwork held in February 2019 using Drone, displays the number of segments in the particular owner of the farming land. It can be seen that the number of segments is eight segments, which consist of plastic shade, agriculture, fallow, and pasture. Otherwise, the number of segments for each landholding varies from 10 - 20 segments. It can predict the number of landholdings within the national park in 2013 varies from 463 - 926 owners (considering the average segment of 10 – 20 for each farmer). Term of the presence of cropping activities inside the national park can be categorised as follows: High possibility of cropping consists of agriculture, and plastic shades class and low possibility of cropping contain fallow and pasture class. The existence of agriculture and plastics class shows that the cropping is functioning in such an area. It also can be categorised as permanent farming land. While fallow, shrubs and pasture class can be considered as temporary farming land. MAP 6 shows the comparison between the high possibility and low possibility of crop existence in 2013.

CROPS POSSIBILITY MAP
IN KERINCI SEBLAT NATIONAL PARK
IN THE YEAR 2013

Sumatra Barat

KERINCI VOLCANO

KERINCI SEBLAT NATIONAL PARK

Pelompek
Lubuk Pauh
Bumbun Duri
Tangkil

Sungai Sikai
Bengkolan Dua
Sungai Rumpun

Giri Mulyo
Gunung Labu
Kebun baru
Jambi
Kersik Tuo
Lindung Jaya
Sangir
Koto Tengah
Koto Periang
Sungai Kering
Sungai Jambu
Koto Panjang
Sungai Sampun
Sungai Lintang
Sungai Tanduk Koto baru
Patok Empat
Koto Tuo
Bedeng Baru
Bento
Kampung Baru
Sako Duo
Bedeng Dua
Sungai Asam
Bedeng Delapan
Batu Hampar
Sungai renah
Sungai Dalam

Legend
Villages
Sealed road
High possibility
Low Possibility
KSNP boundary

Sumatra Barat
Jambi
INDIAN OCEAN
Bengkulu
Legend
STUDY AREA

N
W   E
S

1:100,000

0 0.75 1.5   3   4.5   6
Kilometers

Coordinate system:
WGS 1984 UTM Zone 47 South

MAP 6: Cropping activities within the national park (2013)

MAP 7: Segmentation inside the national park (2013) shows the forest loss inside the national park. The land use in such area consists of eight classes such as agriculture, fallow, and shrubs.
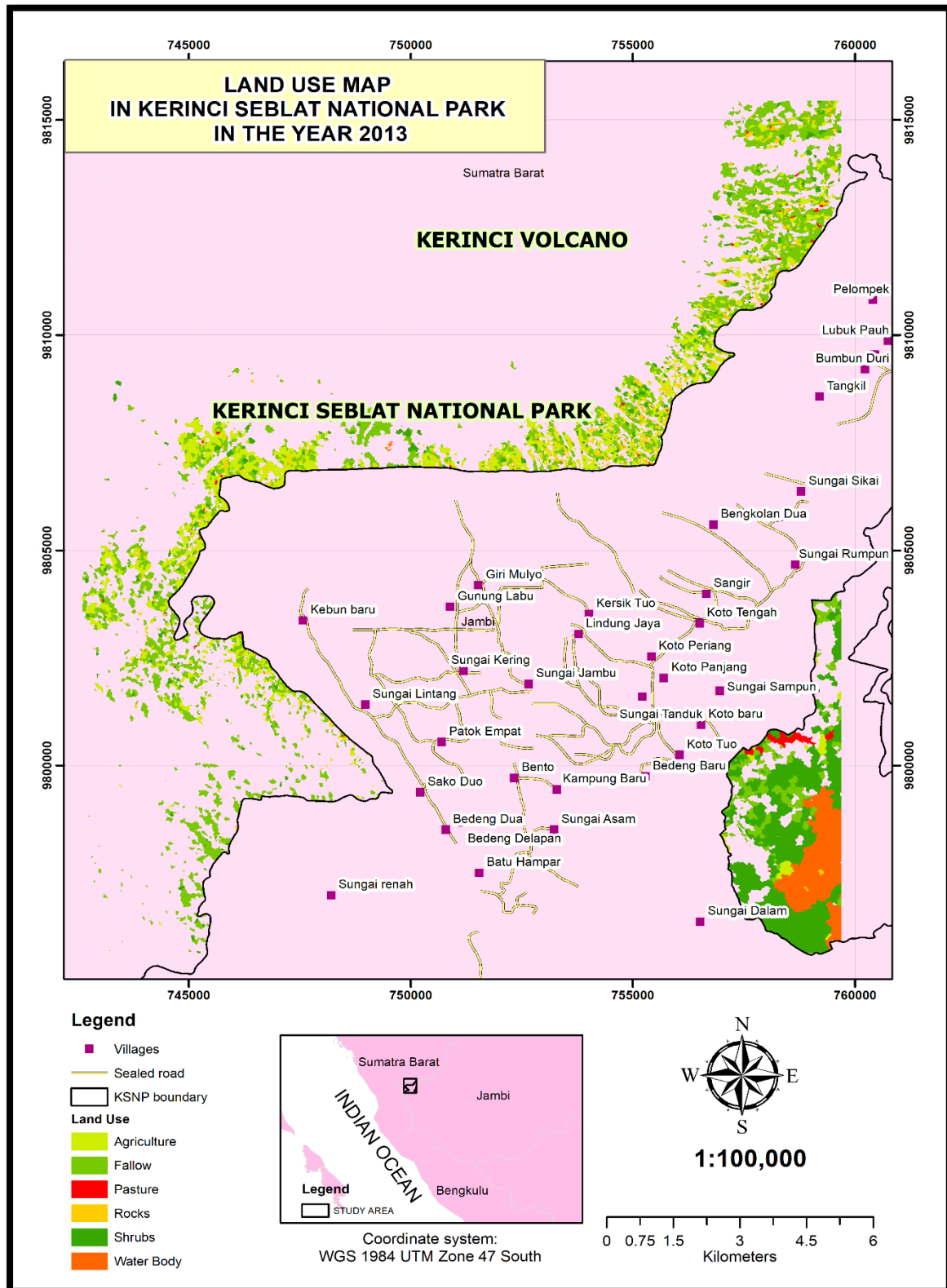
MAP 7: Segmentation inside the national park (2013)

4.5.4 Classification using Machine Learning (Image of 2018)

The SPOT-6 image of 2018 mostly covered by cloud at around fifty per cent of the total area of the study area. Therefore, some spots both inside and outside of the park cannot be classified. Overall, in the study area consist of seven classes that can be determined such as agriculture, fallow, forest, pasture, plastic shade/rocks, shrubs, and tea plantation shown in *Table 31* and Appendix 5

Table 31: Classification of SPOT 2018

	Class	Area (Hectares)	%
	No data	**15816.01**	**46.6**
1	Agriculture	2050.10	6.0
2	Fallow	1048.06	3.1
3	**Forest**	**7587.42**	**22.4**
4	Pasture	227.94	0.7
5	Pyroclastic	2179.83	6.4
6	Shrubs	2920.98	8.6
7	Tea	2091.13	6.2
	Total	33921.47	100.0

In term of the national park area, there are fourth land-use type which can be recognised inside the national park that includes agriculture, plastic shade, fallow and shrubs. The total of such classes/ segmentation is around 1997 with the number of segmentations is around 4258. Such a number can be ascertained as forest loss in Kerinci Seblat National Park. The image of 2013 classification details shown in *Table 32*.

Table 32: Segmentation of deforestation inside the national park in 2018

Class	Number of segmentations	Area (Hectares)	%
Agriculture	315	582.56	29.17
Plastic shade	3132	378.35	18.94
Fallow	178	146.57	7.34
Shrubs	633	890.24	44.57
	4258	1997.2	

MAP 8: Segmentation inside the national park (2018) portrays the land use inside the park. Due to the area mostly covered by cloud, the detecting segmentation of mostly in the northwest of the study area shown black rectangle in the map.
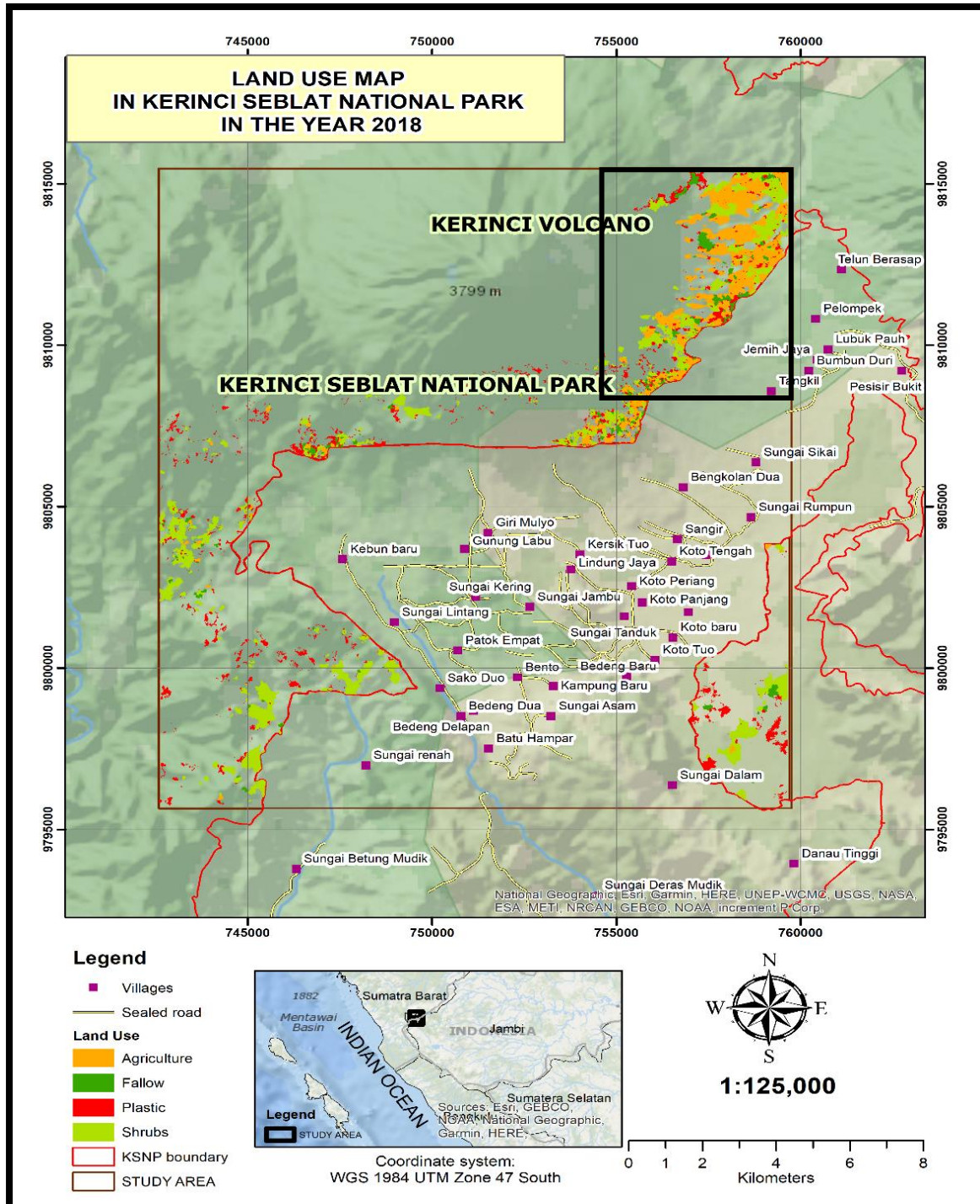
MAP 8: Segmentation inside the national park (2018)

4.5.5 Accuracy Assessment of SPOT-6 Imagery

The overall classification accuracy of Spot-6 images of 2013 is 85.29 % that is shown in Figure 52. The producer's accuracy informs the comparison between corrected classification and reference data (total column). On the other hand, User's accuracy is the comparison between fixed classification and classified data (entire row). It can be seen that the classes that have higher both users' and producer's accuracy are water body and forest class at around 97 % and 94% for producers' accuracy and around 92% for user's accuracy. The lowest percentage consist of three class such as fallow, agriculture and pasture ranges between 74% - 80% both for user's and producer's accuracy. The overall Kappa statistics is at 0.8, meaning that such classification can be categorised as a substantial agreement.

```
ACCURACY TOTALS - SPOT-6 IMAGE OF 2013
----------------

          Class  Reference      Classified    Number  Producers    Users
           Name     Totals          Totals   Correct  Accuracy   Accuracy
    ----------  ----------      ----------   -------  ---------   -----
                         0               0         0       ---        ---
        Forest         50              51        47    94.00%     92.16%
   Agriculture         51              51        40    78.43%     78.43%
        Fallow         48              51        38    79.17%     74.51%
       Pasture         55              51        43    78.18%     84.31%
  Rocks_Plastic        46              51        45    97.83%     88.24%
        Shrubs         56              51        45    80.36%     88.24%
           Tea         54              51        43    79.63%     84.31%
    Water Body         48              51        47    97.92%     92.16%

        Totals        408             408       348

Overall Classification Accuracy =     85.29%

              ----- End of Accuracy Totals -----



KAPPA (K^) STATISTICS
---------------------

Overall Kappa Statistics = 0.8319
```

Figure 52: Accuracy Assessment report image of 2013

Figure 53 portrays the accuracy assessment report of SPOT-6 image of 2018. The overall classification accuracy is 85.71 % with the overall kappa statistics 0.83 (strong agreement). Two classes have higher accuracy than other classes, that is forest and plastic shade/rocks/settlement class. The percentage is 88 % and 94% for producer's accuracy respectively. The user's accuracy is 90% and 92% respectively. The lower accuracy is agriculture, shrubs, and tea class.

```
ACCURACY TOTALS SPOT-6 IMAGE OF 2018
-----------------

        Class  Reference      Classified      Number  Producers      Users
         Name     Totals          Totals     Correct   Accuracy   Accuracy
   ----------  ---------      ----------     -------  ---------    ------

                        0               0          0       ---        ---
  Agriculture          53              51         44    83.02%     86.27%
       Fallow          49              51         42    85.71%     82.35%
       Forest          52              51         46    88.46%     90.20%
      Pasture          47              51         41    87.23%     80.39%
  Plastic_rock         50              51         47    94.00%     92.16%
       Shrubs          55              51         42    76.36%     82.35%
          Tea          51              51         44    86.27%     86.27%

       Totals         357             357        306

Overall Classification Accuracy =      85.71%

            ----- End of Accuracy Totals -----



KAPPA (K^) STATISTICS
---------------------

Overall Kappa Statistics = 0.8333
```

Figure 53: Accuracy Assessment report image of 2018

4.6 SPOT-6 Post Image processing

4.6.1 Dissolve

By using the dissolve tool in Arc Map, the segmentation that exists in the classified image of 2013 can be removed. All the similar class in such segmentation merge and form a new polygon that shown in MAP 9 and MAP 10.
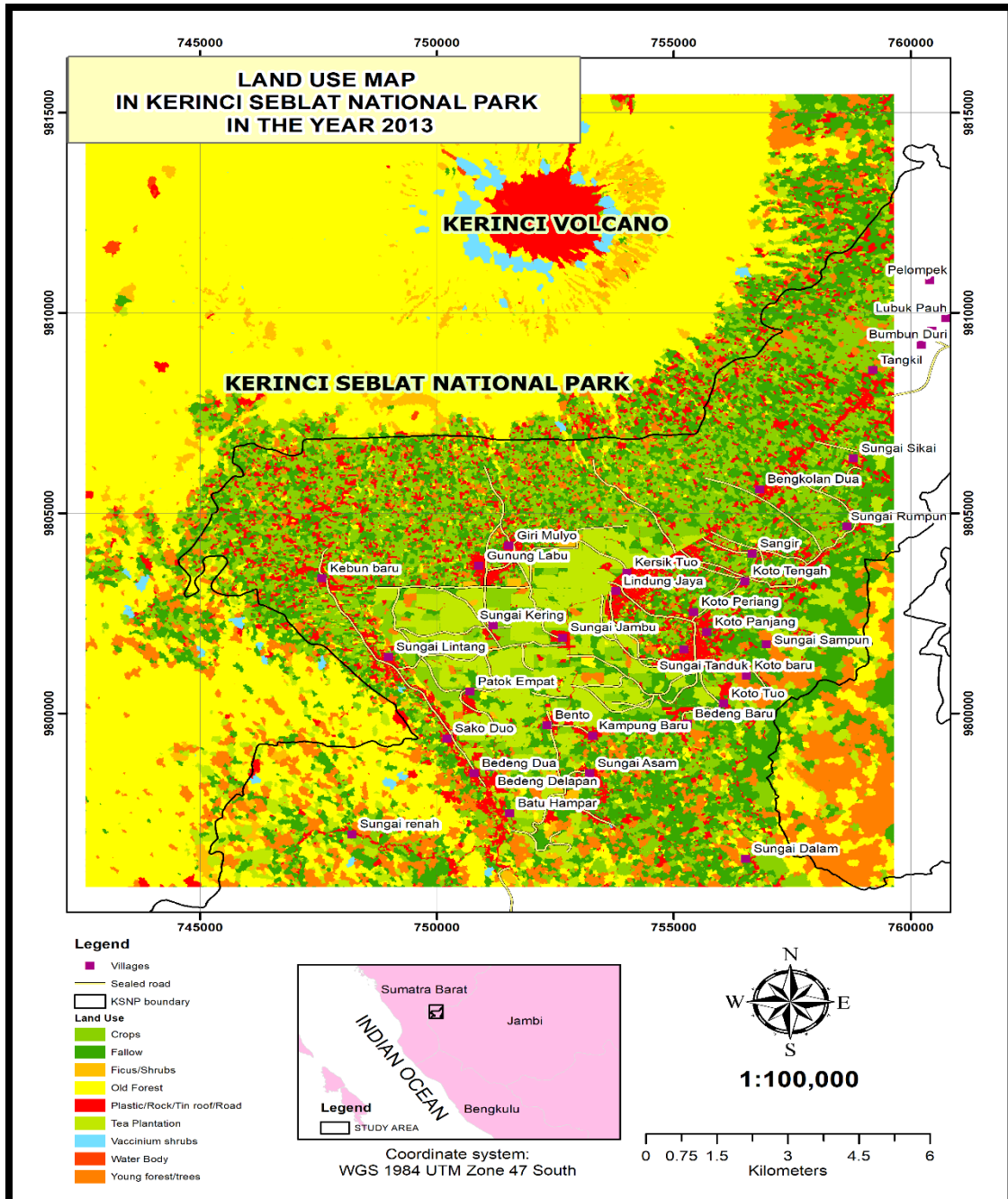
MAP 9: Dissolve Class image of 2013

LAND USE MAP
IN KERINCI SEBLAT NATIONAL PARK
IN THE YEAR 2018

KERINCI VOLCANO

KERINCI SEBLAT NATIONAL PARK

Legend

Villages
Sealed road
KSNP boundary
Land Use
Coffee Plantation States
Crops
Fallow
Ficus/shrubs
Old Forest
Plastics/Rocks/Tin roof/ road
Tea Plantation States
Vaccinium shrubs
Young Forest/trees

Sumatra Barat

INDIAN OCEAN

Jambi

Bengkulu

Legend
STUDY AREA

Coordinate system:
WGS 1984 UTM Zone 47 South

1:100,000

0   0.75 1.5   3   4.5   6
Kilometers

MAP 10: Dissolve image of 2018

V. DISCUSSION

5.1 LANDSAT - PRE-PROCESSING

5.1.1 Geometric evaluation

The Landsat images level-2 downloaded from the USGS were geometrically adjusted by USGS using GCP and digital elevation model. The Root Mean Square Error (RMSE) information can be found at each image metadata files. According to USGS (2019a), the accuracy of image correction relies on two factors, the quality of image and distribution of ground control points (GCP). Lunetta et al. (1999) argued that the classification which aimed to analyse the change detection requires threshold RMSE value at 0.5 pixels or around 15 metres. The geometric calculation provided by USGS was 0.18 and 0.17 for the image of 1998 and 2008, respectively. By using ten sharp points, the geometric correction for the image of 2018 was 1, 63 pixel or around 4.90 metres. It indicates that the image of 2018 was geometrically correct, and such value was under the determined threshold value that was used for change detection.

5.1.2 Cloud Masking

According to USGS (2019b), QA band does not always provide suitable information on cloud and shadow. The CF Mask algorithm has issues to determined, bright targets such as building roof, snow, sand, thin cloud, and so forth. For example, the image of L7-08 presents no cloud, as shown in part A, Figure 54. However, the Cloud Mask algorithm classified such area as the cloud depicted in part B. Therefore, and such area is classified as no data (zero) portrayed in part C. It means that QA band is not always similar t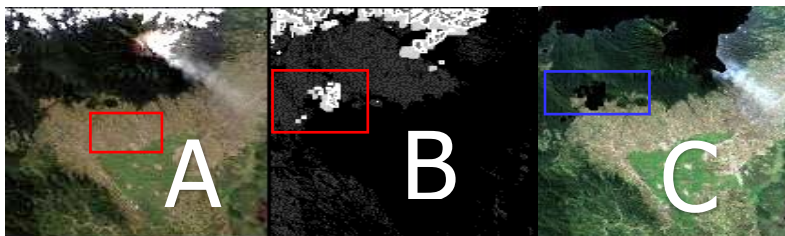o multispectral image. Nevertheless, in general, the QA band can be applied to mask the cloud throughout the Landsat images.

Figure 54: Cloud Mask issues

5.1.3 Gap Filling

According to Potić (2015), NASA has not been successful in amending SLC malfunction of the Landsat 7 Enhanced Thermal Mapper Plus (ETM+) that generate such problem to be perpetual. The gaps span around 14 pixels near the edges (Potić 2015).

In this study, the focal analysis was applied to fill in the gaps throughout the image. The image of 2018 has gaps 11 pixels or 330 metres in length. The focal analysis provided by ERDAS IMAGINE software can be used to fill in such zero value to a new specific value. This function also has three types of window size consists of 3 x 3, 5 x 5 and 7 x 7 window. The window 3 x 3 consist of 9 pixels or 270 metres of the gaps (Landsat pixel = 30 metres). It means that the window cannot complete the fill in the gaps in 330 metres in length. Such a window requires two times to fill in all gaps throughout the images. However, the second process can reach 540 metres, but it affects the non-zero pixels. It around 220 metres, the non-zero pixels changed to new values. The pixel window 5 x 5 has the pixel 25 pixels or 750 metres in length. It means that they fill the gaps process requires only one time to fill in all zeros value. However, this process also changed the non-zero value with a new value based on the statistical mean function. By using the 5 x 5-pixel window, it can be seen that the pixels which were located around 440 metres from the boundary of the gaps were changed to the new pixel value.

5.2 LANDSAT - DIGITAL IMAGE PROCESSING

5.2.1 Maximum Likelihood Classification (MLC)

According to Apan (1997), Maximum likelihood Classification has conventionally been used as a standard for extraction of remotely sensed data. This approach presumes that multivariate normal distribution (Gaussian Model) can delineate spectral class throughout the remotely sensed image. Richards (2013) argues that the Maximum Likelihood Classification (MLC) is the most accurate classifier set against parallelepiped. However, the classifier also has disadvantages as follows (ERDAS 1999):

a. Slower computation compared to minimum distance and parallelepiped

b. The classifier inclines to over classify spectral signatures.

c. It depends profoundly on the normal distribution of the image.

Gilani et al. (2015) argued that Maximum Likelihood Classification (MLC) is appropriately used to classify land use and land cover change because such classifier has simplicity and high efficiency in computation. This research also has shown that the classifier can differentiate between forest and non-forest. The separability of each class can be performed by determining the minimum threshold value of Jeffries-Matusita distance in 1380. In this study, all of the three images shown that the distance between the classes varies from 1411 to 1413. This threshold Jeffries-Matusita value means that between forest and non-forest classes reasonably separate.

In term of classification, the total area of the Landsat image of 2018 was similar to the total area of the study area at around 33,865 hectares. However, the total area of the image of 1998 and 2008 was less than in 2018. It caused in some places were covered by cloud. In this case, such an area was categorised as an unclassified pixel with zero value. Nevertheless, in general, the upward trend of deforestation continues over the year.

5.2.2 Accuracy Assessment of Landsat Imagery

The reference data was obtained by applying the stratified random point selection. Such points then are divided equally for forest and non-forest class. It can be seen that the classification of three remotely sensed images has accuracy at the range between 87% and 90%. The Kappa statistic value of three Landsat images varies from 0.7 to 0.8. According to Landis et al. (1977), the Kappa statistic spans from 0.6 to 0.8 can be categorised as moderate agreement. It means that matrix error is less for such classification.

Visually, the difference between forest and forest can be distinguished through the human's view. It is caused by the forest colour reasonably different compared to the other classes within the study area. The forest also can be categorised as an old-growth forest and the other mostly classified as a new growth plantation, settlement and bare land. Siitonen et al. (2000) contended that the forest ages between 129 and 198 years could be considered as the old-growth forest that can be seen in three

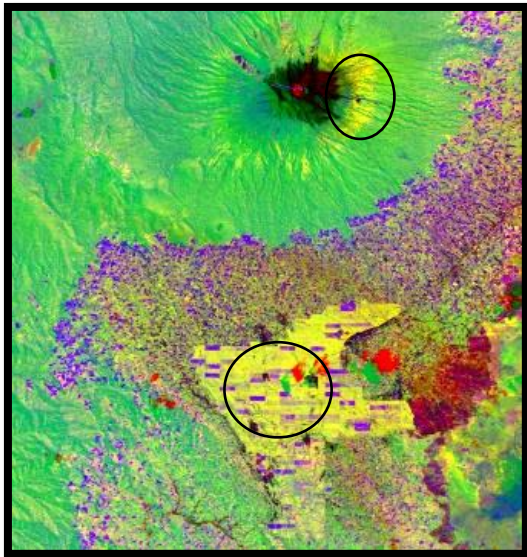images used in this study. Therefore, due to the existence of the outstanding difference between forest and no-forest, the overall classification assessment in this study can reach a high percentage of accuracy at around 88%. However, an addition of the number of classes in particular within the non-forest class can decrease the accuracy of the classification. For example, in Figure 55 (black circle) describes that between tea plantation and other shrubs around the peak of the volcano shown similar spectra. It is also quite demanding to differentiate between shrubs and other types of agriculture with similar spectra. It can be concluded that in the case of the image with lower spatial resolution, the higher the number of classes, the lower classification accuracy can be achieved. Therefore, in obtaining high accuracy and details, such issues can be overcome by using remotely sensed image with high spatial or spectral resolution.

Figure 55: Landsat-5 image of 1998

5.2.3 Change detection

The yellow rectangle, as shown in Figure 56 describes that deforestation and change detection using the image of the 2008 area could not be computed due to the area was covered by cloud. Therefore, deforestation trend in such an area could be shown an upward or downward trend. By using the measurement tool in ArcGIS, the extent of the area is around 200 hectares. However, by using the Google Earth image that
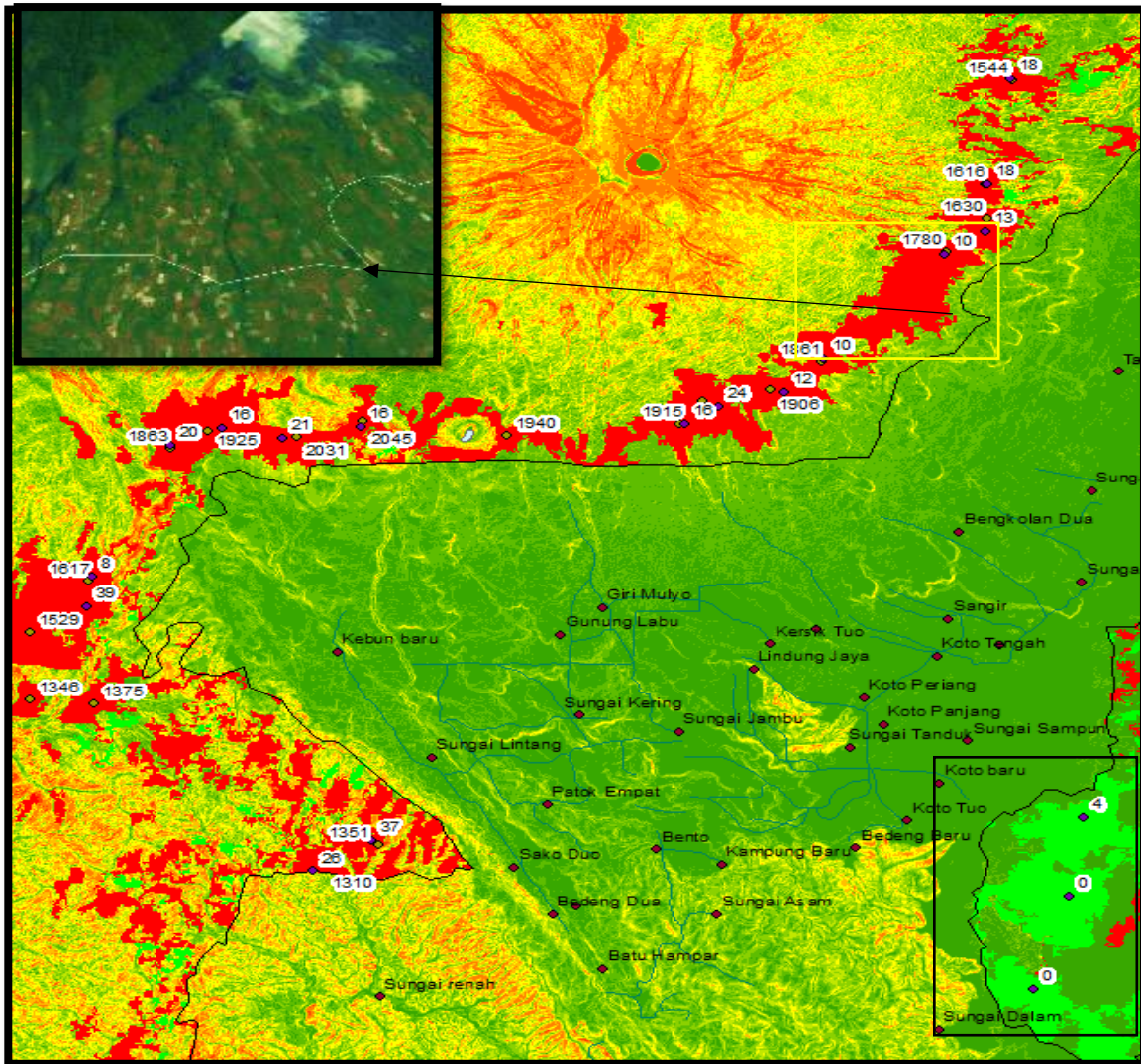
Figure 56: Deforestation around the boundary of the park

was recorded on 6 April 2018 (Inset of Figure 56), it reveals that such an area can accommodate categories as the increasing deforestation. The wetland Swamp forest marked with a black rectangle in figure 33 indicates deforestation is decreasing over the year. According to Kurniati (2008), the area is a wetland which comprises of grassy and weedy area. The area has a lot of old trees, but the size is small due to wet habitat. There is no agriculture area found in this area, but illegal logging occurred in small scale. In general, deforestation could be found in the area, but it did change the overall landscape of the area.

By extracting information from the Digital Elevation Model, it can be seen that the increase of deforestation is located with the average slope varies from 10 to 20 degrees Figure 56. The attitude of the area varies from 1300 meters to 2031 meters above sea level.

5.3 SPOT-6 IMAGE PRE-PROCESSING

ENVI software can perform three types of conversion of the image, such as radiance, TOA reflectance, and Surface Reflectance. Such processing is faster compared to manual calculation using spatial model editor provided by spatial ERDAS IMAGINE. Radiometric calibration and FLAASH tool provided by ENVI was performed in this study to generate a radiance image that then was applied as an input in FLAASH that was applied to create a surface reflectance image.

To generate the image that can be converted to radiance or reflectance image, ENVI provides two options; importing data through metadata, or converting the interleaved of the image that stored with ENVI format. For example, ENVI stores the image slightly different compared to ERDAS IMAGINE. Such software saves the image with Band Interleaved by Line (BIL) and Band Interleaved by Pixel (BIP) format. Conversely, ERDAS IMAGINE saves the image with Band Sequential (BSQ) format. However, the second option requires all parameters such as Gain, Bias, Sun Elevation, irradiance value inputted through EDIT ENVI HEADER attached in ENVI toolbox. In this study, the importing data through metadata of the image is recommend being applied that make the following conversion easy to be performed.

According to Jensen, J (1996), many pre-processing software tools can be applied to improve the quality of the image through the pre-processing image. Such software tools consist of:

a. ACORN (Atmospheric Correction Now)
b. ATREM (The Atmospheric removal Program)
c. FLAASH (Fast Line-of-sight Atmospheric Analysis of Spectral Hypercube)
d. ATCOR (Atmospheric correction)

ATCOR, for instance, is provided by ERDAS IMAGINE software. It also can be used to generate surface reflectance. However, such a tool is purchased separately and not automatically included in ERDAS IMAGINE.

5.4 SPOT-6 DIGITAL IMAGE PROCESSING

5.4.1 FLS Segmentation

According to Aumeeruddy et al. (1994), the type of farmer landholding in Kerinci district can be divided into three main groups.

a. The farmer who owns crops area around 10 – 25 hectares categorised as large landholding.

b. Agriculturalist possesses an agriculture area between 5 and 10 hectares. It was classified as Medium landholding.

c. The farmer occupies the land less than 5 hectares categorised as Small landholding.
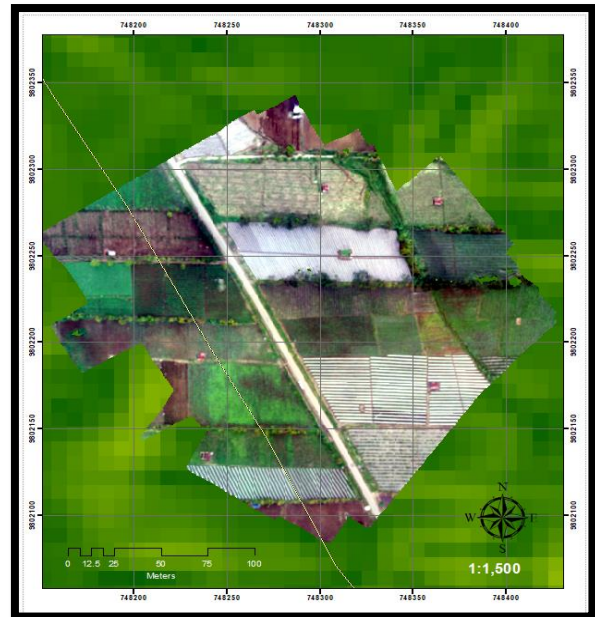
MAP 11: Segmentation of cropping
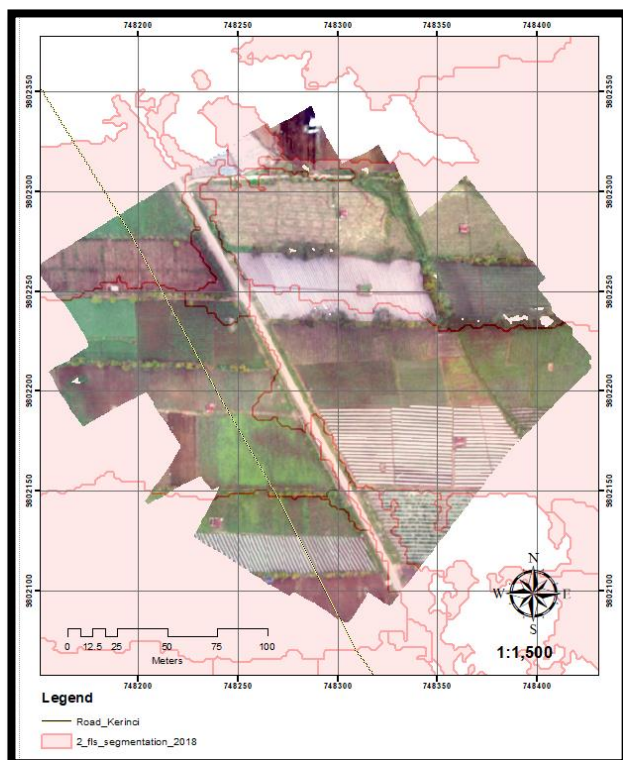
MAP 12: The comparison of FLS segmentation and high spatial image resolution

Based on fieldwork held in February 2018 using a drone shown in MAP 11, the extent of segmentation varies from 0.1 to 1 hectare that shown in MAP 11. It means that segmentation that created through FLS segmentation can represent the landholding of farming land. The number of segmentations can be the baseline to identify how many farmers who occupied such an area.

However, the best FLS segmentation results rely on the value of the relative weights such as spectral, texture, size, and shape. By

comparing FLS segmentation generated in this study with high spatial resolution captured by a drone shows that in one FLS segmentation consist of two or three farmers owned farming land shown in MAP 12. The farming landholding can be investigated for the future researcher used to obtain appropriate FLS segmentation.

5.4.2 Machine learning

The most exceptional classification result through machine learning determined by three aspects, FLS segmentation (or other methods of creating a segment), training data, and the classifier. In this study shows that segmentation and training data has a significant role in obtaining the most excellent result. According to Ong et al. (2001), the excellent segmentation derived from the image has a significant influence in generating a proper classification. Therefore, the classification through OOC, the approaches of determined segmentation can be achieved by using the other approaches of creating segmentation such as fuzzy segmentation, fuzzy region, and fuzzy-region segmentation.

The appropriate training data can be attained by collecting data in the field. A large number of sample point can contribute to obtaining a good accuracy of classification. Therefore, the machine learning approach can gain the maximum result of the application.

5.4.3 Spatial resolution

By using the pan-sharpening image, SPOT-6 images which 1.5-metre spatial resolution provide more information than Landsat, which has 30-metres spatial resolution. However, in this study, such an image cannot differentiate the different type of cropping such as chilli, tomato, between, potatoes and various type of cropping. It was caused by the distribution of such cropping was random. The farmer who has 1 to 5 hectares farming land, growth various type of cropping. Figure 57 taken on January 2019, portrays how the farmers mix all the cropping in the farming land such as coffee, potatoes, and cabbage in the range around 1 − 5

Figure 57: various cropping snapped by Drone

metres. Therefore, all the different type of cropping was grouped into one class, agriculture. It means that to classify such cropping requires the spatial resolution below one metre.

5.4.4 The comparison with previous studies.

This study can provide details information on cropping activities in a specific area within KSNP. The mapping and predicting deforestation pattern, which was conducted by Linkie, Smith and Leader-Williams (2004), shows similar patterns by which deforestation in KSNP tends to increase over the year. However, their research did not provide details information on cropping and other agriculture activities within KSNP, but it provided the pattern and trend of deforestation in KSNP. Moreover, such research also covered all area of the national park in four provinces, Jambi, Bengkulu, West and South Sumatra, which only present general information of deforestation.

VI. CONCLUSION

6.1.1 Research Findings and Outcomes

This research attempts to answer two main questions related to the change of landscape and understanding the structure of cropping activities within the Kerinci Seblat National Park in Indonesia. Overall, this study can achieve the general objectives and aims.

There are two types of satellite images used in this study that are Landsat imagery used to identify the change of cropping and SPOT-6 applied to distinguish the structure of cropping. SPOT image has a higher spatial resolution at 1.5 metres compared to Landsat scenes at 30 metres. Therefore, in identifying the structure of cropping, it requires the images with high spatial resolution. In term of the classifier, Maximum Likelihood Classification (MLC) was utilised to separate two main classes, forest and non-forest. Random Forest (RF) algorithm used to classify the segmentation and the structure of cropping within the national park.

Accuracy assessment report shows that both two approaches obtain a high accuracy varies from 88% to 90% for the Landsat imagery. The high percentage was obtained because this research only applies two types of classification, forest and non-forest. The boundary of two classes also uncomplicated to be distinguished through the human's view. Digitally, signature collection assists the algorithm to differentiate between forest and non-forest. Such classes also have a high value of separability at around 1413, which above the minimum threshold of Jefferies-Matusita distance at 1380. Separate SPOT-6 images classification also gains a better accuracy at around 85% for two dates of the image, 2013 and 2018. It is because the determined classes also have good separability.

There was a significant change within the study area in the last twenty years. In 1998, the forest area was calculated 17102.7 hectares or 51% of total land use, and it decreased to 12071.4 hectares or 35.65% in 2018. However, the image of 2008 cannot be compared to other images due to the different size of the area. It was caused in the northern part of the national park boundary; such area was covered by thick cloud. QA band provided by USGS has not covered the area through cloud mask

processing. Thus, it creates the size of the area smaller than other images. Nevertheless, the study found that the area of forest was 11332.9 hectares or 36.58 % of total land use and non-forest was around 63%.

The structure of cropping that can be identified using SPOT-6 imagery consists of eight classes for the image of 2013 and seven classes for the image of 2018. The unsupervised approach through FLS segmentation has successfully delineated each segment boundary in the study area. There was around 56% of the image of 2013 covered by forest followed by agriculture and fallow at around 11 % and 14% respectively. Conversely, the image of 2018 mostly covers by cloud at around 46%. Thus, some area cannot be classified. Nevertheless, the area with free-cloud cover was mostly dominated by forest at around 22% followed by agriculture and shrubs.

The existence of plastic shade also indicates the presence of agriculture activities in such an area. Both of the images show that most of the agriculture class was covered by plastic shade used to resist pest attacks.

6.1.2 Study Limitations

a. Cloud cover

Throughout the year, the study area mostly covers by cloud, and most of the remotely sensed data collection provides the image with non-free cloud cover. LAPAN has many collections of SPOT-6 images recorded from January to December 2018. Most of the collection is covered by clouds that can be used as an analysis image. Only one image of 2018 was relatively free of clouds (50%) that can be applied in this paper. Therefore, it was entirely tasked to analyse a series of data collection due to such constraints.

b. Ground truth data

This study achieved a high accuracy caused by less of the number of classes. Otherwise, the classification obtains less accuracy caused by the smaller number of ground truth data. Such data also did not cover all of the study areas and the collecting data only reserved for more contrast class, such as forest, pasture, tea plantation and agriculture. Moreover, by adding a new class into the classification, the percentage of accuracy decline significantly. Therefore, to obtain an appropriate result of

classification, the more fieldwork sampled points collected, the easier to control the classification processing.

6.1.3 Radiometric Correction

In term of SPOT images, ENVI software is one of a powerful tool and software to perform the radiometric correction. Such software provides two tools to convert the original image into a new image. Radiometric calibration is used to generate radiance and TOA reflectance, while FLAASH is applied to produce surface reflectance. Such a process automatically computes all parameters used to generate a new image. For example, in obtaining radiance image, Gain and BIAS value automatically loaded through metadata. Therefore, the users do not need to input manually such parameters to a particular equation. Overall, this process can generate a surface reflectance image that can be used for the subsequent processing that was the classification process.

In term of Landsat images, generally, USGS provides two types of image, surface reflectance images level 2 and level 1 that can be downloaded through the USGS website. However, the images categorised as level 1 is not radiometrically corrected. To obtain the corrected image, the radiometric and geometric correction was required to get a surface reflectance image.

6.1.4 The alternative of Artificial intelligence (AI)

Deep learning is part of artificial intelligence. In term of image processing, such machine offers the algorithm to automatically learn and advance the training data algorithm to classify the image. In this study, the classification through machine learning provides a relevant result of classification. Such a process has a similar approach with a supervised classification that also provides a spectral signature collection to obtain training data. However, deep learning as an alternative to traditional machine learning offers the advanced algorithm used to learn features and training sample to create a particular class that represent the object on the surface of the Earth. Such a machine is more complicated than machine learning, but it can improve the result of the classification.

6.1.5 Recommendations for Future Research

To obtain a comprehensive understanding of deforestation in Kerinci Seblat National Park. This study can be a baseline and guideline for the next researches to analyse the drivers of deforestation. The drivers of forest loss can emerge from spatial and physical attributes such as type of soils, weather, slope, elevation, and distance from the nearest settlement, river, and other variables. The drivers also arise due to the social and economic condition of the community around the national park.

In term of classification, this study can be used to predict the future pattern of deforestation through cellular automata model or another model that can represent the future pattern of deforestation.

Regarding spatial resolution, this study shows that with 1.5 metres resolution, the study can differentiate every type of homogenous features within the range of such resolution. Therefore, by increasing the spatial resolution under 1 metre, the method used in this study can identify different type of cropping within the national park. Unmanned Aerial Vehicle (UAV) such as drone can capture the features on the surface of with higher resolution compared to remotely sensed data.
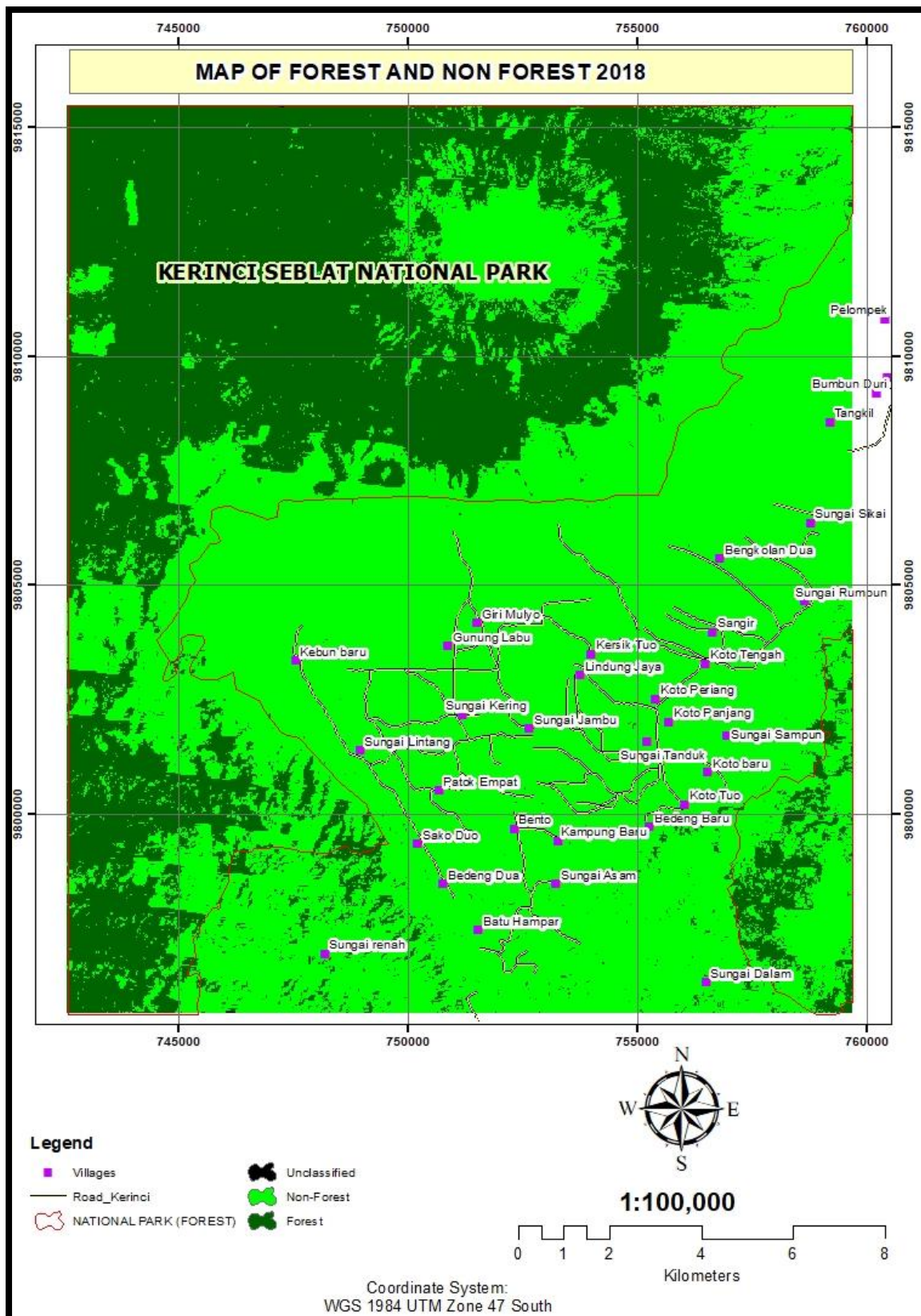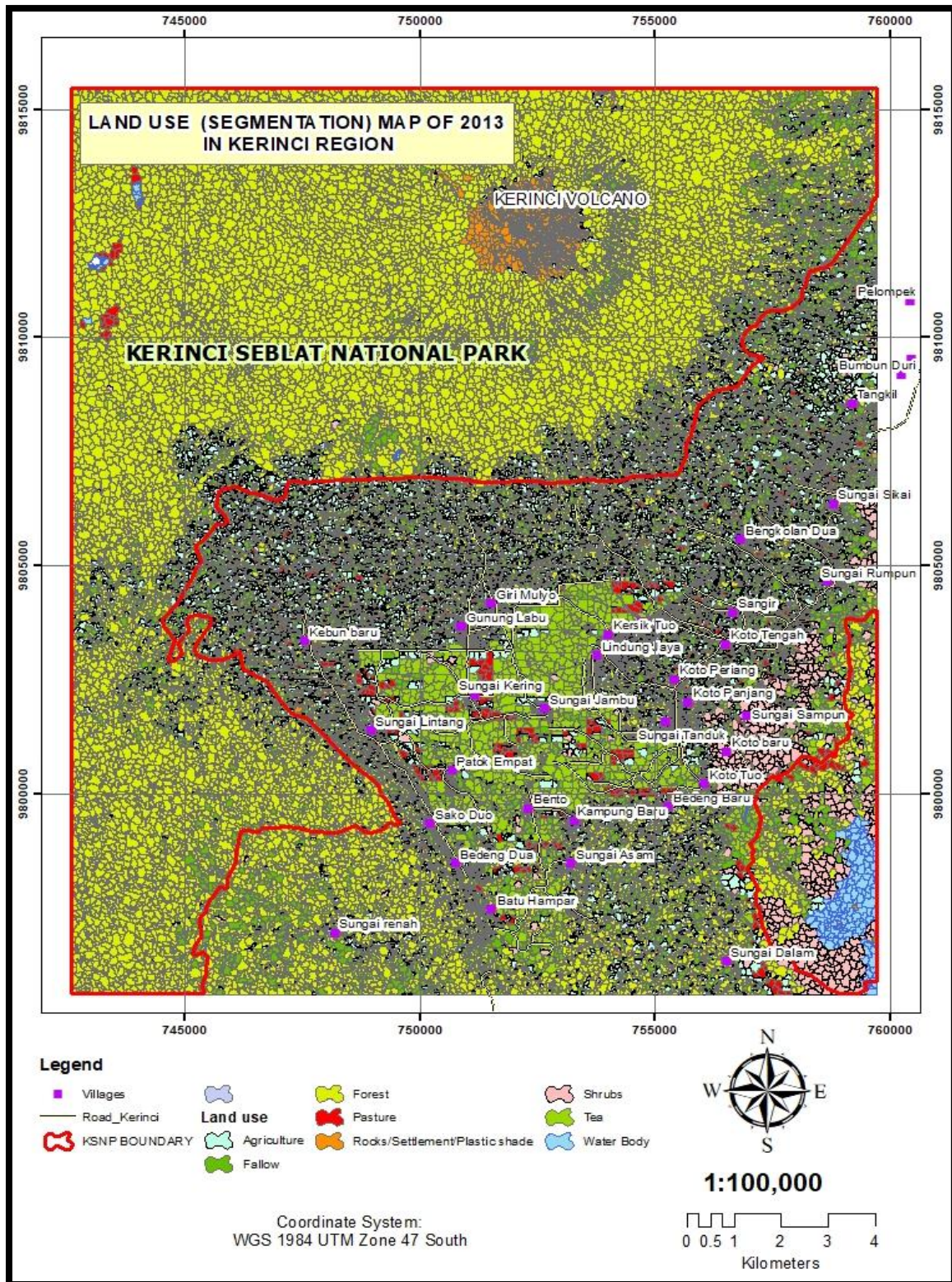
APPENDICES
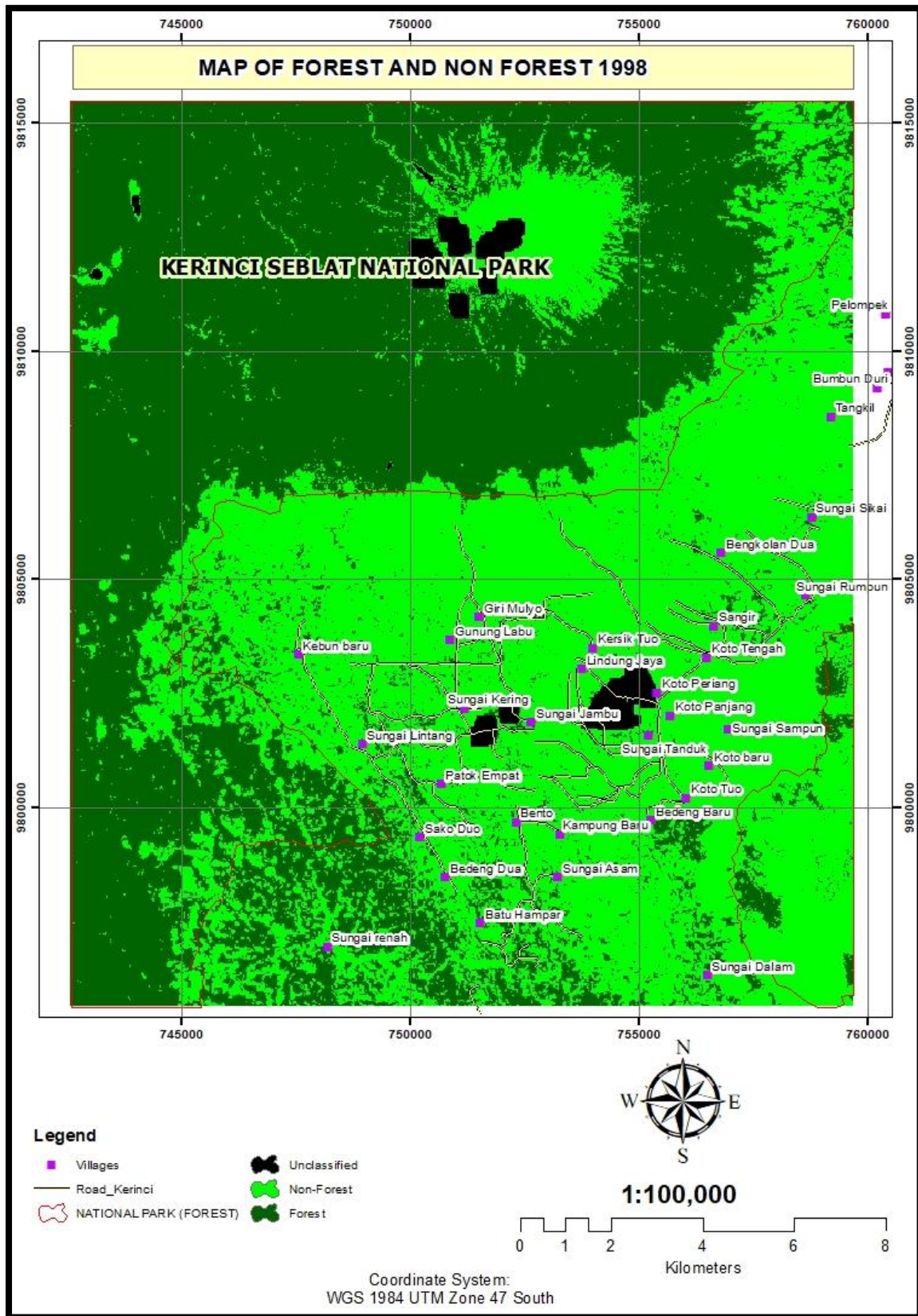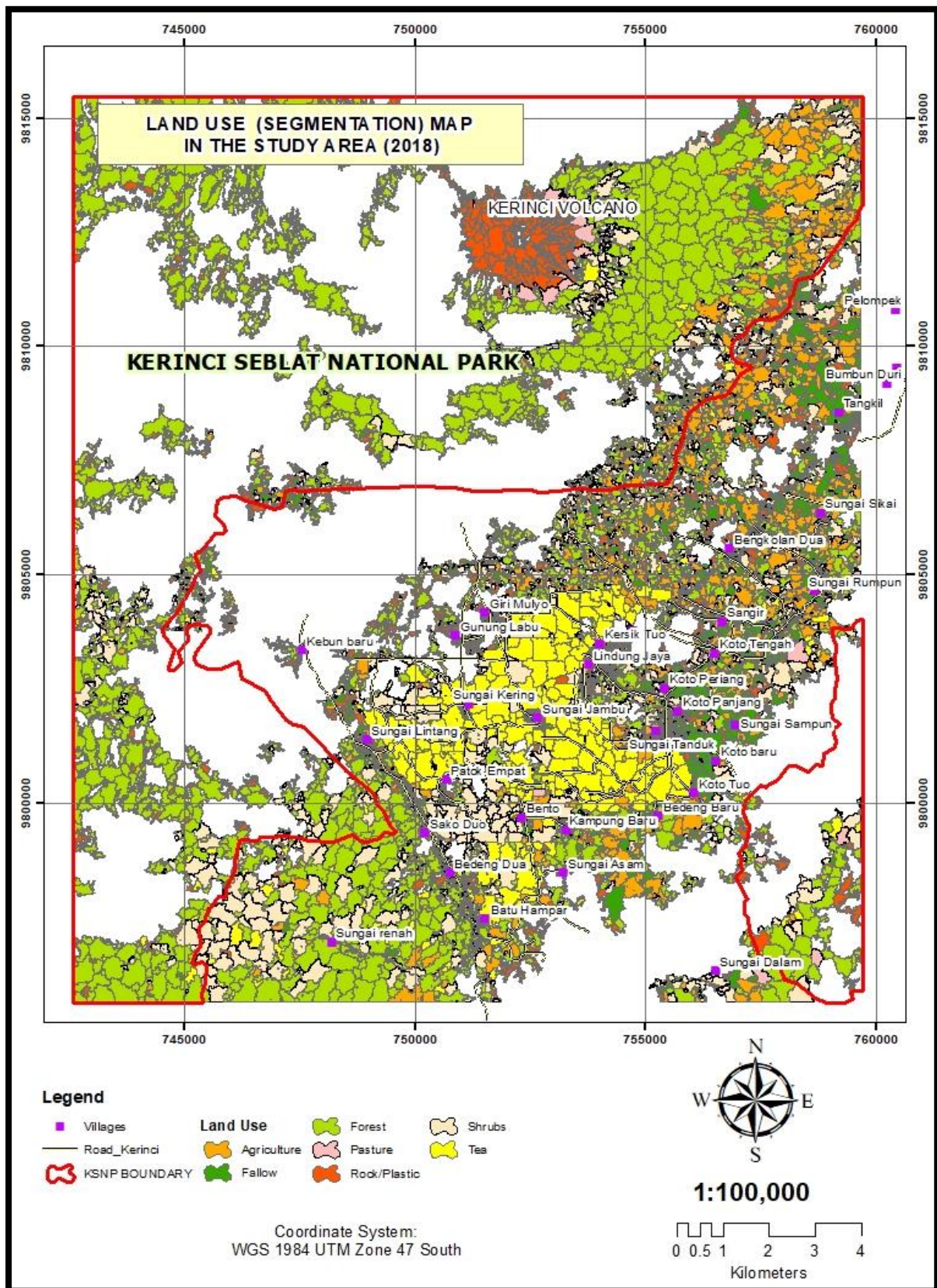

Appendix 1: Forest and Non-forest 1998
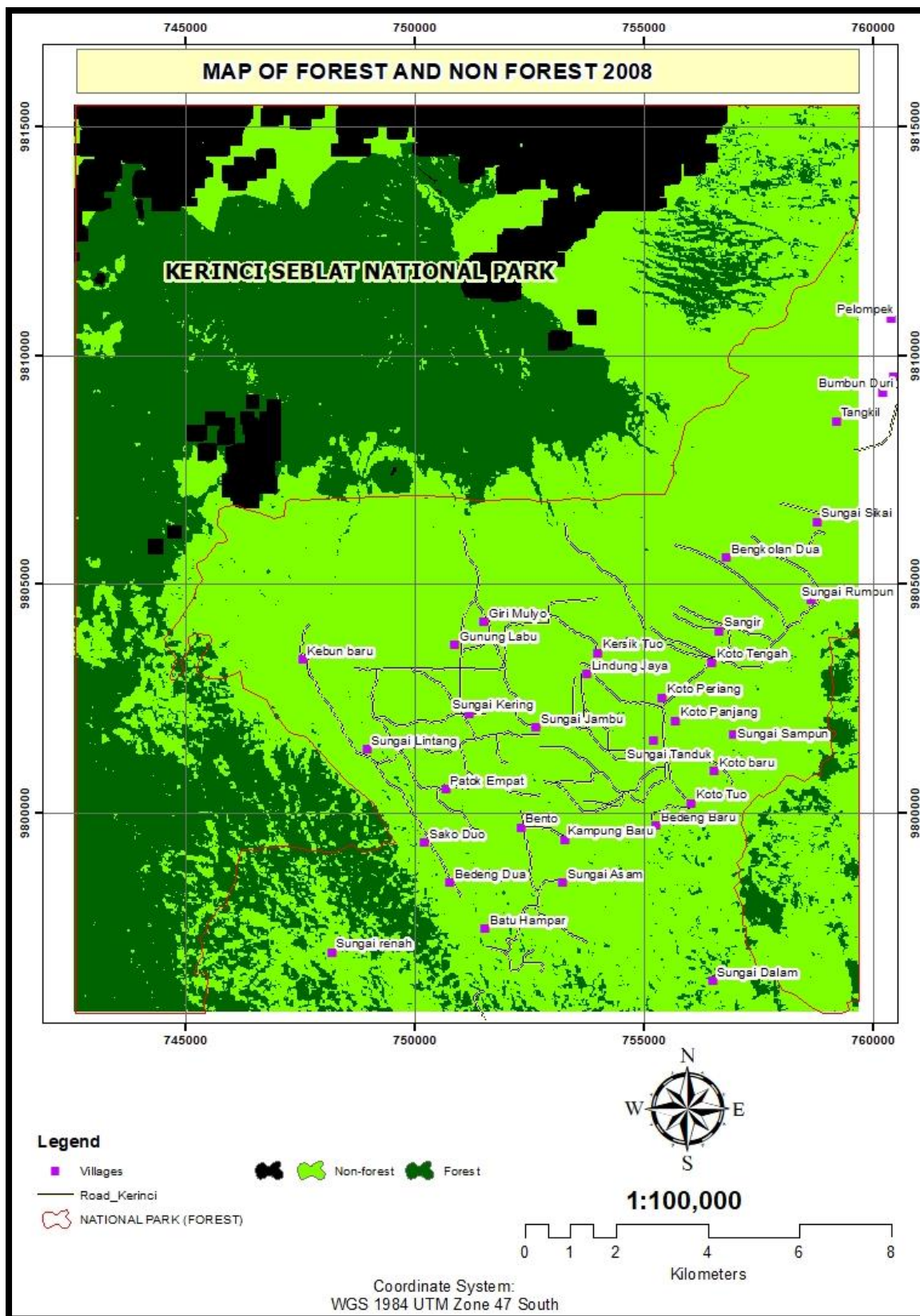
Appendix 2: Forest and Non-forest 2008

Appendix 3: Forest and non-forest map 2018

Appendix 4: Segmentation image of 2013

Appendix 5: Segmentation image of 2018

REFERENCES

Aber, JS, Marzolff, I & Ries, J 2010, *Small-format aerial photography: Principles, techniques and geoscience applications*, Elsevier.

Apan, AJIJoRS 1997, 'Land cover mapping for tropical forest rehabilitation planning using remotely-sensed data', vol. 18, no. 5, pp. 1029-49.

Aumeeruddy, Y & Sansonnens, BJAs 1994, 'Shifting from simple to complex agroforestry systems: an example for buffer zone management from Kerinci (Sumatra, Indonesia)', vol. 28, no. 2, pp. 113-41.

Bettinger, KA 2014, 'On the political edge: Conservation in an era of decentralization and democratization in central Sumatra, Indonesia', The University of Hawai'i at Manoa.

Blaschke, TJIjop & sensing, r 2010, 'Object-based image analysis for remote sensing', vol. 65, no. 1, pp. 2-16.

Borra, S, Thanki, R & Dey, N 2019, *Satellite Image Analysis: Clustering and Classification*, Springer.

Bradford, AJLS 2015, 'Deforestation: Facts, Causes & Effects'.

Breiman, L 1999, '1 RANDOM forest--RANDOM FEATURES'.

Brodský, L & Borůvka, L 2006, 'Object-oriented fuzzy analysis of remote sensing data for bare soil brightness mapping', *Soil & Water Research*, vol. 1, no. 3.

Bruner, AG, Gullison, RE, Rice, RE & Da Fonseca, GA 2001, 'Effectiveness of parks in protecting tropical biodiversity', *Science*, vol. 291, no. 5501, pp. 125-8.

Campbell, JB & Wynne, RH 2011, *Introduction to remote sensing*, Guilford Press.

Camps-Valls, G 2009, 'Machine learning in remote sensing data processing', in *2009 IEEE international workshop on machine learning for signal processing*, pp. 1-6.

Congalton & Russell 1991, 'A review of assessing the accuracy of classifications of remotely sensed data', vol. 37, no. 1, pp. 35-46.

Congalton, Russell, Green & Glen 2008, *Assessing the accuracy of remotely sensed data: principles and practices*, CRC press.

Cooley, T, Anderson, G, Felde, G, Hoke, M, Ratkowski, A, Chetwynd, J, Gardner, J, Adler-Golden, S, Matthew, M & Berk, A 2002, 'FLAASH, a MODTRAN4-based atmospheric correction algorithm, its

application and validation', in *IEEE International Geoscience and Remote Sensing Symposium*, vol. 3, pp. 1414-8.

Dhodhi, MK, Saghri, JA, Ahmad, I, Ul-Mustafa, RJJoP & Computing, D 1999, 'D-ISODATA: A distributed algorithm for unsupervised classification of remotely sensed data on network of workstations', vol. 59, no. 2, pp. 280-301.

Dong, J, Zhuang, D, Huang, Y & Fu, JJS 2009, 'Advances in multi-sensor data fusion: Algorithms and applications', vol. 9, no. 10, pp. 7771-84.

Eklundh, L & Singh, AJIJoRS 1993, 'A comparative analysis of standardised and unstandardised principal components analysis in remote sensing', vol. 14, no. 7, pp. 1359-70.

ERDAS-IMAGINE 2013, *ERDAS IMAGINE FIELD GUIDE*, Erdas.

ERDAS 1999, 'ERDAS field guide'.

FAO-UN 2016, *Global forest resources assessment*.

FAO 2005, *Global Forest Resources Assessment 2005, Progress Towards Sustainable Forest Management. FAO Forestry Paper 147*, FAO Rome.

Faust, NLJEocs & technology 1989, 'Image enhancement', vol. 20, no. supplement 5.

FFI 2018, *A global biodiversity hotspot*, viewed 13 April 2019, <https://www.fauna-flora.org/countries/indonesia>.

Friedl, MA, Brodley, CE, Strahler, AHJIToG & Sensing, R 1999, 'Maximizing land cover classification accuracies produced by decision trees at continental to global scales', vol. 37, no. 2, pp. 969-77.

Gebreslasie, M, Ahmed, F & Van Aardt, JAJIjors 2011, 'Extracting structural attributes from IKONOS imagery for Eucalyptus plantation forests in KwaZulu-Natal, South Africa, using image texture analysis and artificial neural networks', vol. 32, no. 22, pp. 7677-701.

Geneletti, D & Gorte, BJIJoRS 2003, 'A method for object-oriented land cover classification combining Landsat TM data and aerial photographs', vol. 24, no. 6, pp. 1273-86.

Gibbs, HK, Ruesch, AS, Achard, F, Clayton, MK, Holmgren, P, Ramankutty, N & Foley, JAJPotNAoS 2010, 'Tropical forests were the primary sources of new agricultural land in the 1980s and 1990s', vol. 107, no. 38, pp. 16732-7.

Gilani, H, Shrestha, HL, Murthy, M, Phuntso, P, Pradhan, S, Bajracharya, B & Shrestha, BJJoem 2015, 'Decadal land cover change dynamics in Bhutan', vol. 148, pp. 91-100.

Ginting, E 2015, 'Summary of Indonesia's economic analysis'.

Green, GM & Sussman, RW 1990, 'Deforestation history of the eastern rain forests of Madagascar from satellite images', *Science*, vol. 248, no. 4952, pp. 212-5.

Hansen, MC, Roy, DP, Lindquist, E, Adusei, B, Justice, CO & Altstatt, AJRSoE 2008, 'A method for integrating MODIS and Landsat data for systematic monitoring of forest cover and change in the Congo Basin', vol. 112, no. 5, pp. 2495-513.

Holmes, D 2000, 'Deforestation in Indonesia: A View of the Situation in 1999', *Jakarta: World Bank*.

Homer, C, Huang, C, Yang, L, Wylie, B, Coan, MJPE & Sensing, R 2004, 'Development of a 2001 national land-cover database for the United States', vol. 70, no. 7, pp. 829-40.

IBS, IBS 2013, *Population of Kerinci Regency*.

IPBES & UN 2019, *Nature's Dangerous Decline 'Unprecedented' Species Extinction Rates 'Accelerating'* UN, Paris.

James, A, Gaston, KJ & Balmford, A 2001, 'Can we afford to conserve biodiversity?', *AIBS Bulletin*, vol. 51, no. 1, pp. 43-52.

Jensen, J 1996, *Introductory digital image processing: a remote sensing perspective*, Prentice Hall Press.

Jensen, JR 2009, *Remote sensing of the environment: An earth resource perspective 2/e*, Pearson Education India.

Johnson, RA & Wichern, DW 2002, *Applied multivariate statistical analysis*, vol. 5, Prentice Hall Upper Saddle River, NJ.

Kauppi, PE, Ausubel, JH, Fang, J, Mather, AS, Sedjo, RA & Waggoner, PEJPotNAoS 2006, 'Returning forests analysed with the forest identity', vol. 103, no. 46, pp. 17574-9.

Keenan, RJ, Reams, GA, Achard, F, de Freitas, JV, Grainger, A, Lindquist, EJFE & Management 2015, 'Dynamics of global forest area: Results from the FAO Global Forest Resources Assessment 2015', vol. 352, pp. 9-20.

Kim, D-H, Sexton, JO, Noojipady, P, Huang, C, Anand, A, Channan, S, Feng, M & Townshend, JRJRSoE 2014, 'Global, Landsat-based forest-cover change from 1990 to 2000', vol. 155, pp. 178-93.

Krishna, VV, Kubitza, C, Pascual, U & Qaim, MJWD 2017, 'Land markets, property rights, and deforestation: insights from Indonesia', vol. 99, pp. 335-49.

KSNP 2018, *The Zone of Kerinci Seblat National Park 2017*, KSNP, viewed 14 April 2019, <http://tnkerinciseblat.or.id/zonasi/>.

KSNP, TS 2018, *Kerinci Seblat National Park Guide Book*, KSNP, Sungai Penuh.

Kubitza, C, Krishna, VV, Alamsyah, Z & Qaim, MJHe 2018, 'The economics behind an ecological crisis: livelihood effects of oil palm expansion in Sumatra, Indonesia', vol. 46, no. 1, pp. 107-16.

Kubitza, C, Krishna, VV, Urban, K, Alamsyah, Z & Qaim, MJEe 2018, 'Land property rights, agricultural intensification, and deforestation in Indonesia', vol. 147, pp. 312-21.

Kurniati, H 2008, 'Biodiversity and natural history of amphibians and reptiles in Kerinci Seblat National Park, Sumatra, Indonesia'.

Laben, CA & Brower, BV 2000, *Process for enhancing the spatial resolution of multispectral imagery using pan-sharpening*, Google Patents.

Lambin & Eric 1999, 'Monitoring forest degradation in tropical regions by remote sensing: some methodological issues', vol. 8, no. 3-4, pp. 191-8.

Lambin, EF, Geist, HJ & Lepers, E 2003, 'Dynamics of land-use and land-cover change in tropical regions', *Annual review of environment and resources*, vol. 28, no. 1, pp. 205-41.

Lambin, EFJGe & biogeography 1999, 'Monitoring forest degradation in tropical regions by remote sensing: some methodological issues', vol. 8, no. 3-4, pp. 191-8.

Landis, JR & Koch, GGJb 1977, 'The measurement of observer agreement for categorical data', pp. 159-74.

Leader-Williams, N & Albon, S 1988, 'Allocation of resources for conservation', *Nature*, vol. 336, no. 6199, pp. 533-5.

Lee, JSH, Abood, S, Ghazoul, J, Barus, B, Obidzinski, K & Koh, LPJCl 2014, 'Environmental impacts of large-scale oil palm enterprises exceed that of smallholdings in Indonesia', vol. 7, no. 1, pp. 25-33.

Levick, S & Rogers, K 2008, 'Structural biodiversity monitoring in savanna ecosystems: Integrating LiDAR and high-resolution imagery through object-based image analysis', in *Object-Based Image Analysis*, Springer, pp. 477-91.

Liaghat, S & Balasundram, SK 2010, 'A review: The role of remote sensing in precision agriculture', vol. 5, no. 1, pp. 50-5.

Linkie, M, Smith, RJ & Leader-Williams, N 2004, 'Mapping and predicting deforestation patterns in the lowlands of Sumatra', *Biodiversity & Conservation*, vol. 13, no. 10, pp. 1809-18.

Linkie, M, Smith, RJ, Leader-Williams, NJB & Conservation 2004, 'Mapping and predicting deforestation patterns in the lowlands of Sumatra', vol. 13, no. 10, pp. 1809-18.

Lunetta, RS & Elvidge, CD 1999, *Remote sensing change detection*, vol. 310, Taylor & Francis United Kingdom.

Margono, BA, Potapov, PV, Turubanova, S, Stolle, F & Hansen, MCJNcc 2014, 'Primary forest cover loss in Indonesia over 2000–2012', vol. 4, no. 8, p. 730.

Maurer 2013, 'How to pan-sharpen images using the Gram-Schmidt pan-sharpen method-a recipe', vol. 1, p. W1.

Meng, Q, Cieszewski, C, Madden, MJIJoP & Sensing, R 2009, 'Large area forest inventory using Landsat ETM+: a geostatistical approach', vol. 64, no. 1, pp. 27-36.

Millington, A, Blumler, M & Schickhoff, U 2011, *The SAGE handbook of biogeography*, Sage.

MOAR INDONESIA 2017, *Agricultural Statistics in Indonesia*, by Ministry of Agriculture Republic Indonesia , M-R, MINISTRY OF AGRICULTURE REPUBLIC INDONESIA.

Mitri, G & Gitas, IJIJoWF 2004, 'A semi-automated object-oriented model for burned area mapping in the Mediterranean region using Landsat-TM imagery', vol. 13, no. 3, pp. 367-76.

Mueller, M, Segl, K & Kaufmann, HJPr 2004, 'Edge-and region-based segmentation technique for the extraction of large, man-made objects in high-resolution satellite imagery', vol. 37, no. 8, pp. 1619-28.

Myint, SW, Gober, P, Brazel, A, Grossman-Clarke, S & Weng, QJRsoe 2011, 'Per-pixel vs. object-based classification of urban land cover extraction using high spatial resolution imagery', vol. 115, no. 5, pp. 1145-61.

Netanyahu, NS, Le Moigne, J, Masek, JGJIToG & Sensing, R 2004, 'Georegistration of Landsat data via robust matching of multiresolution features', vol. 42, no. 7, pp. 1586-600.

Novack, T, Esch, T, Kux, H & Stilla, UJrs 2011, 'Machine learning comparison between WorldView-2 and QuickBird-2-simulated imagery regarding object-based urban land cover classification', vol. 3, no. 10, pp. 2263-82.

Ok, AO, Akar, O & Gungor, OJEJoRS 2012, 'Evaluation of random forest method for agricultural crop classification', vol. 45, no. 1, pp. 421-32.

Ong, HP & Rajapakse, JC 2001, 'Fuzzy-region-segmentation', in *IJCNN'01. International Joint Conference on Neural Networks. Proceedings (Cat. No. 01CH37222)*, vol. 2, pp. 1374-9.

Oza, S, Panigrahy, S, Parihar, JSJIJoAEO & Geoinformation 2008, 'Concurrent use of active and passive microwave remote sensing data for monitoring of rice crop', vol. 10, no. 3, pp. 296-304.

Pal, MJIJoRS 2005, 'Random forest classifier for remote sensing classification', vol. 26, no. 1, pp. 217-22.

Pendrill, F, Persson, M, Godar, J & Kastner, TJERL 2019, 'Deforestation displaced: trade in forest-risk commodities and the prospects for a global forest transition'.

Pendrill, F, Persson, UM, Godar, J, Kastner, T, Moran, D, Schmidt, S & Wood, RJGEC 2019, 'Agricultural and forestry trade drives a large share of tropical deforestation emissions', vol. 56, pp. 1-10.

Potić, I 2015, 'Simple ETM+ gap fill techniques review', vol. 3, no. 1, pp. 31-7.

Radoux, J, Lamarche, C, Van Bogaert, E, Bontemps, S, Brockmann, C & Defourny, P 2014, 'Automated training sample extraction for global land cover mapping', *Remote Sensing*, vol. 6, no. 5, pp. 3965-87.

Richards, JA 1999, *Remote sensing digital image analysis*, vol. 3, Springer.

—— 2013, 'Supervised classification techniques', in *Remote Sensing Digital Image Analysis*, Springer, pp. 247-318.

Rosenqvist, Å, Milne, A, Lucas, R, Imhoff, M, Dobson, CJES & Policy 2003, 'A review of remote sensing technology in support of the Kyoto Protocol', vol. 6, no. 5, pp. 441-55.

Rudel, TK, Defries, R, Asner, GP & Laurance, WFJCB 2009, 'Changing drivers of deforestation and new opportunities for conservation', vol. 23, no. 6, pp. 1396-405.

Schiewe, JJIAoPRS & Sciences, SI 2002, 'Segmentation of high-resolution remotely sensed data-concepts, applications and problems', vol. 34, no. 4, pp. 380-5.

Schuck, A, Päivinen, R, Hytönen, T & Pajari, B 2002, *Compilation of forestry terms and definitions*, European Forest Institute Joensuu.

Siagian, TH, Purhadi, P, Suhartono, S & Ritonga, HJNh 2014, 'Social vulnerability to natural hazards in Indonesia: driving factors and policy implications', vol. 70, no. 2, pp. 1603-17.

Sihotang, EBS 2018, 'Perkebunan Teh Kayu Aro di Kerinci 1925-1940', *Ilmu Sejarah-S1*, vol. 3, no. 5.

Siitonen, J, Martikainen, P, Punttila, P, Rauh, JJFe & management 2000, 'Coarse woody debris and stand characteristics in mature managed and old-growth boreal mesic forests in southern Finland', vol. 128, no. 3, pp. 211-25.

Singh, IJJotISoRS 1988, 'Evaluation of Landsat TM data for forest cover type and land-use classification in subtropical forests of Kumaon Himalaya (UP)', vol. 16, no. 4, pp. 43-52.

BP STATISTIK 2017, *Environment Statistics of Indonesia*, by STATISTICS, National Statistics.

2017, *Statistik Indonesia 2017*, by Statistics, BPS.

Stehman, SV & Wickham, JDJRSoE 2011, 'Pixels, blocks of pixels, and polygons: Choosing a spatial unit for thematic accuracy assessment', vol. 115, no. 12, pp. 3044-55.

Taylor, PJ 1977, *Quantitative methods in geography:*

an introduction to spatial analysis, Houghton Mifflin.

Thomas, M & Orden, D 2004, *Agricultural Policies in Indonesia: Producer Support Estimates 1985-2003*.

USGS 2019a, *Geometry Correction*, viewed 1 May 2019, <https://www.usgs.gov>.

—— 2019b, *Landsat 4-7 Surface Reflectance Quality Assessment*, <https://www.usgs.gov/>.

Vogelmann, JE, Xian, G, Homer, C & Tolk, BJRSoE 2012, 'Monitoring gradual ecosystem change using Landsat time series analyses: Case studies in selected forest and rangeland ecosystems', vol. 122, pp. 92-105.

Waheed, T, Bonnell, R, Prasher, SO & Paulet, EJAwm 2006, 'Measuring performance in precision agriculture: CART—A decision tree approach', vol. 84, no. 1-2, pp. 173-85.

Wolf, PR & Dewitt, BA 2000, *Elements of photogrammetry: with applications in GIS*, vol. 3, McGraw-Hill New York.

Yusri, D 2016, 'Perspectives of Sustainable Collaborative Management: A Case Study in Kerinci Seblat National Park, Sumatra-Indonesia', Georg-August-Universität Göttingen.

Zhang, G 2013, 'Spectral-Spatial Based Remote Sensing Image Classification'.